EUROPEAN ORGANIZATION FOR NUCLEAR RESEARCH

August 31, 2018

D-hadron correlations in pp collisions at $\sqrt{s_{\rm NN}}$ = 5.02 TeV

F. Colamaria, S. Kumar, M. Mazzilli

Abstract

In this note, we present the analysis of azimuthal correlations of D mesons and primary charged π,K,p,e,μ performed in the ALICE central barrel in pp collisions at $\sqrt{s_{\rm NN}}$ = 5.02 TeV, from 2017 data taking. The analysis is performed in an extended $p_{\rm T}$ range and with additional observables with respect to pp 2013 data analysis. After a description of the analysis strategy, corrections and systematic uncertainties, the results obtained for prompt D^0, D^{*+} and D^+ mesons in different ranges of transverse momentum of the D meson and of the associated particles are presented. The results are then compared to perturbative QCD inspired Monte Carlo models and also with pp at 7 and 13 TeV analysis results for the common $p_{\rm T}$ ranges as well as with the 2016 p-Pb results.

Contents

1 Introduction and Motivation

The study of the azimuthal correlations of heavy-flavour particles and charged particles at the LHC energies provides a way to characterize charm production and fragmentation processes in pp collisions. The measurement also provide a way to probe our understanding of QCD in the perturbative regime, accessible in a large kinematic range given the large mass of heavy quarks. Flavour conservation in QCD implies that charm quarks are always produced as pairs of quarks and anti-quarks. The azimuthal correlations obtained using a meson carrying a heavy quark as trigger particle with the other charged particles in the same event give the possibility to study the underlying charm production mechanism in detail. In particular, prompt charm quark-antiquark pair production is back to back in azimuth at first order in leading-order perturbative-QCD (pQCD). If a hadron from the quark hadronization is taken as trigger particle, a near-side (at $\Delta\varphi = 0$) and an away-side (at $\Delta\varphi = \pi$) peaks would appear in the azimuthal correlation distributions, coming from the fragmentation of the quark pair. Heavy quarks produced from the splitting of a massless gluon can be rather collimated and may generate sprays of hadrons at small $\Delta\varphi$. Finally, for hard-scattering topologies classified as "flavour-excitation", a charm quark undergoes a hard interaction from an initial splitting ($g \rightarrow c\bar{c}$), leading to a big separation in rapidity of the hadrons originating from the antiquark (quark) with respect to the trigger D meson and contribute to a rather flat term to the $\Delta\varphi$-correlation distribution.

In the following note, we first describe the analysis strategy for the pp 2017 data sample at $\sqrt{s}$ = 5 TeV in all its steps, followed by the list of analysis corrections and the estimation of systematic uncertainties. Finally the results of $\Delta\varphi$ correlations, and quantitative observable extracted to fits to those distributions, obtained for prompt D^0, D^+ and D^{*+} in different ranges of transverse momentum for the D-meson (trigger particle) and the associated particles are presented.

The extension of the momentum ranges (both for D mesons and associated particles) with respect to the 2010 and 2016 pp datasets (at $\sqrt{s}$ = 7 TeV and $\sqrt{s}$ = 13 TeV, respectively), as well as the improved precision in the common ranges allow a more thorough investigation of the charm quark fragmentation properties (multiplicity of tracks as a function of momentum, geometrical profile of charm jets, p_T distribution of the tracks inside the jet). This can also allow us to put better constraints of charm fragmentation and charm jet properties provided by models. Furthermore, 2017 pp data sample allows us a direct and more reasonable comparison with 2016 p-Pb data, since it has the same center-of-mass energy and, thanks to the higher precision and statistics, it was possible to exploit the azimuthal correlations in the same (extended and more differential) pT ranges of both the trigger and the associated particle of the 2016 p-Pb data sample (with the exclusion of the $p_T > 3$GeV range only for the associated tracks). This new pp reference data, together with new p-Pb 2016 data will help to study cold nuclear matter effects affecting the charm fragmentation in p-Pb with better precision. In addition, this new pp data can also be used as solid and precise references in view of an analysis on a Pb-Pb sample at the same energy, which will be taken during the last weeks of 2018 data taking.

2 Data/Monte Carlo samples and event selection

The data used for the analyses were the AOD samples of the following four datasets: LHC17p_FAST, LHC17p_CENT_woSDD, LHC17q_FAST and LHC17q_CENT_woSDD (in all the cases, exploiting the pass1 reconstruction). The reason for choosing these data samples (in particular, those without the drifts for the CENT cluster) is explained later on, in this section. Exactly as done in the p–Pb 2016 data sample, also split in a similar fashion, it was verified, by looking at D-meson and associated charged track η and φ distributions, and at the mixed-event correlation distributions for each sub-samples, that no visible differences is present for the four periods (though the 17q samples taken alone suffer from very large statistical uncertainties), hence it was possible to perform the analysis directly on the merged samples without any bias.

The Monte Carlo productions adopted for this study were:

1. LHC18a4a2_fast, a HF production (HIJING with GEANT3) anchored to LHC17p,q with enrichment of heavy quarks (charm and beauty) in each of the event, produced by PYTHIA6 with Perugia2011 tune, and with forced hadronic decays of the charmed hadrons. This production was used for D-meson efficiency evaluation, purity estimation and Monte Carlo closure test.

2. LHC17l3b_fast, minimum-bias sample produced with DPMJET generator, used for the evaluation of the tracking efficiencies.

Table 1 shows the list of runs used for the analysis, for each of the data taking periods, and of the Monte Carlo productions used to evaluate the corrections:

The trigger mask request for the event selection is kINT7. Only events with a reconstructed primary vertex within 10 cm from the centre of the detector along the beam line are considered. This choice maximises the detector coverage of the selected events, considering the longitudinal size of the interaction region, and the detector acceptances, without introducing sizeable η dependencies for the reconstruction efficiencies in the considered pseudorapidity ranges. Beam-gas events are removed by offline selections based on the timing information provided by the V0 and the Zero Degree Calorimeters, and the correlation between the number of hits and track segments in the SPD detector. This is automatically performed in the Physic Selection, a positive outcome of which is required during our event selection. The pile-up cuts for out-of-bunch pile-up protection are also invoked when calling the Physics Selection task. The minimum-bias trigger efficiency is 100% for events with D mesons with $p_{\mathrm{T}} > 1$ GeV$/c$. For the analyzed data samples, the probability of pile-up from collisions in the same bunch crossing is below 2% per triggered event (in most of the runs, well below 1%). Events in which more than one primary interaction vertex is reconstructed with the SPD detector are rejected (via a call to AliRDHFCuts::kRejectMVPileupEvent method with default parameters), which effectively removes the impact of pile-up events on the analysis. Out-of-bunch tracks are also effectively rejected by the Physics Selection pile-up cuts, and also by the request of at least one point in the SPD, which has a very limited time acquisition window (300 ns).

Since data collected during pp 2017 data taking are distinguished into two categories - one including SDD detector (CENT_wSDD sample) and the second one without the SDD in the reconstruction, or in the acquisition (CENT_woSDD and FAST samples, respectively), a study of performance of the D-hadron correlation analysis with respect to the data samples employed has been carried out for D^{*+} and D^{+} mesons (more sensitive to the presence of the SDD w.r.t. the D^{0}, due to their reconstruction from three decay tracks), very similar of what was done for the p-Pb 2016 data sample (refer to p-Pb 2016 analysis note at [7]), reaching exactly the same conclusion, of a more solid analysis being obtained using more uniform samples (FAST and CENT_woSDD), at the price of a slight reduction of the statistical precision.

3 Analysis strategy

The analysis follows the same strategy one used in 2016 p-Pb and pp data samples (see published paper [2] and analysis notes [8], [7]). Correlation pairs are formed by trigger particles (D mesons) reconstructed and selected in the following $p_{\mathrm{T}}^{\mathrm{trig}}$ ranges: $3 < p_{\mathrm{T}}^{\mathrm{trig}} < 5$ GeV/c, $5 < p_{\mathrm{T}}^{\mathrm{trig}} < 8$ GeV/c, $8 < p_{\mathrm{T}}^{\mathrm{trig}} < 16$ GeV/c, $16 < p_{\mathrm{T}}^{\mathrm{trig}} < 24$ GeV/c (the possibility of extending the analysis in $2 < p_{\mathrm{T}}^{\mathrm{trig}} < 3$ was also exploited. Further details are furnished in the next paragraph). Associated particles (charged tracks) have been reconstructed in the following $p_{\mathrm{T}}^{\mathrm{assoc}}$ regions: $p_{\mathrm{T}}^{\mathrm{assoc}} > 0.3$ GeV/c, $0.3 < p_{\mathrm{T}}^{\mathrm{assoc}} < 1$ GeV/c, $p_{\mathrm{T}}^{\mathrm{assoc}} > 1$ GeV/c, $1 < p_{\mathrm{T}}^{\mathrm{assoc}} < 2$ GeV/c, $2 < p_{\mathrm{T}}^{\mathrm{assoc}} < 3$ GeV/c. In this analysis, the particle identification defines the trigger particle rather than a momentum cut and therefore the momentum range of the associated particles is not constrained by that of the trigger particle. Our definition of associated particle includes primary particles of the following species: pion, kaon, proton, electron, muon. The primary particle definition comprises particle coming from the primary vertex of interaction, including those coming from strong and electromagnetic decay of unstable particles, and particles deriving from the decay of hadrons with charm or beauty. We therefore include any charged π,K,p,e,μ except those coming from weak decays of strange particles and particles produced in the interaction with the detector material. This definition corresponds to that used in the method AliAODMCParticle::IsPyhysicalPrimary(). All associated particles surviving the selection cuts and not matching the adopted criterion are considered as a contamination whose contribution has to be corrected for.

The analysis is performed through the following steps:

1. **D meson selection and signal extraction.** For each single event, "trigger" particles are defined as the selected D meson candidates (D^0, D^+ and D^{*+}) within a given $p_{\mathrm{T}}^{\mathrm{trig}}$ range. The detection strategy for D mesons at central rapidity is the same performed for the analyses of the D-meson production at central rapidity [1], and also applied for the D-h analysis on 2010 pp, 2016 pp and 2016 p-Pb samples ([8], [7]). It is based on the reconstruction of decay vertices displayed from the primary vertex by a few hundred μm and on the identification of the decay-particle species. The identification of the charged kaon and pion in the TPC and TOF detectors is also used, to further reduce the background at low p_{T}. An invariant-mass analysis is then used to extract the raw signal yield, using the same fit functions described in [2]. The D mesons are selected in the rapidity range varying from $|y| < 0.5$ at low p_{T} to $|y| < 0.8$ for $p_{\mathrm{T}} > 5$ GeV/c.

2. **Correlation of D candidates with associated tracks.** Particle pairs are formed by correlating each trigger particle with the charged primary particles passing the track selection (excluding those coming from the decay of the D-meson candidate) in a specified p_T^{assoc} interval (which can overlap with the $p_{\mathrm{T}}^{\mathrm{trig}}$ range) and in the pseudo-rapidity range $|\eta| < 0.8$. For the D^0 meson, also the low-momentum pion tracks from feed-down of D^{*+} mesons are removed via 3σ invariant mass cut on the $M(K\pi\pi) - M(K\pi)$ difference. This because these soft pion are not related to the charm quark fragmentation chain. For D meson candidates in the invariant mass signal region, defined by a $\pm$ 2σ interval around the D meson mass peak, the azimuthal angle difference $\varphi^{\mathrm{assoc}} - \varphi^{\mathrm{trigg}} \equiv \Delta\varphi$ and the pseudorapidity difference $\eta^{\mathrm{assoc}} - \eta^{\mathrm{trig}} \equiv \Delta\eta$ are evaluated and stored to build two-dimensional correlation distribution.

3. **Correction for limited acceptance and detector inhomogeneities with Event Mixing** The angular correlation distribution may be affected, even for uncorrelated pair of particles, by structures not due to physical effects, but originating from the limited detector acceptance, as well as from angular inhomogeneities in the trigger and track reconstruction efficiencies as a function of $\Delta\varphi$ and $\Delta\eta$. Effects of this kind are removed using the Event Mixing technique. In this technique, the analysis is executed on the same data sample of the standard one (called "same event" analysis,

SE), but the trigger particles found in each event are correlated to charged particles reconstructed in different events ("Mixed Events" analysis, ME) with similar characteristic, in particular concerning the event multiplicity and z position of the primary vertex (see Section 3.3.1).

The differential yield of associated particles per trigger particle is obtained by

$$\frac{1}{N_{\mathrm{trig}}}\frac{\mathrm{d}^2N^{\mathrm{pair}}}{\mathrm{d}\Delta\eta\,\mathrm{d}\Delta\varphi} = B_{ME}(0,0)\times\frac{S(\Delta\eta,\Delta\varphi)}{B_{ME}(\Delta\eta,\Delta\varphi)}, \tag{1}$$

where N^{pair} is the total number of correlated D-hadron pairs. The functions $S(\Delta\eta,\Delta\varphi)$ and $B_{ME}(\Delta\eta,\Delta\varphi)$ are the signal and the mixed event background distributions, respectively. The later is normalized to its value in $(\Delta\eta,\Delta\varphi) = (0,0)$, i.e. $(B(0,0))$. Further details on the mixed-event correction are provided in the next section.

4. **Subtraction of background correlation from signal distribution.** The invariant mass signal region also includes background D-meson candidates. Their contribution to the raw correlation distribution is subtracted as follows. For each p_{T} bin, the mean and the sigma of the invariant mass spectrum are extracted. For D^0 and D^+, a "background" region is defined in the sidebands of the mass distribution as the interval 4 $\mathrm{GeV}/c^2 < |m - m^{\mathrm{pdg}}| < 8$ GeV/c^2 (for the D^{*+} meson, only the right sideband is used). The angular correlation distribution for background candidates in this region is extracted and normalized with respect to the background in the signal region estimated from the mass fit. This normalized background correlation distribution is then subtracted from the raw signal one to obtain the signal correlation distribution. The normalization factor is the ratio of the number of background candidates under the signal peak (obtained by integrating the background of the fit function within the signal region) over the number of background candidates in the sidebands (obtained via bin-counting in the sideband region). An example of the signal region, sideband and sideband-subtracted 1D correlation distributions (along $\Delta\varphi$) is shown in figure 1, together with the comparison of the three distributions after the normalization to the number of triggers.

5. **Correction for D meson efficiency and associated track efficiency.** After filling the signal and background correlation distributions, it is necessary to take into account also for the correlations with tracks, those are not reconstructed, or not passing the quality selection due to poor reconstruction. In the same way, the loss of D-mesons which are not reconstructed, or do not pass the selection, impacts the correlation distribution shape. Hence, each pair is weighted by the inverse of the product of the associated track and D meson reconstruction efficiency, ε_{trk} and ε_{trig}. Further details are provided later on in this section.

6. **Projection in $\Delta\varphi$.** The limited statistics available does not allow to study the two dimensional $(\Delta\eta,\Delta\varphi)$ distribution, which is therefore projected to the $\Delta\varphi$ axis by integrating on $|\Delta\eta| < 1$. Despite, in principle, our maximum $\Delta\eta$ acceptance is of $|\Delta\eta| < 1.6$, removing the large $|\Delta\eta|$ regions allow us to reject angular regions with very low statistics, where fluctuations would be amplified by a large mixed-event correction, and avoid the so-called wings effect.

   As the difference in the azimuthal angle is periodic ($\Delta\varphi = 0 = 2\pi$), the $\Delta\varphi$-range is limited to the essential range of 2π. The $\Delta\varphi$-limits are chosen to be $[-\pi/2, 3\pi/2]$ in order to provide a good visibility of the correlation pattern, which peaks around 0 and π.

7. **Correction for the contamination of secondary particles** The DCA to primary vertex cut, applied during the associated track selection, has the role of removing the secondary particles from the associated track sample. Secondary particles are indeed produced either from long-lived strange hadrons or from interaction of particles with the detector material. A residual contamination from secondary tracks is hence expected in the correlation distributions. This contamination

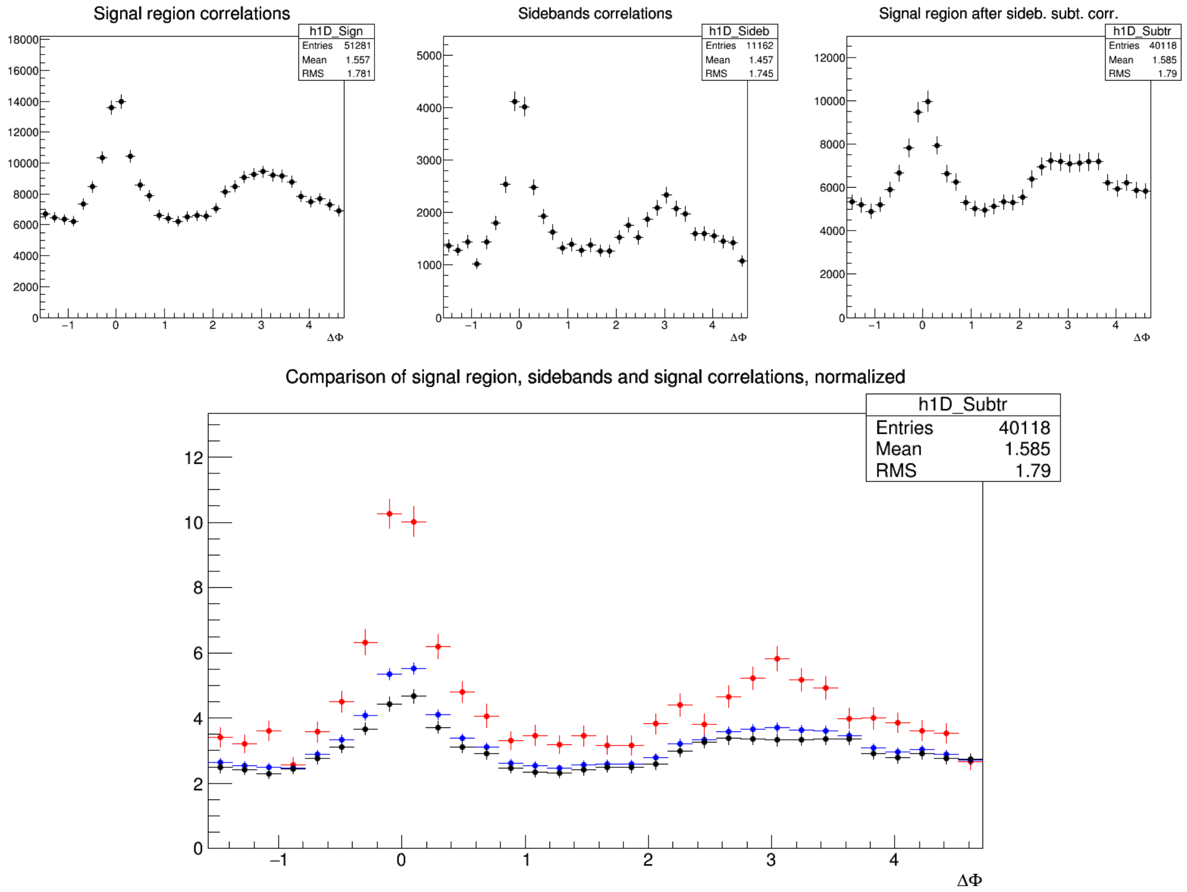

Figure 1: Top: Example of D^{*+}-h signal region (left), sideband (middle), and signal minus sideband (right) correlation distributions. Bottom: signal region per-trigger normalized correlation distribution (blue), sideband region per-trigger normalized correlation distribution (red), background-subtracted per-trigger normalized correlation distribution (black).

is estimated from Monte Carlo simulation based on Pythia as described more in detail in the next section. The background-subtracted event-mixing corrected correlations are multiplied by a purity factor to encounter this contribution.

8. **Correction for bias on B to D decay topologies** The presence of the topological cuts for the D-meson selection indirecly induce a bias on the topology of the B to D decay topologies, favouring cases with a small opening angle between the D-meson and the other tracks from the B decay. This affects the feed-down component of the data correlation distributions. This effect is corrected for with a procedure described in the subsection 3.3.3.

9. **Correction for feed-down of D meson from b-hadron decay** The selection strategy employed for the D meson candidates selection enhances the fraction of reconstructed D mesons coming from the decay of a b-hadron. Typical values, with the cuts used for the D-meson selection, are of the order of 10% or less. The correlation distribution of these secondary D mesons will be sensitive to the properties of beauty jets and beauty hadron decay, which in general differ from those relative to charm jets and hadrons. The procedure used to subtract this contribution is described in the next paragraphs of this section.

10. **Study of correlation properties.** The properties of the azimuthal correlation distribution are quantified by fitting the distribution with a function composed of two Gaussian functions, modelling the near and the away side peaks, and a constant term describing the baseline. The mean of the

Gaussian are fixed at $\Delta\varphi = 0$ and $\Delta\varphi = \pi$. To accomplish the 2π periodicity of the $\Delta\varphi$ variable, the Gaussian functions are "duplicated" with mean shifted by $\Delta\varphi = 2\pi$ and $\Delta\varphi = -2\pi$. The fitting procedure is described in details in Section 5.

3.1 Mass plots and cut optimization

The invariant mass distributions of D^0, D^{*+} and D^+ in the various p_T ranges are shown in Figs. 2, 3, Figs. 4, 5 and Figs. 6, 7 respectively. Note that the distributions are weighted by the D-meson selection and reconstruction efficiency, to allow a correct normalization of the correlation distributions, which have also these weights.

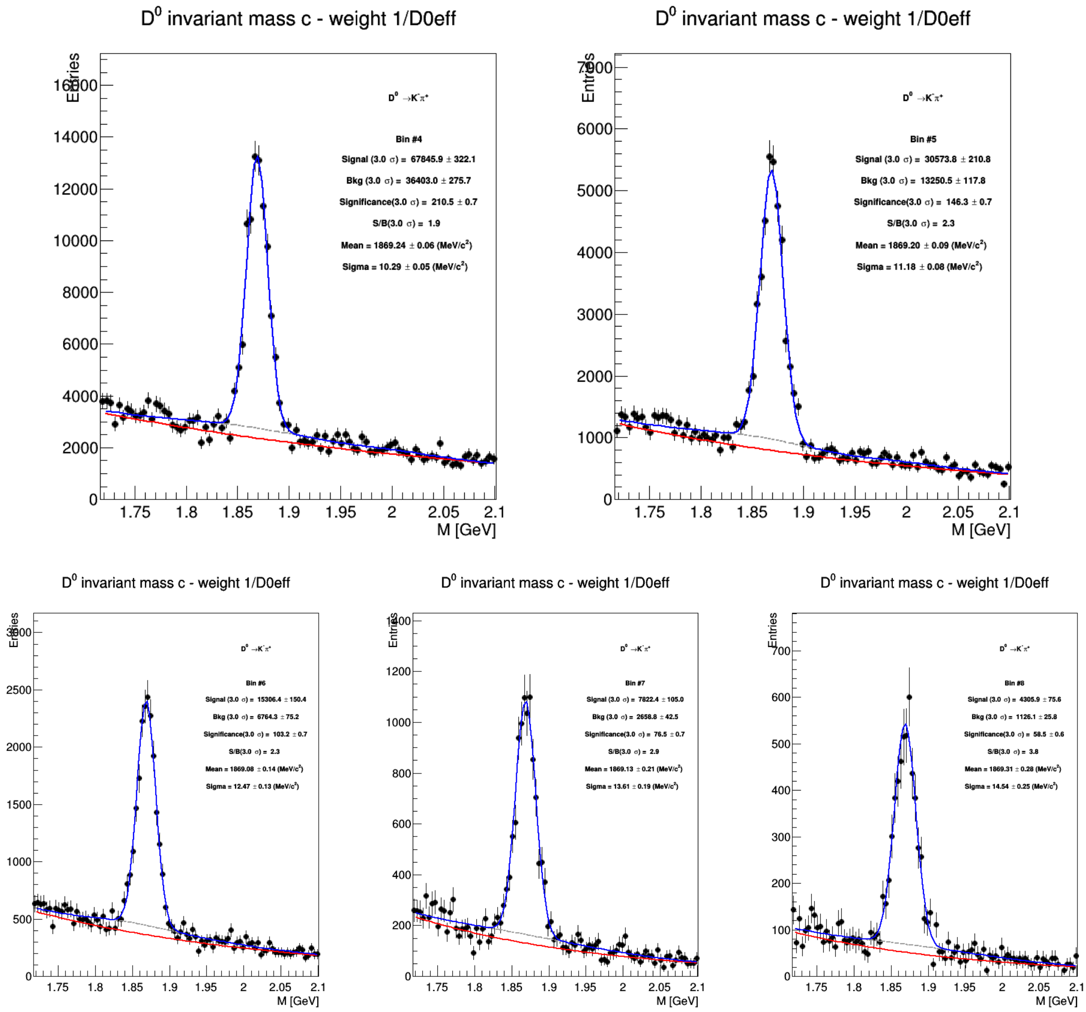

Figure 2: Invariant mass distributions of D^0 corrected with efficiency in different p_T regions. Top: $3 < p_T^D < 4$ GeV$/c$ (left), $4 < p_T^D < 5$ GeV$/c$ right), Bottom: $5 < p_T^D < 6$ GeV$/c$ (left), $6 < p_T^D < 7$ GeV$/c$ (middle), $7 < p_T^D < 8$ GeV$/c$ (right).

For the D^{*+}, 3 sets of cuts were compared (the 2016 p-Pb, 2016 pp and the standard D2H 2017 pp cuts). The best performance was obtained with 2016 p-Pb cuts in most of the p_T bin analysed. Indeed, despite the looser cuts applied from D2H allow to have higher signal, the p-Pb set of cuts assured a better S/B factor without loosing too much signal. This allows us to reduce fluctuations induced by the sideband subraction, that is the limiting factor for the analysis performance. The same holds for the D^+, but with the addition of cuts on the normalized decay length in xy plane and of the normalized difference between measured and expected daughter track impact parameters (topomatic cut).

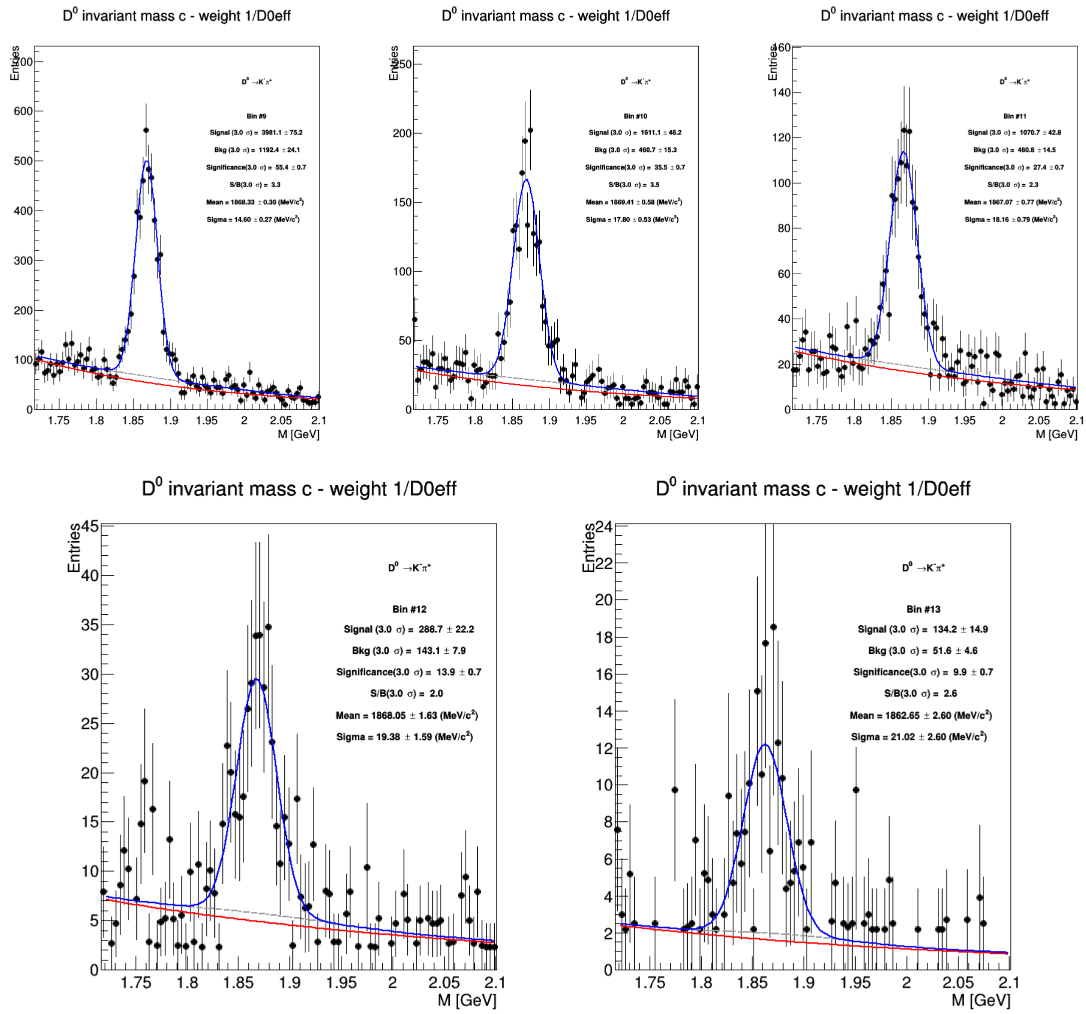

Figure 3: Invariant mass distributions of D^0 corrected with efficiency in different p_T regions. Top: $8 < p_T^{\mathrm{D}} < 10$ GeV/c, $10 < p_T^{\mathrm{D}} < 12$ GeV/c (middle), $12 < p_T^{\mathrm{D}} < 16$ GeV/c (right), Bottom: $16 < p_T^{\mathrm{D}} < 24$ GeV/c.

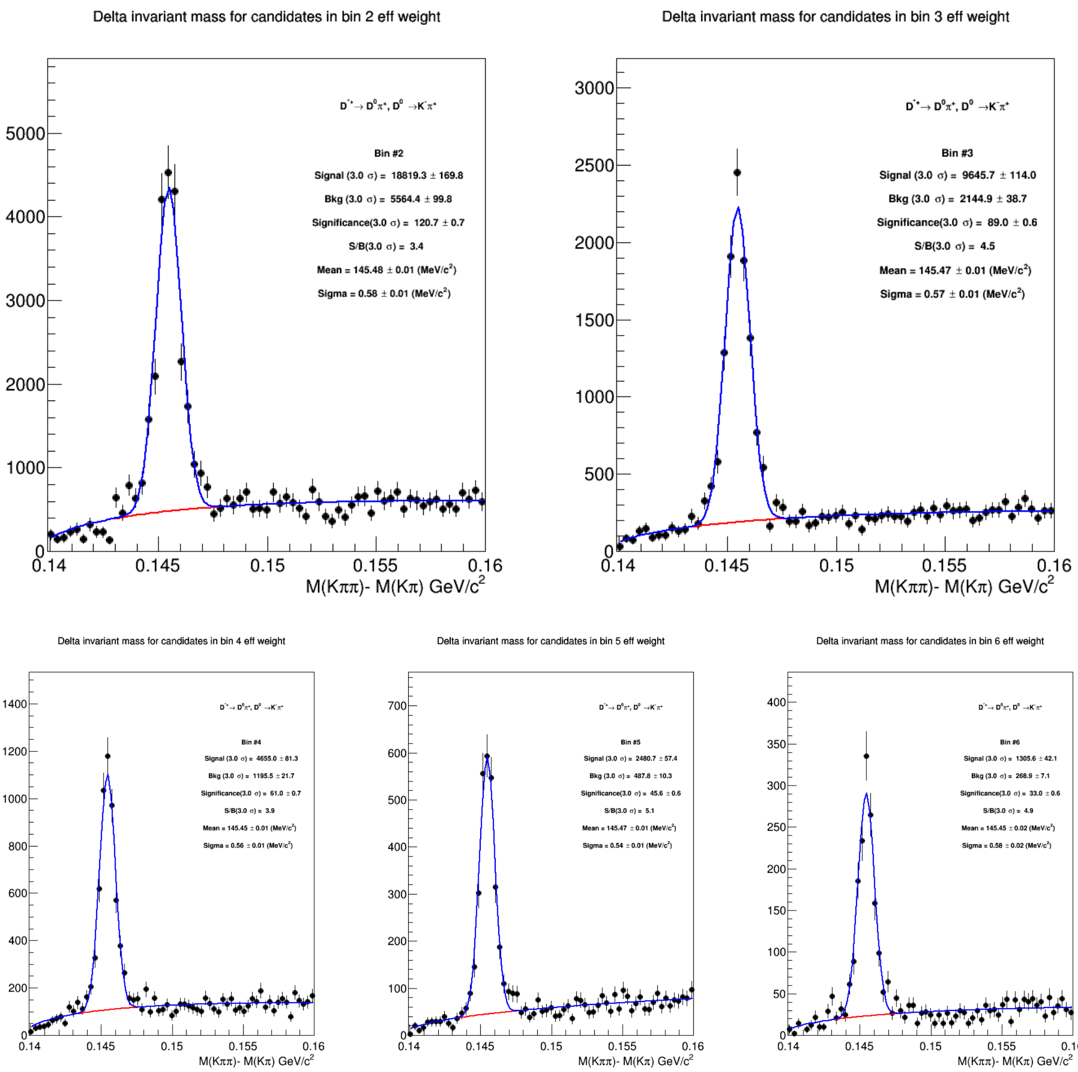

Figure 4: Invariant mass distributions of D^{*+} corrected with efficiency in different p_T regions. Top: $3 < p_T^D < 4$ GeV$/c$ (left), $4 < p_T^D < 5$ GeV$/c$ right), Bottom: $5 < p_T^D < 6$ GeV$/c$ (left), $6 < p_T^D < 7$ GeV$/c$ (middle), $7 < p_T^D < 8$ GeV$/c$ (right).

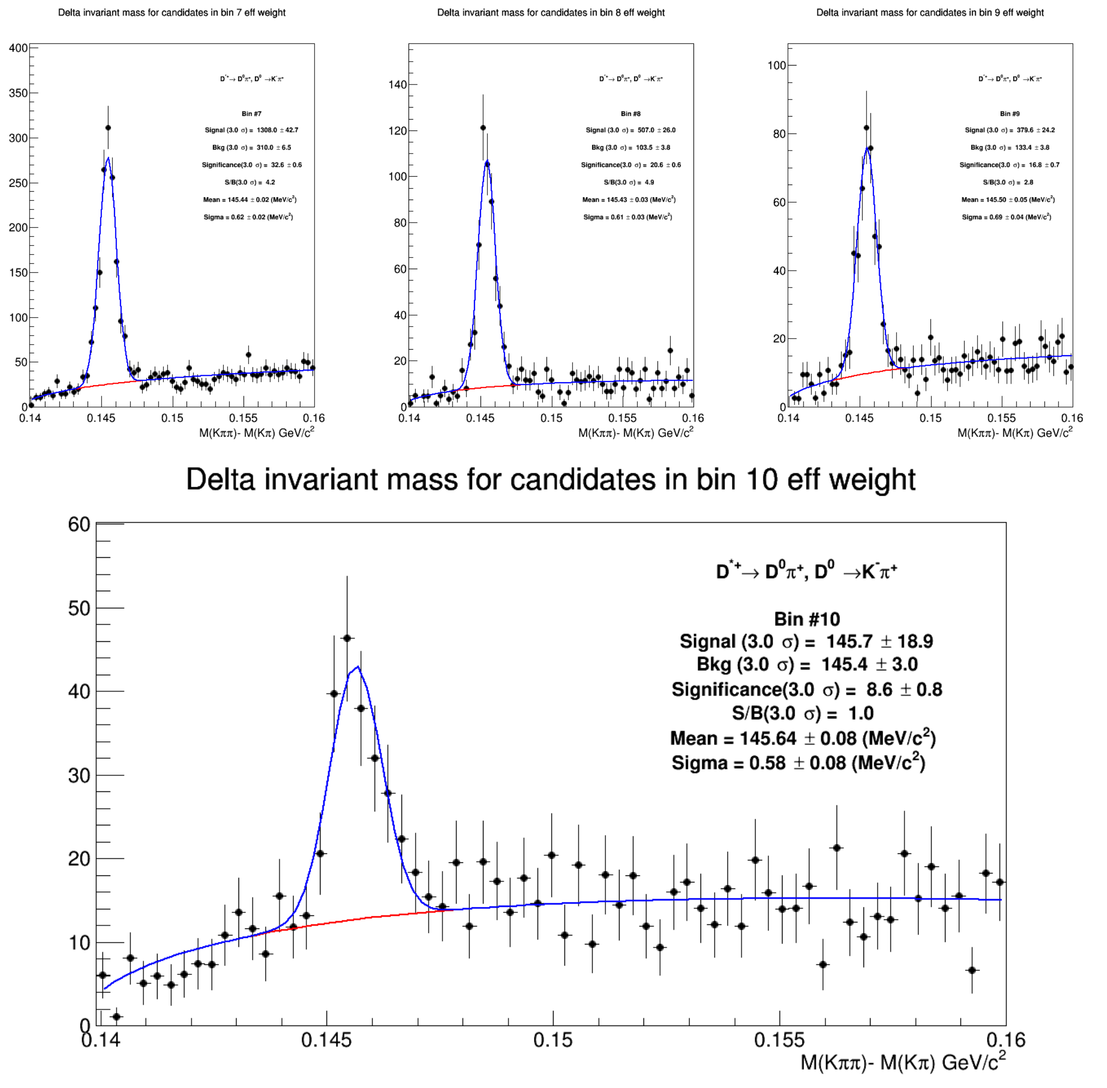

Figure 5: Invariant mass distributions of D^{*+} corrected with efficiency in different p_T regions. Top: $8 < p_T^D < 10$ GeV/c, $10 < p_T^D < 12$ GeV/c (middle), $12 < p_T^D < 16$ GeV/c (right) and Bottom: $16 < p_T^D < 24$ GeV/c .

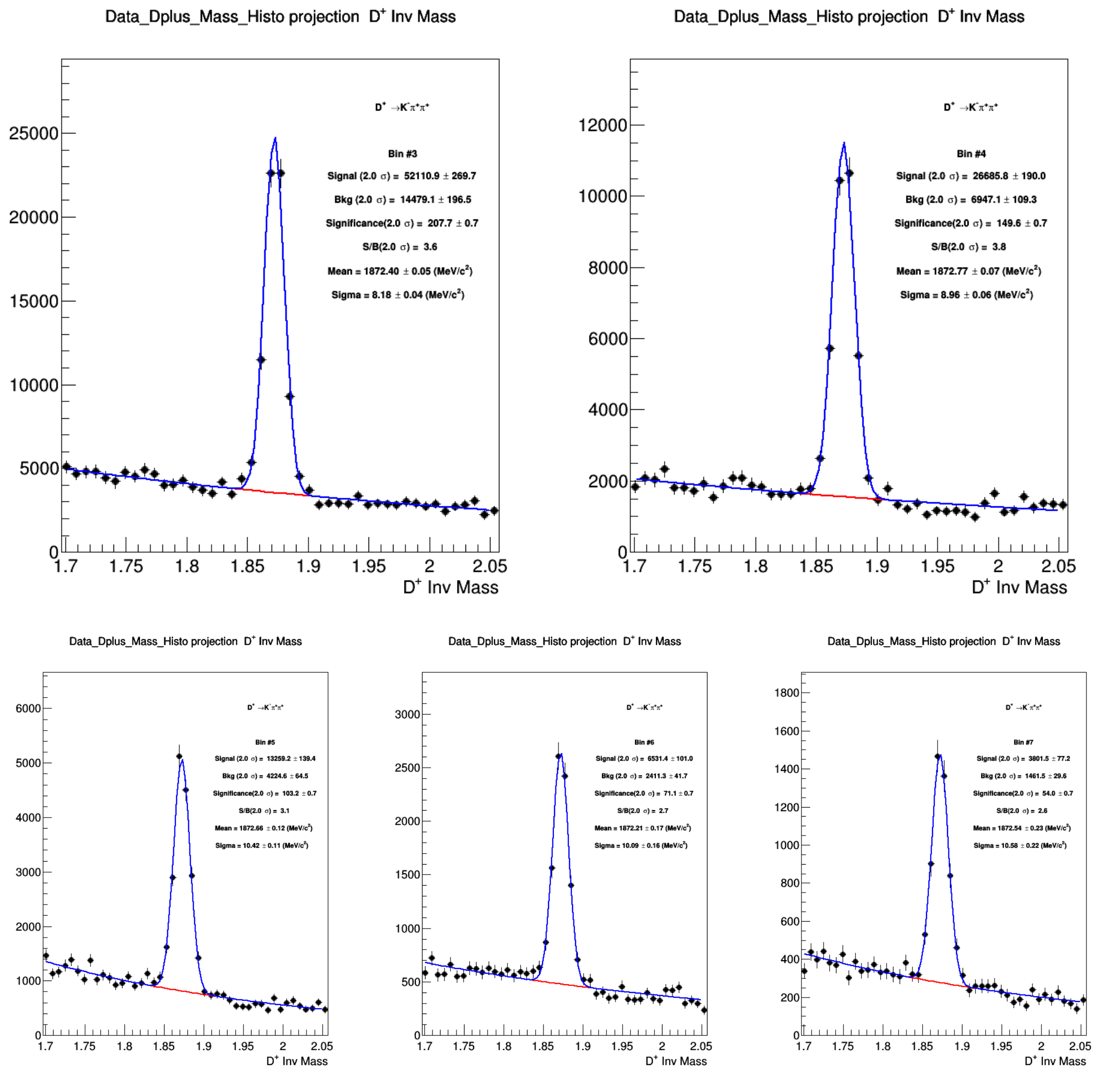

Figure 6: Invariant mass distribution of D^{+} corrected with efficiency in different p_T regions. Top: $3 < p_T^{D} < 4$ GeV$/c$ (left), $4 < p_T^{D} < 5$ GeV$/c$ right), Bottom: $5 < p_T^{D} < 6$ GeV$/c$ (left), $6 < p_T^{D} < 7$ GeV$/c$ (middle), $7 < p_T^{D} < 8$ GeV$/c$ (right);.

A particular cut optimization was instead performed for the D^0 meson. Twelve cut sets were tried, with the goal of increasing the S/B factor, in order to reduce fluctuations induced by the sideband subraction as explained. In Figure 8 the D^0-h correlation distributions are shown for the different cut sets, in exemplary kinematic regions (5 to 8 GeV$/c$), together with the bin-by-bin relative statistical uncertainty on the data points. The best cut set (option B, cyan colour) was defined starting from the standard cuts used for the p-Pb 2016 cross section analysis, with a tightened selection on the cosine of the pointing angle, and with the addition of a cut on the normalized decay length in xy plane (from 5 to 3 units with increasing $p_{\mathrm{T}}^{\mathrm{D}}$ and of a selection on the normalized difference between measured and expected daughter track impact parameters (topomatic cut) at 3 sigma.

3.1.1 Extension to vey-low p_{T} of D mesons

Thanks to the higher statistic of the 2017 pp data sample, we tried to enlarge our correlation studies to very-low p_{T} of the trigger particle. Indeed, the Figure 9 shows the good performance on the invariant mass extraction for all the 3 D-mesons with $2 < p_T^{D} < 3$ GeV$/c$.

The extension of the analysis to this p_{T} interval is of high interest for the jet structure characterizion. Indeed, this study allow us to investigate a kinematic region in which the trigger particle has compatible or even lower momentum with respect to the associated particles. This give us the possibility to better understand the production processes. In fact, for example, at the Leading Order (LO) for $p_{\mathrm{T}}(trig) \sim p_{\mathrm{T}}(ass)$ we don't expect any peak on the near-side region. A peak could arise only from Next-to-Leading-Order production process.

Despite the good statistics, it wasn't enough to perform the correlation analysis. Indeed, the correlation distribution peaks are very small, due to the small energy of the parton, resulting in few tracks being produced in the fragmentation oon top of the D meson. Hence, the correlation peaks were smothened by the baseline fluctuations (of the same order of magnitude of the peak itself), especially on the away-side region, where indeed most of the fit failed.

3.2 Code used for the analysis

The code used for D meson-hadron correlation analysis is fully committed in AliPhysics. The analysis classes can be found in $ALICE_ROOT/PWGHF/correlationHF/. The D meson specific classes where the aforementioned steps are carried out are AliAnalysisTaskDStarCorrelations, AliAnalysisTaskSED0Correlations and AliAnalysisTaskDplusCorrelations. The classes which are common to the D meson specific analysis which includes the associated particle cuts and the correlation observables are AliHFAssociatedTrackCuts, AliHFCorrelator, AliHFOfflineCorrelator, AliReducedParticle and AliDhCorrelationExtraction. Several additional classes and macros in the same folder deal with the correction steps.

3.3 Further details on corrections

3.3.1 Event Mixing

The event-mixing technique is used for correcting the raw correlation distribution for effects arising from the detector limited acceptance in rapidity and detector spatial inhomogeneities. The calculation of the Event Mixing correlation distribution is performed online. An event pool is created, where events preceding the one containing a D candidate are stored based on their properties (position of the vertex along the z axis and multiplicity). Each time a D meson candidate is found in an event, only the events contained in the same pool as the event under analysis is used to evaluate the correlations for the event mixing correction.

The multiplicity and z vertex position bins for the pools used in the p-Pb analysis (for both approaches) are the following:

- Multiplicity bins: $(0,20);(20,35);(35,+\infty)$
- Vertex z (cm) = $(-10,-2.5);(-2.5,2.5);(2.5,10)$

In an ideal case, the mixed event distribution is expected to have a constant flat distribution as function of $\Delta\varphi$ and a triangular shaped distribution in $\Delta\eta$ deriving from the limited η acceptance of the detector. In case, instead, of detector inefficient regions, or holes, in the same angular position for D meson and associated tracks, these structures produce an excess of correlations at $\Delta\varphi = 0$ in the $\Delta\varphi$ distribution, plus possibly other structures depending on the relative position of the inefficient regions and on their number. The mixed-event distribution is used as a weight in each correlation bin, i.e, the corrected correlation distribution is calculated as follows:

$$\frac{dN^{corr}(\Delta\varphi\Delta\eta)}{d\Delta\varphi d\Delta\eta} = \frac{\frac{dN^{SE}(\Delta\varphi\Delta\eta)}{d\Delta\varphi d\Delta\eta}}{\frac{dN^{ME}(\Delta\varphi\Delta\eta)}{d\Delta\varphi d\Delta\eta}} \frac{dN^{ME}(0,0)}{d\Delta\varphi d\Delta\eta} \tag{2}$$

In Eq.2, the last term stands for the average of the bins in the region $-0.2 < \Delta\eta < 0.2$, $-0.2 < \Delta\varphi < 0.2$ (multiple bins are used to minimize the effect of statistical fluctuations on the normalization of the mixed-event plots). This kind of normalization, adopted in the analysis of hadron-hadron correlations, relies on the fact that at $(\Delta\eta, \Delta\varphi) = (0,0)$ the trigger and associated particle experience the same detector effects. In the D meson case this is true only on average and not at very low p_{T}, since D mesons are reconstructed from particles that can go in different detector region. However, $(\Delta\eta, \Delta\varphi) = (0,0)$ is in any case the region with maximum efficiency for the pairs (both correlated and uncorrelated). Thus the same convention was adopted.

The mixed-event correlation distributions are built in both D meson signal and sideband regions. Both are corrected with the relative distributions. An example of the mixed-event distributions, and of the outcome of the mixed-event correction, is provided in Figures 10 and 11. The expected triangular shape in $\Delta\eta$, for the mixed-event distributions, addresses the effect of the limited detector pseudo-rapidity acceptance. Note that the mixed-event distribution is limited to the interval $|\Delta\eta| < 1$: the decision to limit the mixed-event correction, and thus the whole analysis, to this range was taken in order to avoid the so-called “wing effect”, i.e. the wing-like structures arising in the correlation distribution at large $\Delta\eta$ due to the limited filling of the correlation bins in that region.

Type	Production	Run list	nEvents
Monte-Carlo	LHC18a4a2_fast (c/b enriched) [GEANT3]	282343, 282342, 282341, 282340, 282314, 282313, 282312, 282309, 282307, 282306, 282305, 282304, 282303, 282302, 282247, 282230, 282229, 282227, 282224, 282206, 282189, 282147, 282146, 282127, 282126, 282125, 282123, 282122, 282120, 282119, 282118, 282099, 282098, 282078, 282051, 282050, 282031, 282025, 282021, 282016, 282008,282367, 282366, 282365 = **[44 runs]**	23M
	LHC17l3b_fast (Minimum Bias sample) [GEANT3]	282008, 282016, 282021, 282025, 282031, 282050, 282051, 282078, 282098, 282099, 282118, 282119, 282120, 282122, 282123, 282125, 282126, 282127, 282146, 282147, 282189, 282206, 282224, 282227, 282229, 282230, 282247, 282302, 282303, 282304, 282305, 282306, 282307, 282309, 282312, 282313, 282314, 282340, 282341, 282342, 282343, 282365, 282366, 282367 = **[44 runs]**	23M
Data	LHC17p_pass1_FAST	282343, 282342, 282341, 282340, 282314, 282313, 282312, 282309, 282307, 282306, 282305, 282304, 282303, 282302, 282247, 282230, 282229, 282227, 282224, 282206, 282189, 282147, 282146, 282127, 282126, 282125, 282123, 282122, 282120, 282119, 282118, 282099, 282098, 282078, 282051, 282050, 282031, 282025, 282021, 282016, 282008 = **[41 runs]**	985M total
	LHC17p_pass1_CENT_woSDD	282343, 282342, 282341, 282340, 282314, 282313, 282312, 282309, 282307, 282306, 282305, 282304, 282303, 282302, 282247, 282230, 282229, 282227, 282224, 282206, 282189, 282147, 282146, 282127, 282126, 282125, 282123, 282122, 282120, 282119, 282118, 282099, 282098, 282078, 282051, 282050, 282031, 282030, 282025, 282021, 282016, 282008 = **[42 runs]**	
	LHC17q_pass1_FAST	282367, 282366, 282365 = **[3 runs]**	
	LHC17q_pass1_CENT_woSDD	282367, 282366, 282365 = **[3 runs]**	

Table 1: Data Set and Run list

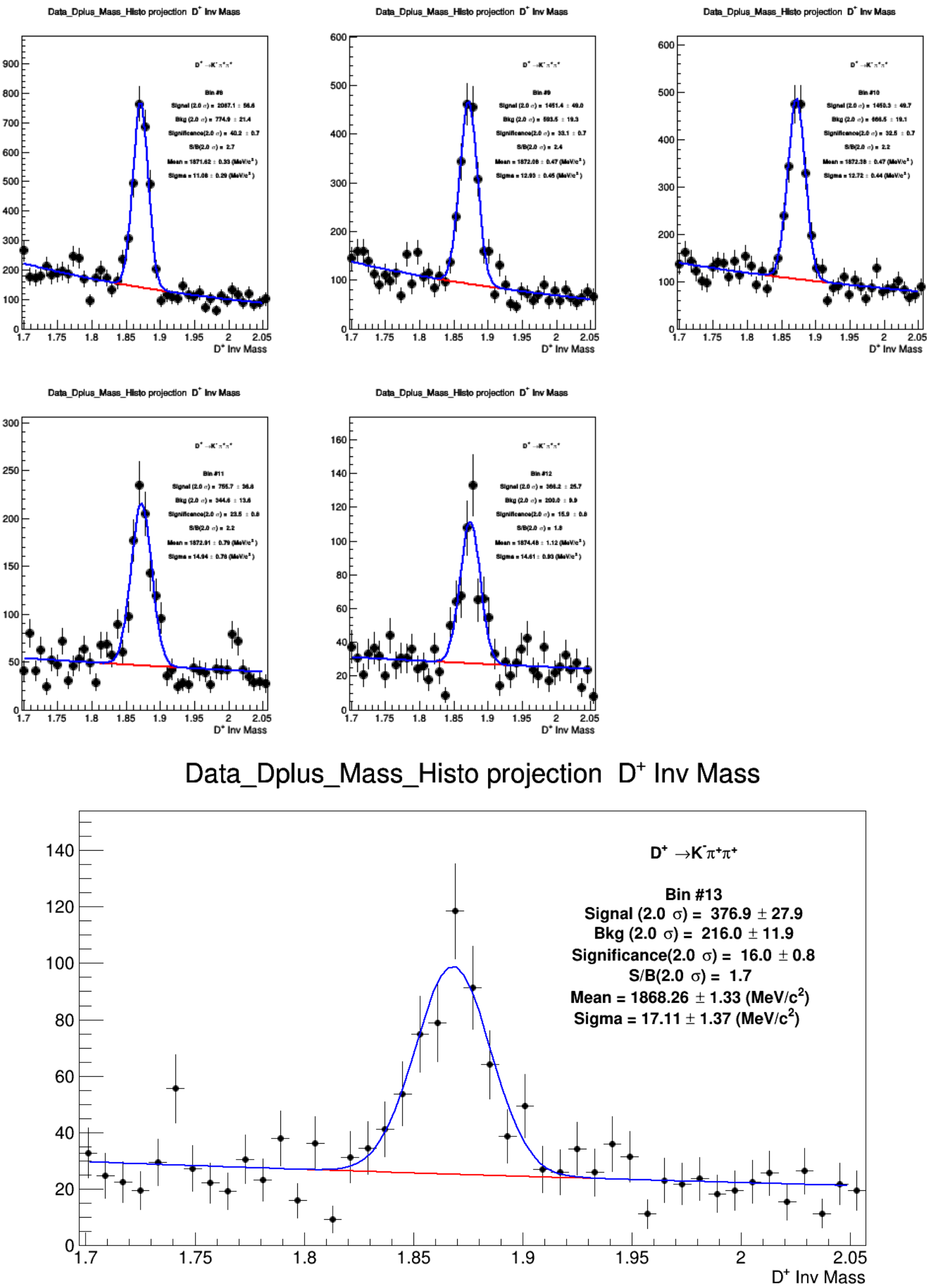

Figure 7: Invariant mass distribution of D^{+} corrected with efficiency in different p_T regions. Top: $8 < p_T^{D} < 10$ GeV$/c$, $10 < p_T^{D} < 12$ GeV$/c$ (middle), $12 < p_T^{D} < 16$ GeV$/c$ (right) and Bottom: $16 < p_T^{D} < 24$ GeV$/c$.

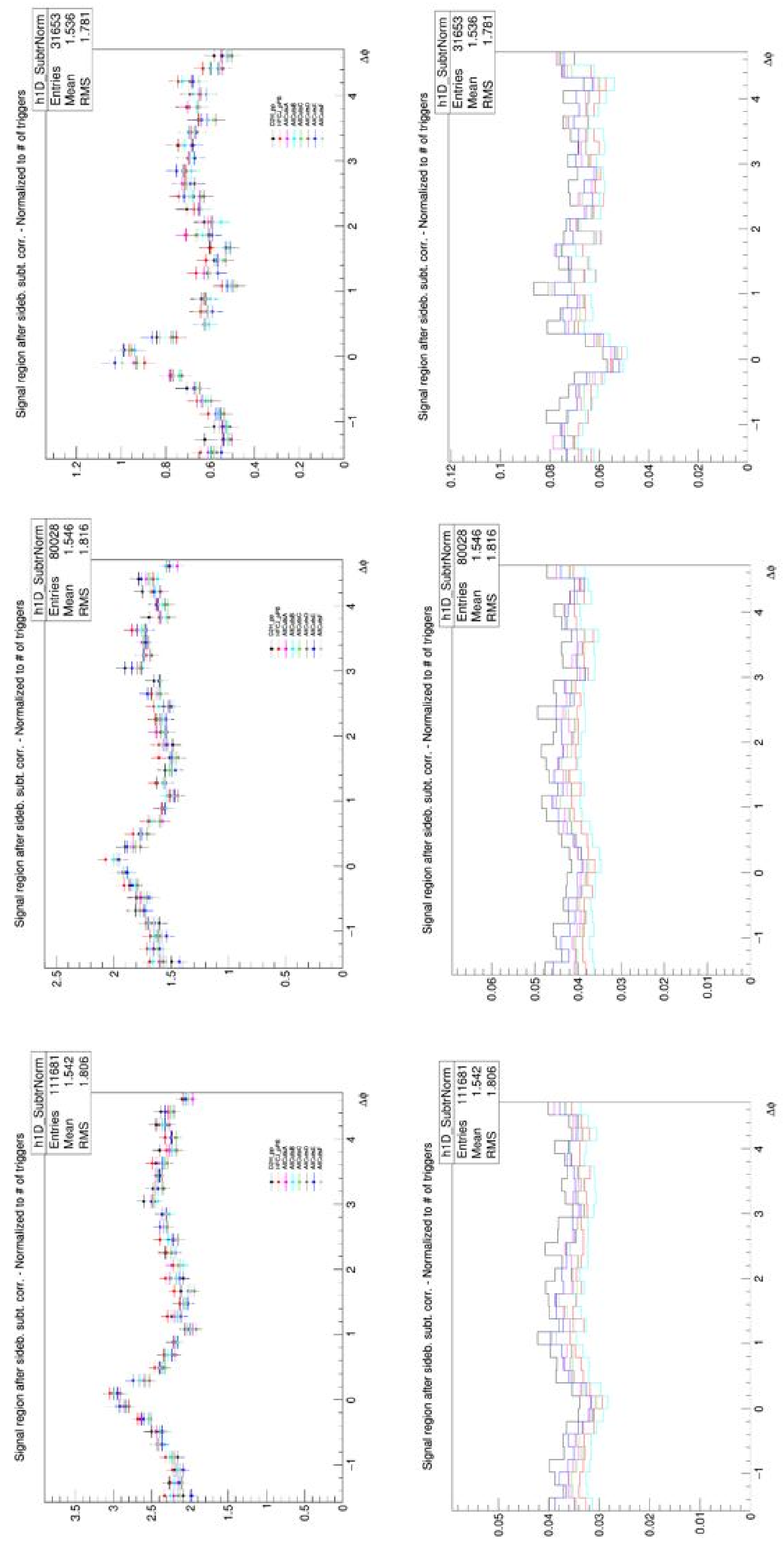

Figure 8: D^0-h correlation distributions with different cut options (top) and point-by-point relative statistical uncertainty (bottom) for $5 < p_T^D < 8\mathrm{GeV}/c$ for associated track $p_T > 0.3\mathrm{GeV}/c$ (left), $03 < p_T < 1\mathrm{GeV}/c$ (middle), $p_T > 1\mathrm{GeV}/c$ (right)

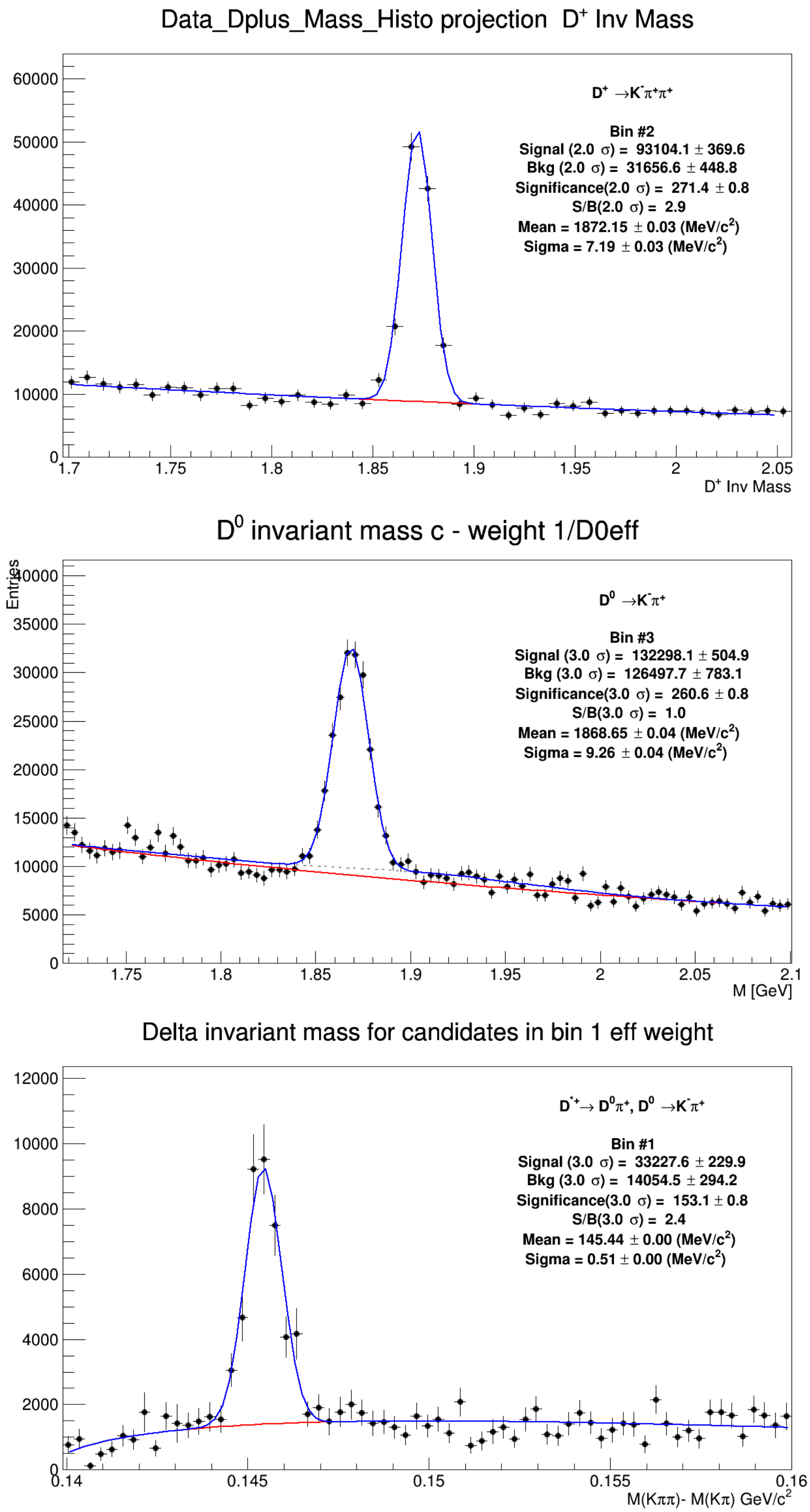

Figure 9: Invariant mass distribution of D^+ (top), D^0 (mid) and D^{*+} (bottom) corrected with efficiency for $2 < p_T^D < 3$.

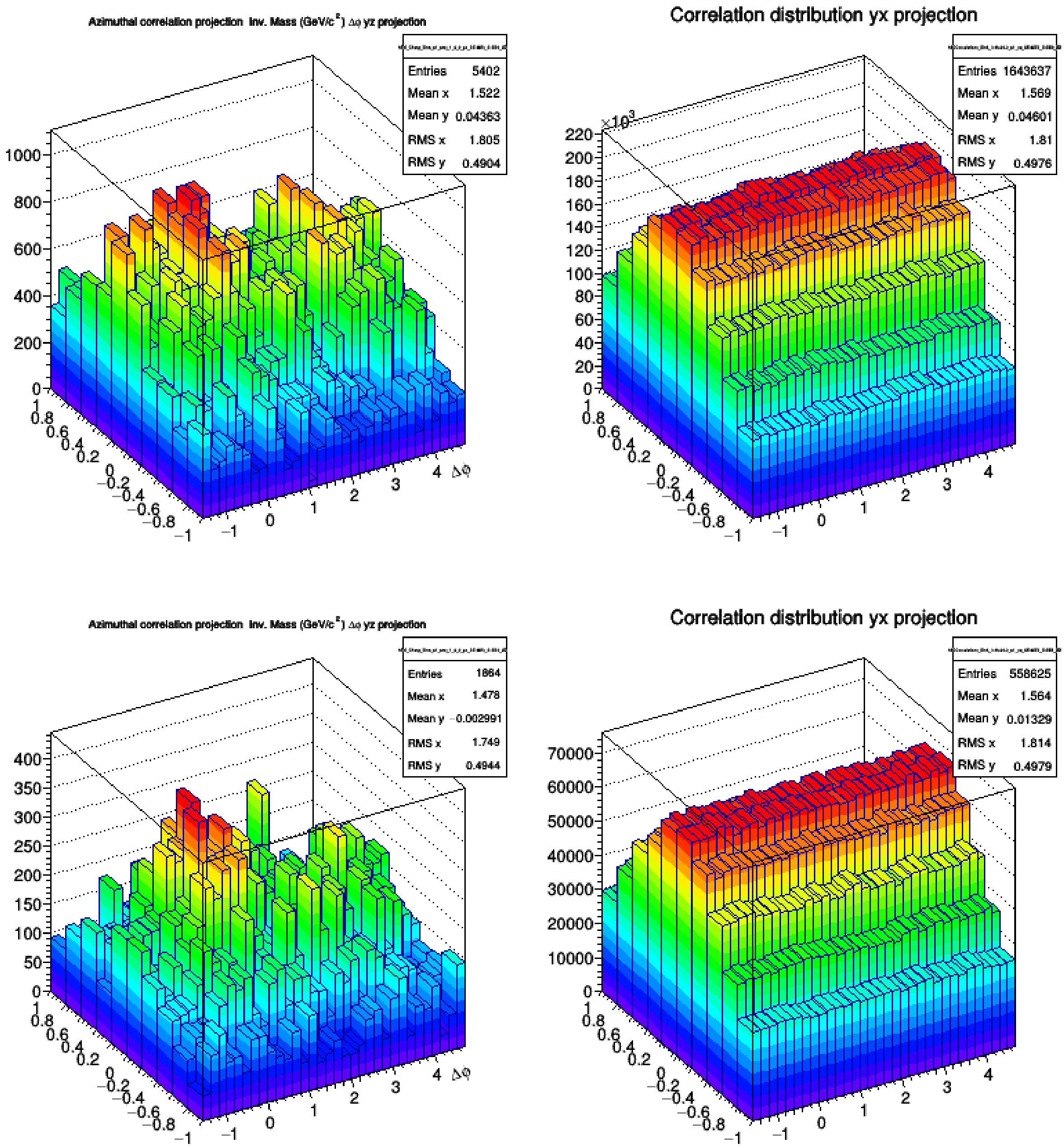

Figure 10: D^{*+} meson $(\Delta\varphi, \Delta\eta)$ correlation for in the signal region (top row) and sidebands (bottom row) from pool1, for Single Event (left) and Mixed Event analysis (center) for high p_T: $3 < p_T < 5$ GeV/c with associated $p_T > 0.3$ GeV/c. The right column shows the SE/ME corrected distributions.

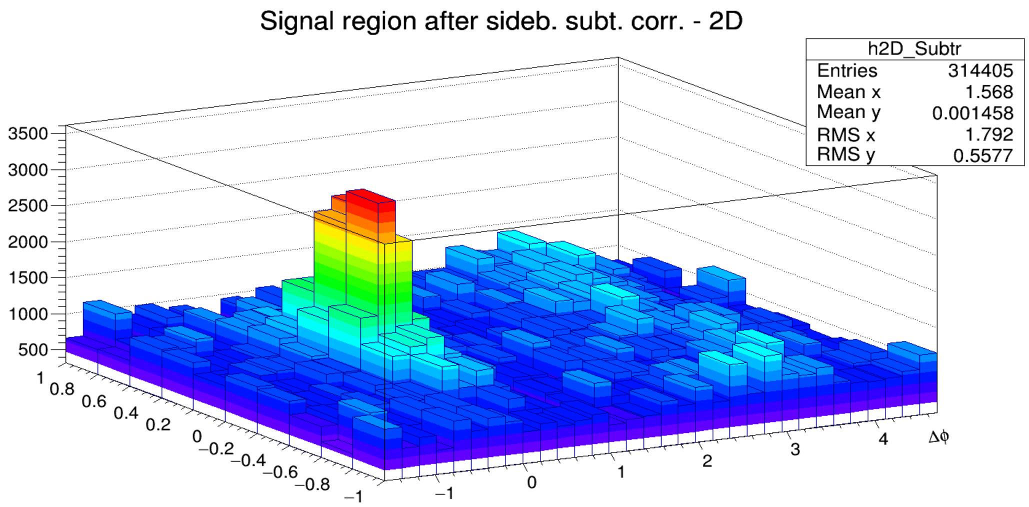

Figure 11: $(\Delta\varphi, \Delta\eta)$ correlation distribution of D^{*+}-h with $8 < p_{\mathrm{T}} < 16$ GeV/c and associated track p_{T} Threshold: $p_{\mathrm{T}} > 0.3$ GeV/c, after the mixed-event correction.

3.3.2 Tracking and D-meson trigger efficiency

(i) Tracking efficiency - The tracking efficiency was calculated by obtaining the ratio between the yield at the reconstructed level and generated level, for a defined "type" of particles (in our case non-identified particles) and it is estimated differentially in p_T, η, and z_{vtx} of the charged particles.

Tracking efficiency maps were produced as TH3D histograms (p_T, η, z_{vtx}) obtained from MC analysis on the minimum-bias samples LHC17l3b_fast and LHC17l3b_cent_woSDD anchored to LHC17p,q data samples, considering only primary pions, kaons, protons, electrons and muons, and applying at reconstructed level the track selections (summarized in Table 2). These efficiency maps were used in the analysis tasks to extract single track efficiencies; each correlation pairs found in the data analysis was inserted in correlation plots with a weight of **1/efficiency value**. The 1D (p_{T} dependence) tracking efficiency for all the five species as well as the tracking efficiency specie by specie are shown in Fig. 12.

Details of cuts at event level and particle/track selection at different steps are listed in Table 2 .

MC Generated	
Stages	Cuts
1.MC Part with Generated Cuts	**After Event Selection** Charge PDG Code Physical Primary
2. MC Part with Kine Cuts	**Kinematics Cuts** $-0.8<\eta<0.8$ $p_{\mathrm{T}} > 0.3$ (GeV/c)
MC Reconstructed	
4. Reco tracks	**After Event Selection** Physical Primary
5. Reco tracks with Kine Cuts	**Kinematics Cuts** $-0.8<\eta<0.8$ $p_{\mathrm{T}} > 0.3$ (GeV/c)
6. MC true with Quality Cuts	**Quality Cuts** SetRequireSigmaToVertex(kFALSE) SetDCAToVertex2D(kFALSE) SetMinNCrossedRowsTPC(70) SetMinRatioCrossedRowsOverFindableClustersTPC(0.8) SetMinNClustersITS(2) SetMaxChi2PerClusterTPC(4) SetMaxDCAToVertexZ(1) SetMaxDCAToVertexXY(1) SetRequireTPCRefit(TRUE) SetRequireITSRefit(FALSE)
7. Reco tracks with Quality Cuts	**Same as step 6**

Table 2: The list of event and particle/track selection cuts used in the estimation of single track efficiency

(ii) D meson efficiency - Due to limited statistics, the correlation analysis is performed in quite wide p_{T} bins and in each of them the reconstruction and selection efficiency of D mesons is not flat, in particular in the lower p_{T} region. We correct for the p_{T} dependence of the trigger efficiency within each $\mathrm{p_T}$-bin.

This correction is applied online, by using a map of D meson efficiency as a function of p_{T} and event multiplicity (in terms of SPD tracklets in $|\eta| < 1$) extracted from the enriched Monte Carlo sample LHC18a4a2_fast. The η dependence was neglected due to the statistics of the available Monte Carlo sample, which rule out the possibility of performing a 3D study.

To properly count the number of trigger particles used to normalize the correlation distributions, N_{trig}, each D meson is weighted with the inverse of its efficiency in the invariant mass distribution. The main role of the correction for the D meson efficiency is to account for the p_{T} dependence of the correlation distribution within a given D meson p_{T} interval. Indeed, only the p_{T} shape of the D meson efficiency within the correlation $p_{\mathrm{T}}^{\mathrm{trig}}$ ranges is relevant while the average value in the p_{T} range is simplified due to the normalization of the correlation distribution to the number of trigger particles.

Efficiency plots for D^0, D^+ and D^{*+} mesons are shown in Figs. 13 and 14, for prompt and feed-down D mesons, respectively.

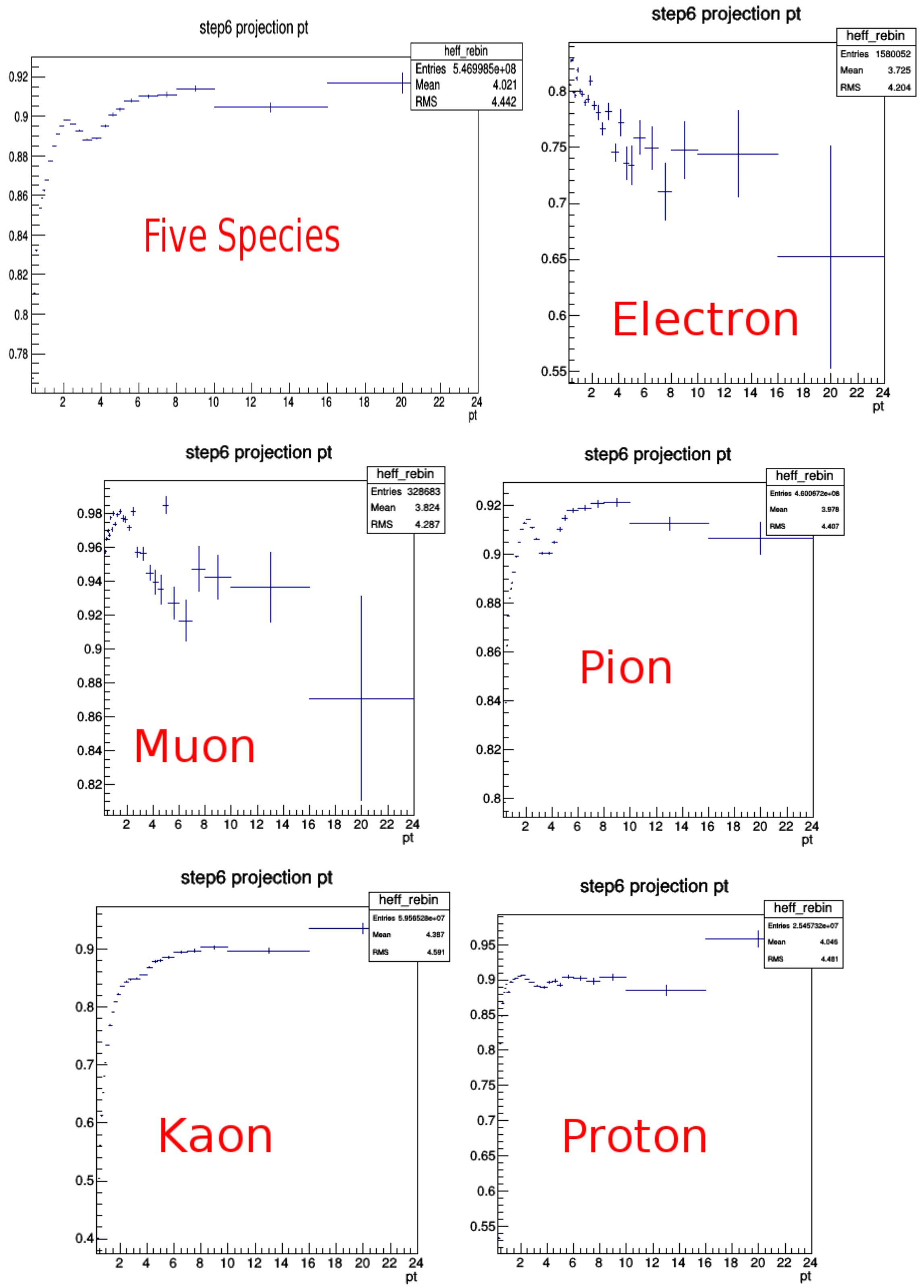

Figure 12: 1D (vs p_{T}) tracking efficiency map for standard track selection, evaluated for five species (electron, muon, pion, kaon and proton) and also different species using data sample LHC17l3b_fast.

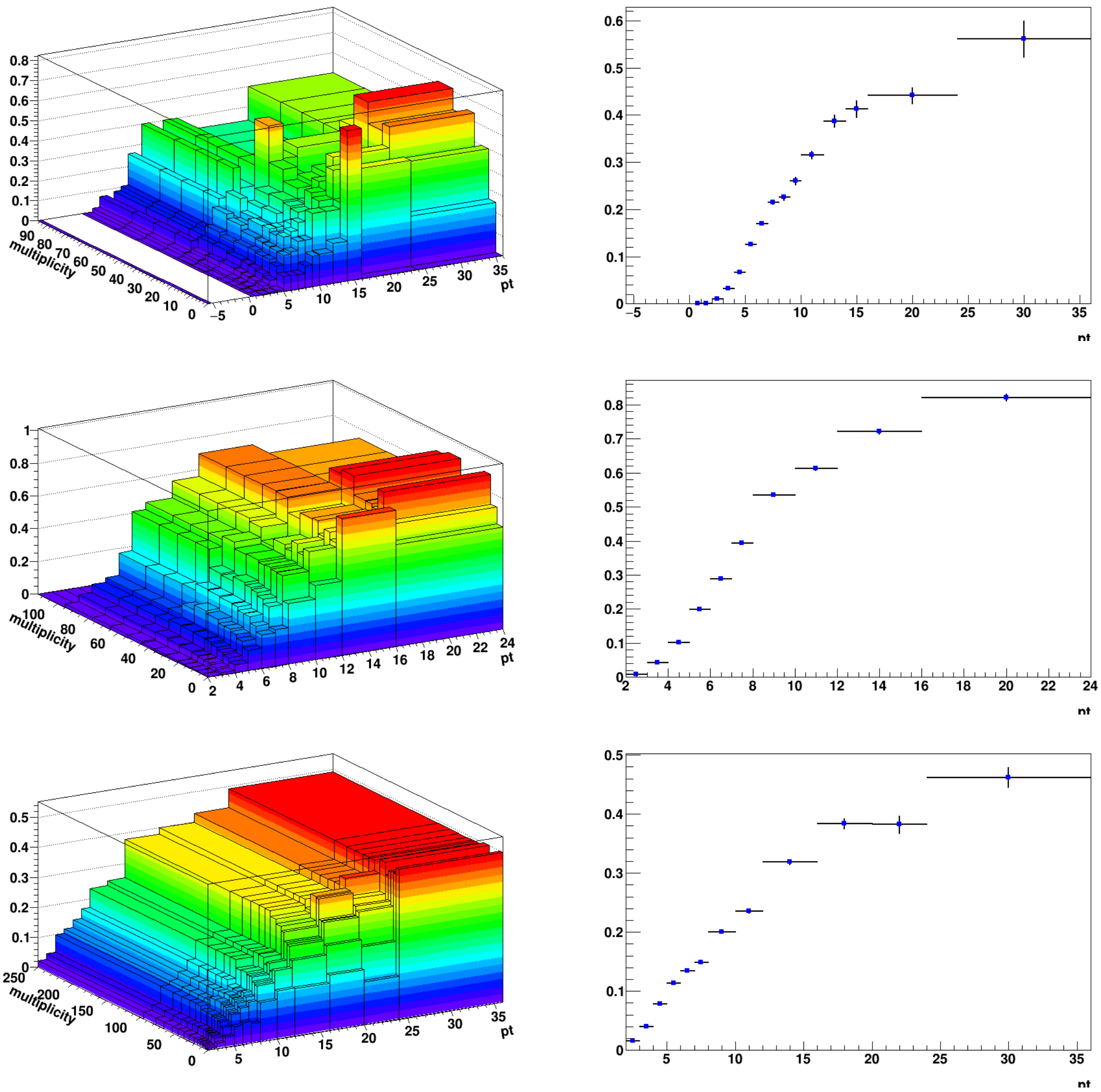

Figure 13: Top panel: (p_T, multiplicity) dependence (left) and p_T dependence (right) of prompt D^+ meson efficiency. Mid panel: (p_T, multiplicity) dependence (left) and p_T dependence (right) of prompt D^{*+} meson efficiency. Bottom panel: (p_T, multiplicity) dependence (left) and p_T dependence (right) of prompt D^0 meson efficiency.

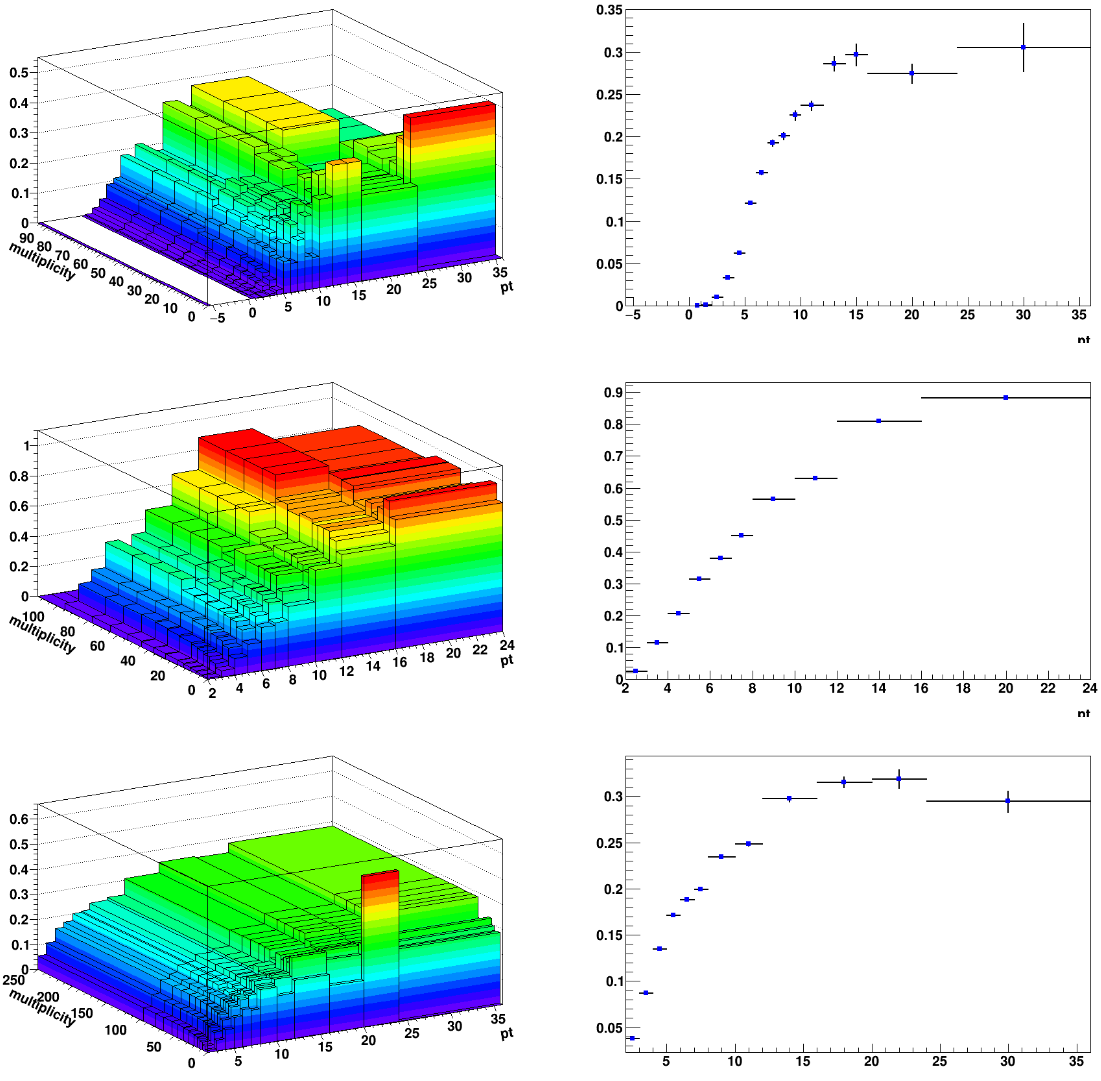

Figure 14: Top panel: (p_{T}, multiplicity) dependence (left) and p_{T} dependence (right) of feed-down D^{+} meson efficiency. Mid panel: (p_{T}, multiplicity) dependence (left) and p_{T} dependence (right) of feed-down D^{*+} meson efficiency. Bottom panel: (p_{T}, multiplicity) dependence (left) and p_{T} dependence (right) of feed-down D^{0} meson efficiency.

3.3.3 Correction for bias on B to D decay topologies

To verify the consistency of the analysis chain and of the corrections applied to the correlation distributions extracted from data, a Monte Carlo closure test was setup and tried on the D^0-h analysis.

On the Monte Carlo enriched with charm and beauty quarks (LHC18a4a2_fast, with GEANT3), the correlation analysis was performed both at kinematic level and at reconstructed level. At kinematic level, only acceptance cuts were applied on the D mesons and the associated particles, using the Monte Carlo information for the identification of the D mesons and the hadrons in the event and rejecting the non-primary particles. At reconstructed level, the analysis was performed as if it were executed on data, applying the event selection, the acceptance cuts for D mesons and the associated particles, selecting the D meson candidates with filtering cuts on their daughters, topological cuts and PID selection, and then keeping only the true D mesons by matching with the Monte Carlo truth; non-primary particles were rejected by means of the DCA selection. Event mixing correction was applied both at reconstructed and at kinematic level, where it takes into account just the effects of the acceptance cuts. In addition, at reconstructed level, the efficiency corrections for D mesons and associated tracks were also applied.

The consistency check was performed to verify whether, after having applied all the corrections to the azimuthal correlation plots at reconstructed level, the results were compatible with the ones at kinematic level. Hence, the ratios of fully corrected reconstructed plots over kinematic plots were evaluated in all the D^0 p_T bins and for the various p_T thresholds for the associated tracks, separating the contributions for the different origins of particles and triggers. The ratios, shown in Figure 15 for exemplary kinematic regions (covering anyway the full span of the measurement), denote a good compatibility with 1, within the uncertainties, of the average reconstructed over generated ratios, in particular for the all D-non HF track case (blue curves), apart from small downward deviations at low p_T, which will be cured with a 2-3% asymmetric systematic uncertainty, as also previously done in the pp 2010 and p–Pnb 2013 analyses.

The major exceptions to the previous conclusion are clearly the structures in the near side region for the beauty origin case. It was verified that these structures are induced by our topological selection for the D mesons. Indeed, in cases in which the D meson triggers come from B hadrons, applying the topological cuts (especially the cosine of the pointing angle) tends to favour cases with a small angular opening between the products of the B hadron decay (i.e. the D meson trigger itself and other particles), with respect to cases where the B decay particles are less collinear.

In the Monte Carlo closure test, this situation is reflected in the correlation distributions at reconstructed level, where the topological selection is applied, while it does not occur at kinematic level. Hence, in the reconstructed/kinematic ratio, the distribution would show an excess for $\Delta\varphi = 0$ (due to the favoured decays with small opening angle), which is then compensated by a depletion for larger values of $\Delta\varphi = 0$ (corresponding to B decays with larger angles, which are disfavoured). These structures are prominent at low D^0 p_T, where the topological cuts are tighter, and tend to disappear at higher p_T, where the selections are released. They are also larger in the higher associated track p_T ranges, where the fraction of B-hadron decay tracks dominate the overall correlation distributions.

The data correlation distribution need to be corrected for this bias, and in particular for the enhancement of b-origin correlation pairs at the centre of the near side region, which would influence the near-side peak features. In order to do this, the amount of the b-origin excess is evaluated from the Reco/Kine ratio, by considering the b-D^0-all tracks case (dark green points). The excess at Reco level (affecting data) is quantified as a $\Delta\varphi$ modulation **modul** for the five points an each side of the $\Delta\varphi = 0$ value (or, equivalently, on the first five points of the reflected distributions, which start from $\Delta\varphi = 0$. This is done separately in each p_T range. Then, the correction is done by applying this modulation to the data correlation distributions, but taking into account that only the correlation entries from B$\rightarrow$D are affected, while the c$\rightarrow$D correlations need to be left unaltered. In particular, it has to be considered that:

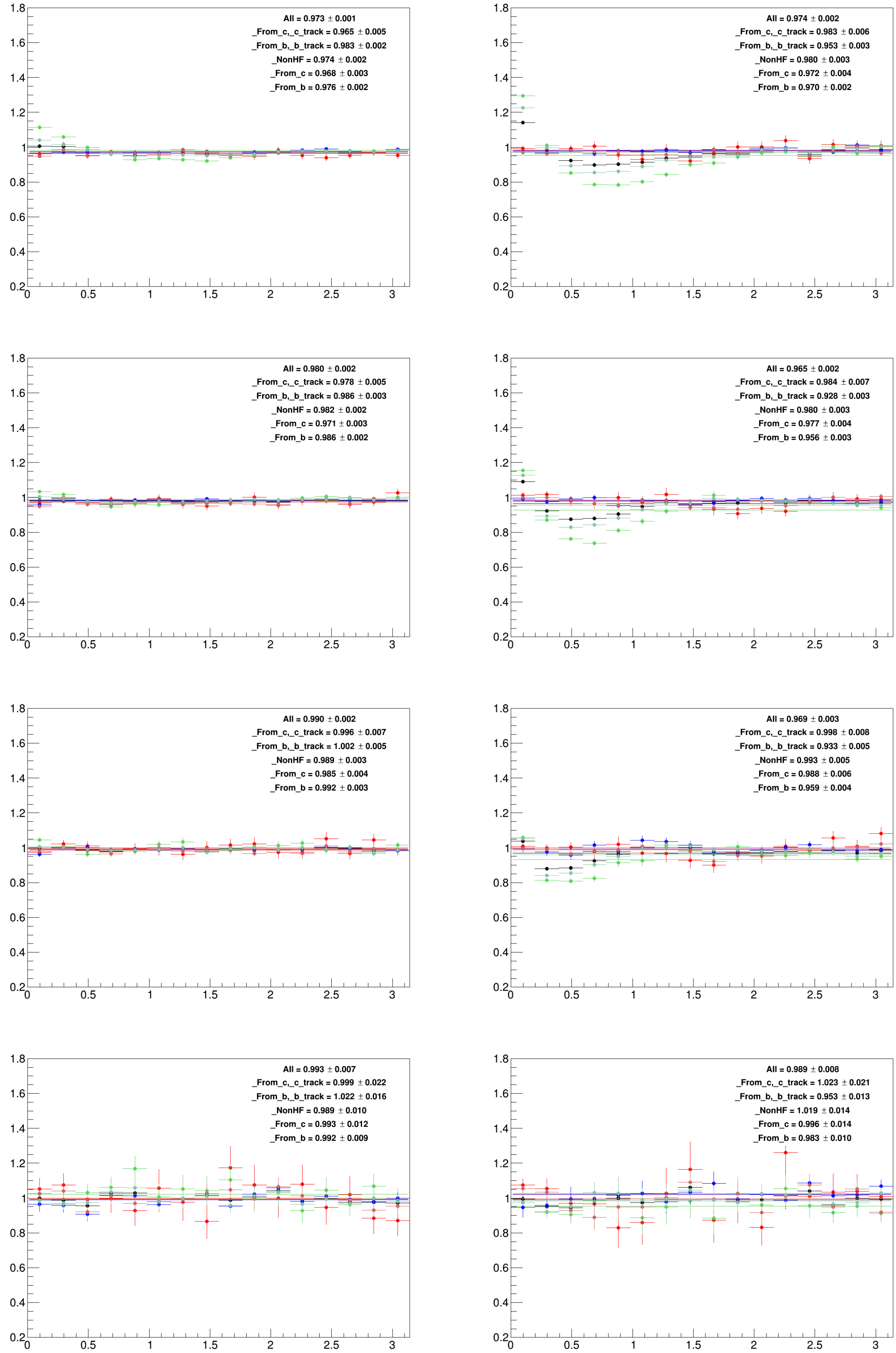
All = 0.973 ± 0.001
_From_c,_c_track = 0.965 ± 0.005
_From_b,_b_track = 0.983 ± 0.002
_NonHF = 0.974 ± 0.002
_From_c = 0.968 ± 0.003
_From_b = 0.976 ± 0.002
All = 0.974 ± 0.002
_From_c,_c_track = 0.983 ± 0.006
_From_b,_b_track = 0.953 ± 0.003
_NonHF = 0.980 ± 0.003
_From_c = 0.972 ± 0.004
_From_b = 0.970 ± 0.002
All = 0.980 ± 0.002
_From_c,_c_track = 0.978 ± 0.005
_From_b,_b_track = 0.986 ± 0.003
_NonHF = 0.982 ± 0.002
_From_c = 0.971 ± 0.003
_From_b = 0.986 ± 0.002
All = 0.965 ± 0.002
_From_c,_c_track = 0.984 ± 0.007
_From_b,_b_track = 0.928 ± 0.003
_NonHF = 0.980 ± 0.003
_From_c = 0.977 ± 0.004
_From_b = 0.956 ± 0.003
All = 0.990 ± 0.002
_From_c,_c_track = 0.996 ± 0.007
_From_b,_b_track = 1.002 ± 0.005
_NonHF = 0.989 ± 0.003
_From_c = 0.985 ± 0.004
_From_b = 0.992 ± 0.003
All = 0.969 ± 0.003
_From_c,_c_track = 0.998 ± 0.008
_From_b,_b_track = 0.933 ± 0.005
_NonHF = 0.993 ± 0.005
_From_c = 0.988 ± 0.006
_From_b = 0.959 ± 0.004
All = 0.993 ± 0.007
_From_c,_c_track = 0.999 ± 0.022
_From_b,_b_track = 1.022 ± 0.016
_NonHF = 0.989 ± 0.010
_From_c = 0.993 ± 0.012
_From_b = 0.992 ± 0.009
All = 0.989 ± 0.008
_From_c,_c_track = 1.023 ± 0.021
_From_b,_b_track = 0.953 ± 0.013
_NonHF = 1.019 ± 0.014
_From_c = 0.996 ± 0.014
_From_b = 0.983 ± 0.010

Figure 15: Ratios of fully corrected azimuthal correlation plots at reconstructed level over azimuthal correlation plots at kinematic level, in the two D^0 p_T bins, for the different associated p_T ranges. Black points: All D^0-all hadrons, normalized by all D^0 triggers; light red points: D^0 from c-hadrons from c, normalized by c-D^0 triggers; dark red points: D^0 from c-all hadrons, normalized by c-D^0 triggers; light green points: D^0 from b-hadrons from b, normalized by b-D^0 triggers; dark green points: D^0 from b-all hadrons, normalized by b-D^0 triggers; blue points: All D^0-hadrons from light quarks, normalized by all D^0 triggers. The panels show the ranges: $3 < p_T$(D)$<$ 5 GeV/c , $0.3 < p_T$(assoc)$<$ 1 GeV/c (1st row-left); $3 < p_T$(D)$<$ 5 GeV/c , p_T(assoc)$>$ 1 GeV/c (1st row-right); $5 < p_T$(D)$<$ 8 GeV/c , $0.3 < p_T$(assoc)$<$ 1 GeV/c (2nd row-left); $5 < p_T$(D)$<$ 8 GeV/c , p_T(assoc)$>$ 1 GeV/c (2nd row-right); $8 < p_T$(D)$<$ 16 GeV/c , $0.3 < p_T$(assoc)$<$ 1 GeV/c (3rd row-left), $8 < p_T$(D)$<$ 16 GeV/c , p_T(assoc)$>$ 1 GeV/c (3rd row-right); $16 < p_T$(D)$<$ 24 GeV/c , $0.3 < p_T$(assoc)$<$ 1 GeV/c (4th row-left), $16 < p_T$(D)$<$ 24 GeV/c , p_T(assoc)$>$ 1 GeV/c (4th row-right).

– On data, the B$\rightarrow$D correlation pairs are only a fraction (1-f_{prompt}) of the total.

– The amplitude of B$\rightarrow$D$|_{\text{amplit}}$ correlation pattern is different (greater) than the amplitude of the c$\rightarrow$D$|_{\text{amplit}}$ correlation pattern:

Thus, the following equation is applied to get the corrected $C(\Delta\varphi)_{\text{corr}}$ data points starting from the raw ones, $C(\Delta\varphi)_{\text{raw}}$:

$$C(\Delta\varphi)_{\text{corr}} = C(\Delta\varphi)_{\text{raw}} \cdot [\frac{\mathrm{c} \rightarrow \mathrm{D}|_{\text{amplit}}}{(\mathrm{B}+\mathrm{c}) \rightarrow \mathrm{D}|_{\text{amplit}}} \cdot f_{\text{prompt}} + \frac{\mathrm{B} \rightarrow \mathrm{D}|_{\text{amplit}}}{(\mathrm{B}+\mathrm{c}) \rightarrow \mathrm{D}|_{\text{amplit}}} \cdot (1 - f_{\text{prompt}}) \cdot \frac{1}{\textbf{modul}}] \quad (3)$$

where $(\mathrm{B}+\mathrm{c}) \rightarrow \mathrm{D}|_{\text{amplit}} = \mathrm{c} \rightarrow \mathrm{D}|_{\text{amplit}} \cdot f_{\text{prompt}} + \mathrm{B} \rightarrow \mathrm{D}|_{\text{amplit}} \cdot (1 - f_{\text{prompt}})$, and where the two amplitudes are evaluated from the Monte Carlo distributions at reconstructed level (so, including the bias), and f_{prompt} with the procedure described in 3.3.5. Applying the **modul** factor to the beauty part of the data correlation distributions brings its value back to the generated level case, effectively removing the bias. The effect of the correction is a shift of the data points in the near-side region (in general, downward in the first and second points, the upward in the others). The maximum value of the shift is of about 5%, at the centre of the near-side peak, for the lowest D-meson p_T range ($3 < p_T < 5$ GeV/c) and the highest associated track p_T range ($p_T > 3$ GeV/c). The typical values are instead of a couple of percentage points. The correction is zero in the highest D-meson p_T range. To take into account for possible inaccuracies in the definition of the modulations, or in their rescaling, a systematic uncertainty is applied on the corrected data points, with value $|C(\Delta\varphi)_{\text{corr}} - C(\Delta\varphi)_{\text{raw}}|/\sqrt{(}12)$, on each side of the data points affected by the bias (symmetric uncertainty).

3.3.4 Secondary track contamination

The secondary tracks inside the associated track sample, due to interaction of primary track with the detector material or to decays of strange hadrons, are mostly removed by the DCA cuts applied during the cut selection phase (DCA(xy) < 1 cm, DCA(z) < 1 cm). Anyway, a small fraction of secondary tracks survives this cut, and the data correlation distributions have to be corrected for this residual contamination. The fraction of surviving secondary tracks is evaluated via a study on the LHC18a4a2_fast sample, by counting the number of tracks accepted by the selection whose corresponding generated-level track doesn't satisfy the IsPhysicalPrimary() call, and dividing this number by the total number of accepted tracks. The outcome of the check is reported in Figure 16. As it's visible, no more than about 4.5% secondary tracks pass the selection (6% in the lowest associated p_{T} range). Moreover, the fraction of residual secondary tracks is rather flattish along the $\Delta\varphi$ axis, as shown, for exemplary p_{T} regions, in Figure 17, where the inhomogeneities are generally not larger than about 1%. Anyway, to take into account these modulations, which vary from bin to bin, the purity correction was performed differentially though the azimuthal axis (i.e. applied bin-per-bin on the azimuthal correlation distributions). In addition, this was important to consider since though these structures are small, they could be amplified after the subtraction of the baseline, when going to the yield evaluation.

In particular, three approaches were tried, by multiplying the data correlation distribution in each kinematic range by:

- the MC primary/inclusive histogram (blue histogram in Fig. 17)
- a polynomial fit applied to the MC primary/inclusive histogram (red curve in Fig. 17)
- a moving average, considering 3 points, of the MC primary/inclusive histogram (red histogram in Fig. 17)

Each approach has pros and cons, since directly using the primary/inclusive histogram gives a correction strongly dependent on the statistical fluctuations, while using the fit or the moving average smoothen the fluctuation, but also the structures with a physical origin (and the fit misses a periodicity condition). For this reason, a comparison of the outcome of the correction after applying either of the approaches (and the old 'flat' correction approach) was performed, which gave full compatibility (within less than 1%) of the correlation distributions corrected with either approach. The moving average approach was chosen as standard correction procedure.

It was also verified with the same Monte Carlo study that applying the DCA selection rejects less than 1% primary tracks (tagged as false positives) from the associated track sample, and less than 1% of heavy-flavour origined tracks, again with a flattish azimuthal distribution, inducing hence a fully negligible bias on the data correlation distributions. This is shown in Figure 18. This was also verified for specific charm-origin and beauty-origin tracks, due to their larger DCA with respect to primary tracks from light quarks. In this case, the fraction of rejected charm and beauty tracks stays below 1% in all the kinematic ranges apart from the associated track p_{T} regions 0.3-1 and > 0.3 GeV/c , where the rejection can be as high as 2%. In these kinematic ranges, though, the data correlation distributions are dominated by non-heavy-flavour tracks, as it was verified from the simulations, hence the overall bias is still contained below 1%, thus negligible.

These studies were performed on an enriched Monte Carlo sample, which could not fully reproduce the relative abundances of the species. Anyway, for events with a reconstructed D-meson, this bias is expected to be minor, and only these events are used in the data analysis. In any case, the percentages obtained from the study were found to be consistent within 1%.

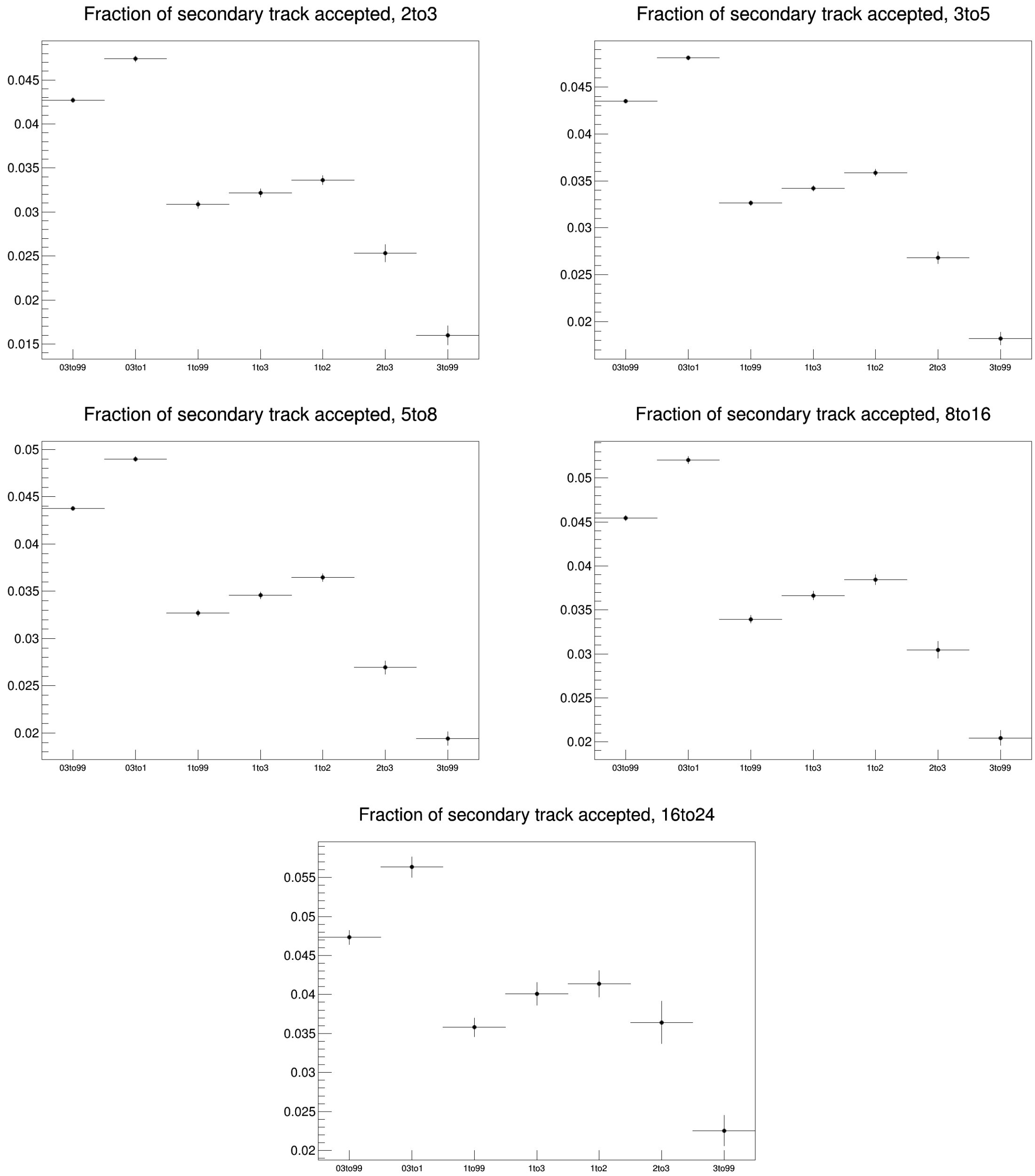

Figure 16: Fraction of secondary tracks over total amount of tracks which pass the DCA selection. The four panel show the fractions for the D-meson p_{T} ranges: 2-3, 3-5, 5-8, 8-16, 16-24, respectively. Inside each panel, the associated track p_{T} ranges are shown on the x-axis.

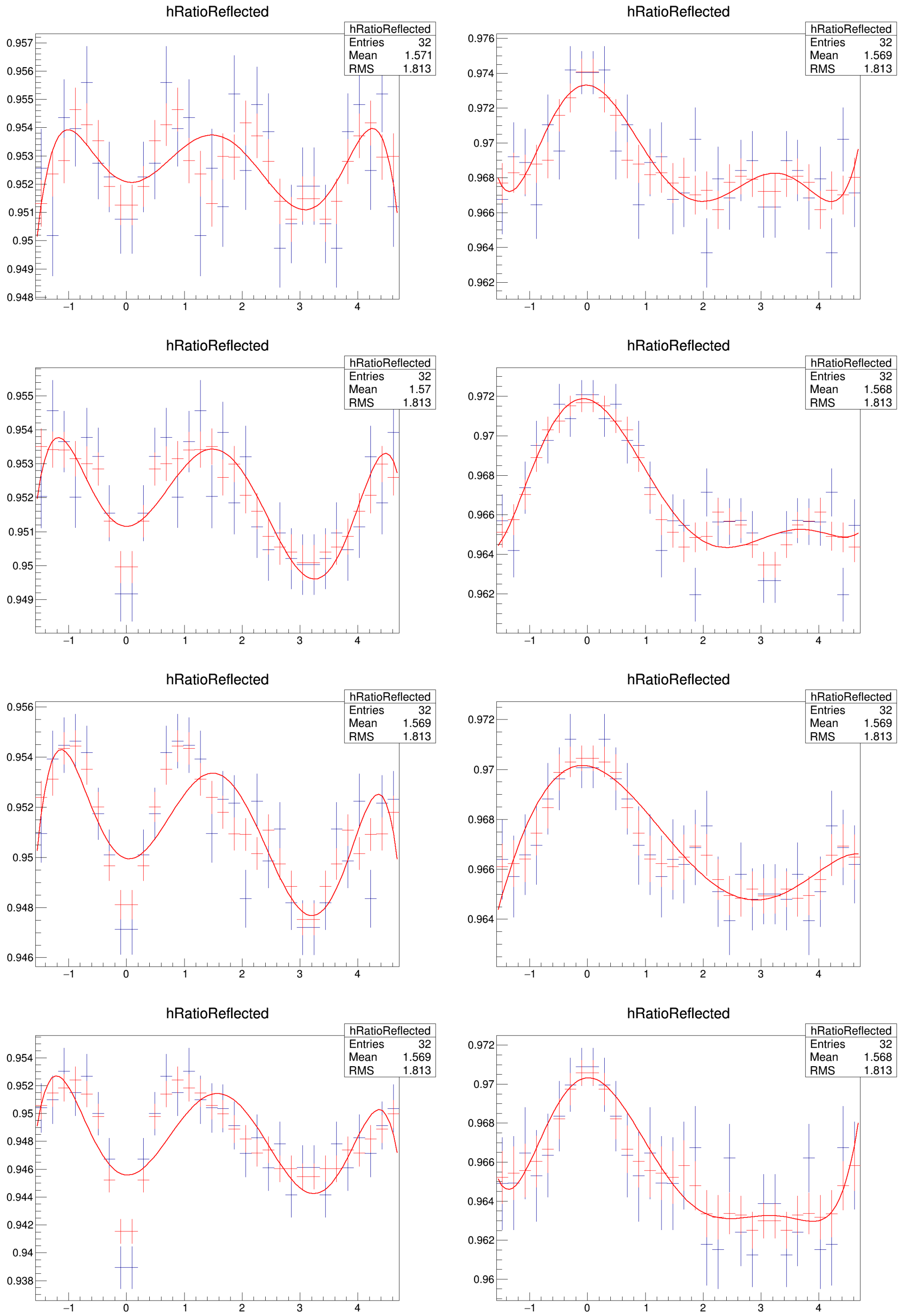

Figure 17: Fraction of primary track in the reconstructed associated track sample (blue histogram). The polynomial fit function (red curve) and the 3-point moving average (red histogram) are also superimposed. The p_{T}(D) ranges are 2-3, 3-5, 5-8, 8-16 GeV/c, respectively for each row, and $0.3 < p_{\mathrm{T}}(\mathrm{assoc}) < 1$, $p_{\mathrm{T}}(\mathrm{assoc}) > 1$ GeV/c inside each row.

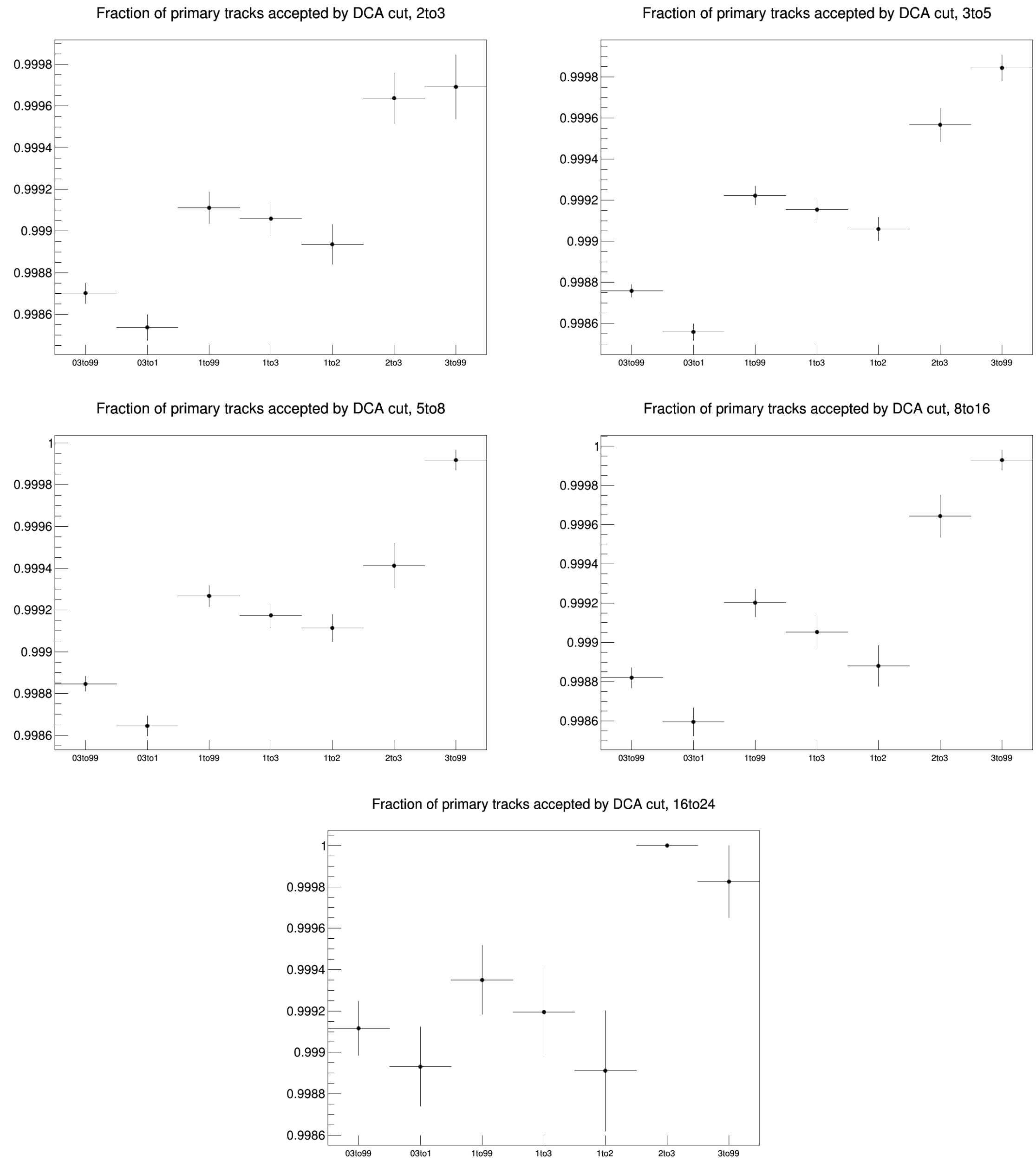

Figure 18: Fraction of primary tracks rejected by the DCA selection. The four panel show the fractions for the D-meson p_{T} ranges:2-3, 3-5, 5-8, 8-16, 16-24, respectively. Inside each panel, the associated track p_{T} ranges are shown on the x-axis.

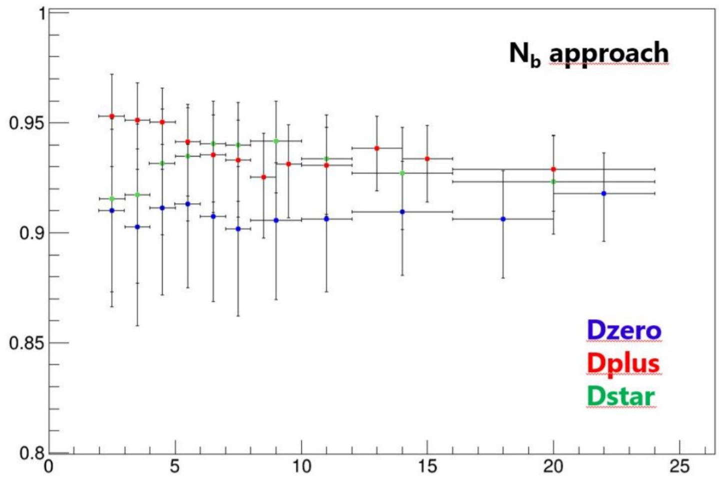

Figure 19: f_{prompt} as a function of the p_{T} for D^0, D^{*+} and D^+ estimated on the basis of FONLL predictions

3.3.5 *Beauty feed-down*

The contribution of correlations of D meson from b-hadron decay is subtracted from the data correlation distributions as:

$$\tilde{C}_{\mathrm{prompt\ D}}(\Delta\varphi) = \frac{1}{f_{\mathrm{prompt}}}\left(\tilde{C}_{\mathrm{inclusive}}(\Delta\varphi) - (1 - f_{\mathrm{prompt}})\tilde{C}^{\mathrm{MC\ templ}}_{\mathrm{feed-down}}(\Delta\varphi)\right). \tag{4}$$

In the above equation, $\tilde{C}_{\mathrm{inclusive}}(\Delta\varphi)$ and $\tilde{C}_{\mathrm{prompt\ D}}(\Delta\varphi)$ are per-trigger azimuthal correlation distributions before and after feed-down contribution subtraction, f_{prompt} is the fraction of prompt D meson and $\tilde{C}^{\mathrm{MC\ templ}}_{\mathrm{feed-down}}$ is a template of the azimuthal correlation distribution for the feed-down component obtained from home-made Monte Carlo simulation at generated level, using PYTHIA6 with Perugia2011 tune. In order to avoid biases related to the different event multiplicity in real and simulated events, the correlation distribution was shifted to have its minimum coinciding with the baseline of the data azimuthal-correlation distribution before feed-down subtraction. More details on the procedure can be found in [8].

The value of f_{prompt} (Figure 19), which depends on D-meson species and varies as a function of the p_{T}, is estimated on the basis of FONLL predictions for the production of feed-down D mesons at central rapidity, in pp collisions at $\sqrt{(s)} = 5$ TeV, and using the reconstruction efficiency of prompt and feed-down D mesons, following the so-called N_{b} approach defined in [1]. Typical values are about 8-10% for the D^0, about 4-7% for the D^+ and about 5-8% for the D^{*+}, fully consistent with the value obtained for the p–Pb data sample, with rather similar cut selections.

4 Systematic uncertainties on $\Delta\varphi$ correlation distributions

4.1 Uncertainty on S and B extraction

The systematic uncertainty for the D meson yield extraction was determined separately for the three mesons. It was obtained by evaluating the value of the signal candidate from the invariant mass spectra with the following differences with respect to the standard approach:

- Changing the background fit function, for D^0 and D^+ (tried with polynomials of 1st and 2nd order) and for D^{*+} (tried with polynomials of 2nd order and a power function);
- Changing the range in which the signal is extracted from the Gaussian fit;
- Reducing the range of invariant mass axis in which the signal region is defined (and S and B are extracted);
- Rebinning the invariant mass distributions before the fit for D^0 and D^+
- Extracting S and B via integral of the fit functions or B via bin counting and S via integral of the Gaussian function.

Both the value of the yield and the sidebands correlations normalization factor are affected by changing the yield extraction approach, while the rest of the procedure to extract the azimuthal correlation distribution is the same as in the standard analysis. The fully corrected azimuthal correlation plots were evaluated, for each of these approaches, in all D meson p_T bins and for each value of associated tracks p_T threshold. The ratios of the correlation distributions obtained with the standard yield extraction procedure and by differentiating the approach were evaluated. From the average of these ratios, which are found to be flat versus $\Delta\varphi$, a systematic uncertainty can be extracted, which was taken of 1% for $3 < p_T(D) < 16$ GeV/c and of 2% in $16 < p_T(D) < 24$ GeV/c. No dependence versus the associated track p_T was assumed, since from a physics point of view we don't expect a modification of the signal and sideband values to have a dependence of this kind. Figures **??**, show the ratios obtained by the above mentioned procedure for exemplary p_T ranges, which anyway span over the full kinematic ranges analyzed, for D^0-h correlations. Figures **??** and **??** show the same ratios for D^{*+}-h, D^+-h as well.

4.2 Uncertainty on background correlation shape

The systematic uncertainty for the subtraction of the background correlations includes the effects due to a potentially biased description of the background correlation shape, which is evaluated from of the sidebands correlations. In particular, the background correlation shape could present some hidden invariant mass dependence. To estimate this uncertainty, the invariant mass range of the sidebands definitions was varied with respect to the default values. For the D^0 meson, the usual range of the sidebands is 4 to 8 σ from the centre of the peak of the Gaussian fit and it was modified, for both sidebands to:

- inner half (4 to 6 σ from the centre of the peak);
- outer half (6 to 8 σ from the centre of the peak)
- extended to 4 to 10 σ (in case this is possible without exceeding the fitting range of the mass plots)

Slightly different variations, but with the same reasoning, were considered for the D^+ meson.

For the D^{*+} meson, the usual range of sideband in invariant mass spectra is 5 to 10 σ (only on the right side) from the centre of the peak of the Gaussian fit of the invariant mass spectra, and it was modified to:

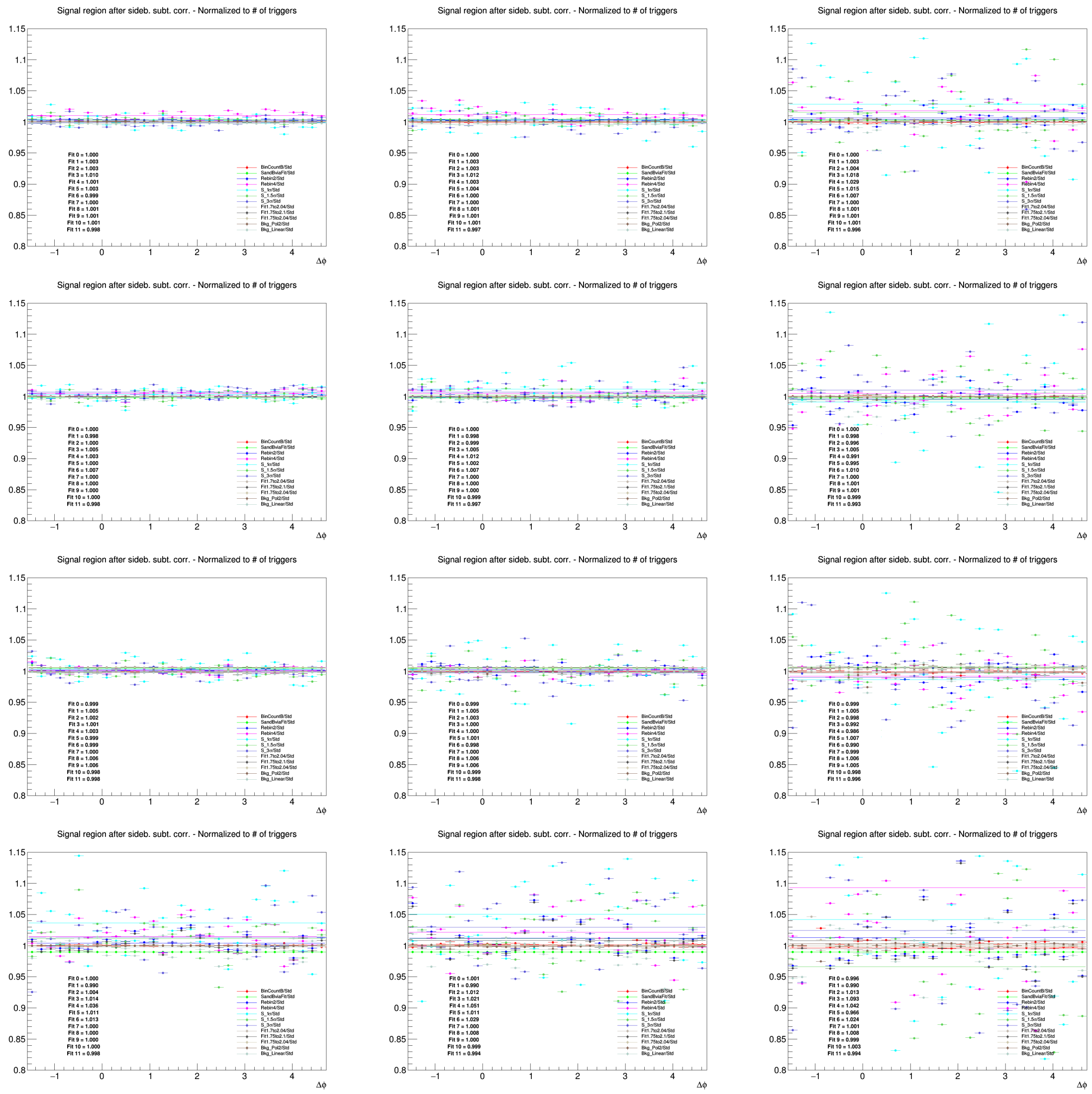

Figure 20: Ratios of D^0-h correlation plots obtained changing S and B extraction procedure over those obtained with standard yield extraction procedure. Rows: $p_T(D^0)$ 3-5, 5-8, 8-16, 16-24 GeV/c. In each row, the panels show the associated track p_T ranges 0.3-1, 1-2, >3 GeV/c, respectively.

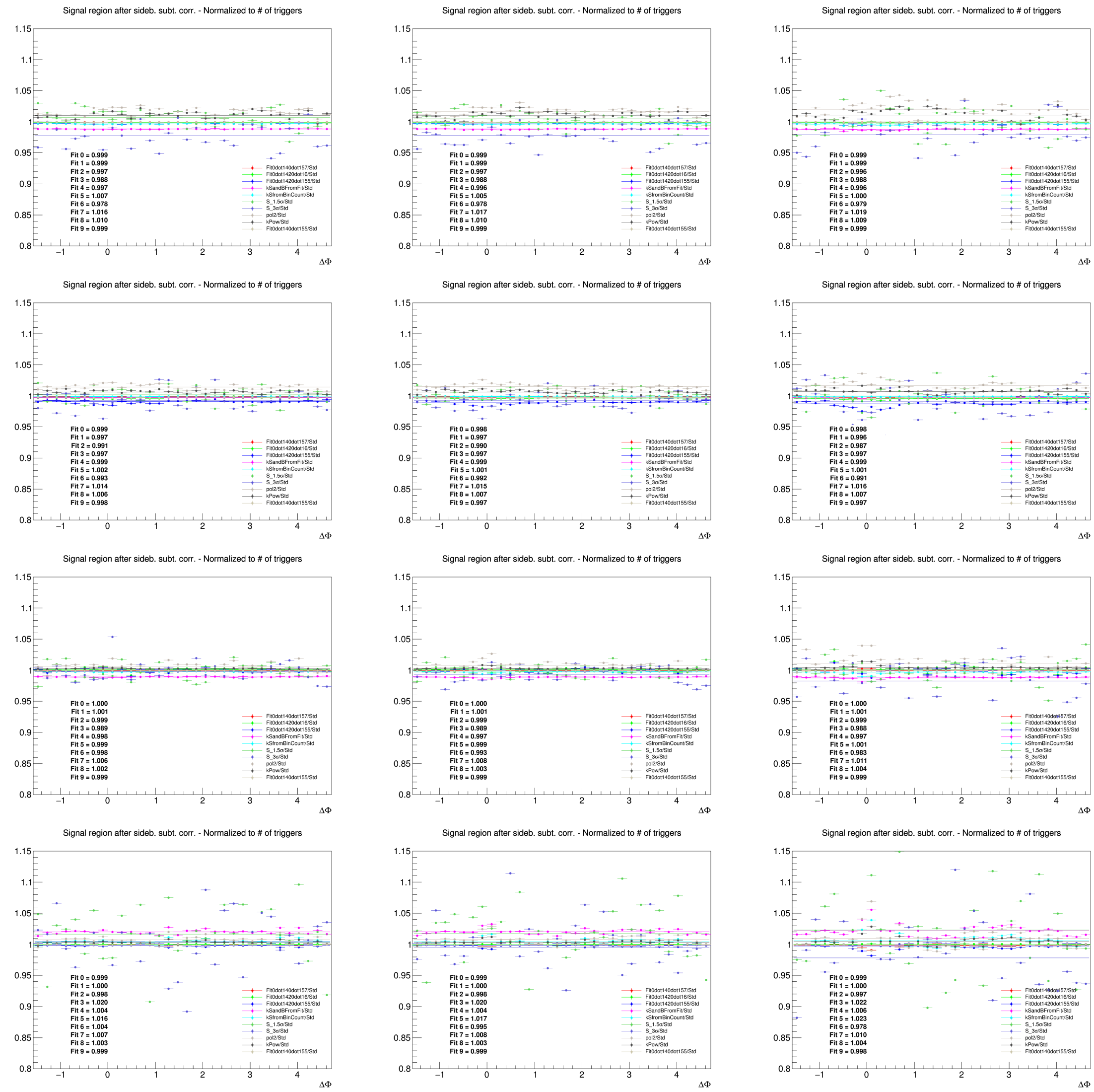

Figure 21: Ratios of D^{*+}-h correlation plots obtained changing S and B extraction procedure over those obtained with standard yield extraction procedure. Rows: $p_T(D^{*+})$ 3-5, 5-8, 8-16, 16-24 GeV/c. In each row, the panels show the associated track p_T ranges >0.3 GeV/c, 0.3-1 GeV/c and >1 GeV/c, respectively.

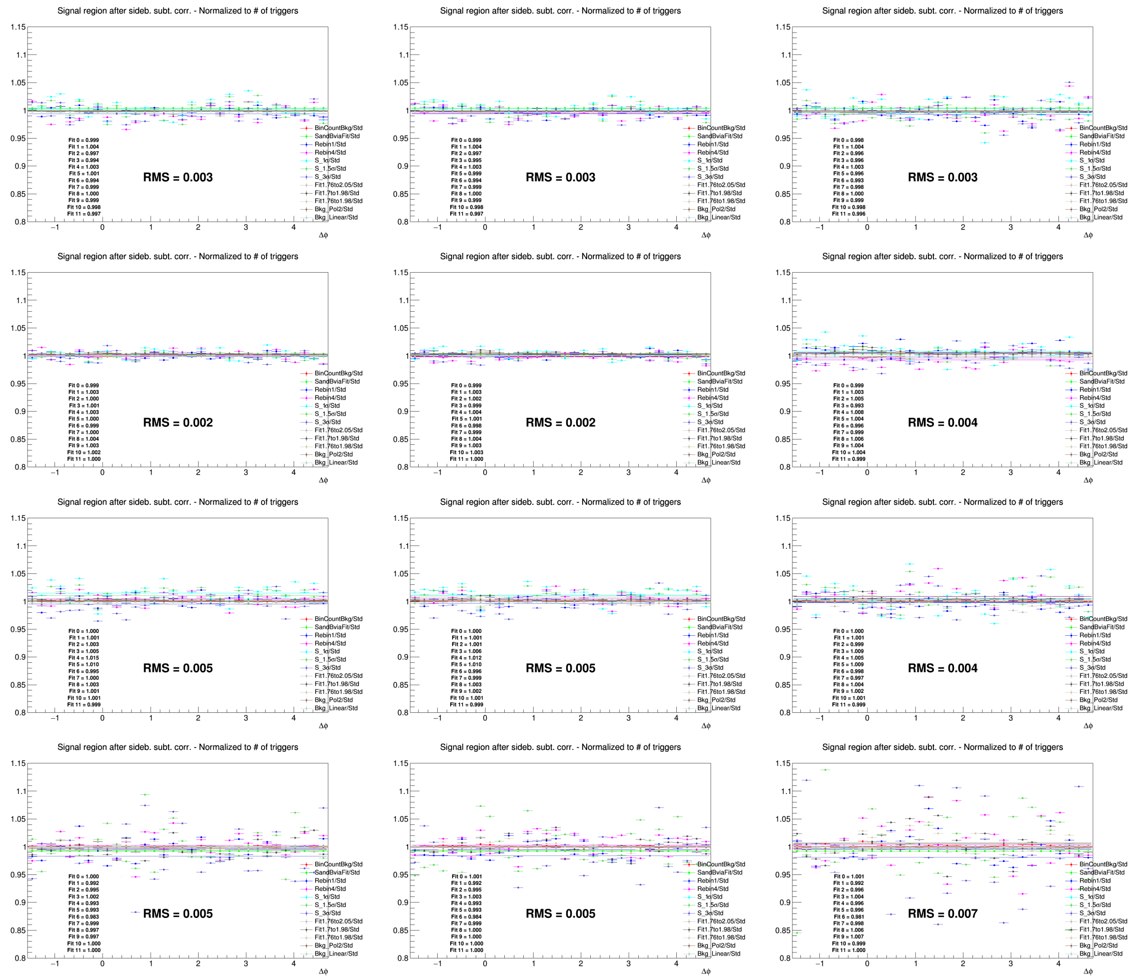

Figure 22: Ratios of D^+-h correlation plots obtained changing S and B extraction procedure over those obtained with standard yield extraction procedure. Rows: $p_T(D^+)$ 3-5, 5-8, 8-16, 16-24 GeV/c. In each row, the panels show the associated track p_T ranges 0.3-1 GeV/c, >0.3 GeV/c, and >1 GeV/c, respectively.

– inner half (5 to 8 σ from the centre of the peak);

– outer half (8 to 13 σ from the centre of the peak);

– extended to 5 to 13 σ from the centre of the peak;

– extended to 6 to 16 σ from the centre of the peak.

The rest of the procedure for the azimuthal correlations distribution was unchanged, and the ratios of the fully corrected azimuthal correlation plots obtained with the standard sidebands range and the correlation plots extracted with different sidebands definitions, were evaluated for each D-meson p_T bin and associated tracks p_T threshold. Results of this check are shown in Figures **??**, **??** and **??** for D^0, D^{*+}, D^+ respectively, for exemplary p_T ranges, spanning over the full kinematic regions analysis. From the values of the ratios extracted from the checks, which do not show any azimuthal dependence a systematic uncertainty for the background subtraction can be evaluated. Also no dependence versus the associated track p_T was assumed also in this case. The uncertainty was hence taken of 1% for all the mesons in $3 < p_T(D) < 16$ GeV/c and of 2%, 2.5% and 4% (for D^+, D^0, D^{*+} respectively) in $16 < p_T(D) < 24$ GeV/c.

4.3 Uncertainty on D-meson cut stability

To study the systematics due to the topological selections on the D meson, the cut variation approach was used. For each D-meson, alternate sets of released and tightened selection cuts were applied to extract the correlation distribution, varying in particular the cosine of the pointing angle, the maximum DCA among the daughter tracks and the product of the daughter track impact parameters. For each set of cuts new 2D (p_T vs multiplicity), D meson efficiency map was computed. In Figures **??**, **??**, **??** (for D^0, D^{*+} and D^+, respectively) the ratio of the different 1D efficiencies with the alternate cuts with respect to the default cut selection is chosen, to highlight how the different selections effectively varied the efficiency values, especially at low p_T, where cuts are more effective.

Figure **??**, **??**, **??** show the ratio of the correlation distributions with alternate cut sets over those with the standard approach, for exemplary p_T ranges covering the full kinematic region of interest for the analyses. The ratios are reasonably flat in $\Delta\varphi$, hence a flat systematic was evaluated as systematic uncertainty from D-meson the cut variations. For the D^0, the uncertainty was considered of 2% for all the p_T ranges of trigger and tracks analyzed. For the D^{*+}, the uncertainty was considered of 1.5% for $3 < p_T(D) < 8$ GeV/c and of 1% for $8 < p_T(D) < 24$ GeV/c. For the D^+, the uncertainty was considered of 1% for $3 < p_T(D) < 16$ GeV/c and of 2% for $16 < p_T(D) < 24$ GeV/c.

4.4 Uncertainty on tracking efficiency evaluation

The systematic uncertainty for the tracking efficiency includes the effects related to the set of filtering cuts defined for the associated tracks selection (mainly requests on the quality of reconstructed tracks for the TPC and ITS detectors). This uncertainty was determined by repeating the full analysis using different selections for the cuts on the associated tracks with respect to the usual selection (TPC only tracks with at least 2 points in the ITS). The alternative selections were: pure TPConly selection, meaning TPC tracks with no requests on the number of hits in the ITS, and TPC+ITS selection, which requires filterbit 4 with, in addition, at least 3 points in the ITS, ITS refit and a hit in at least an SPD layer. The ratios of the azimuthal correlation distributions with different sets of tracks selection over distributions with standard selection were evaluated, and are shown in Figures **??** and **??** for D^0-h correlations. Their values were used to determine a systematic uncertainty, which as the previous ones could be assigned flat in $\Delta\varphi$, and which was estimated of 3% in all the ranges of p_T analyzed.

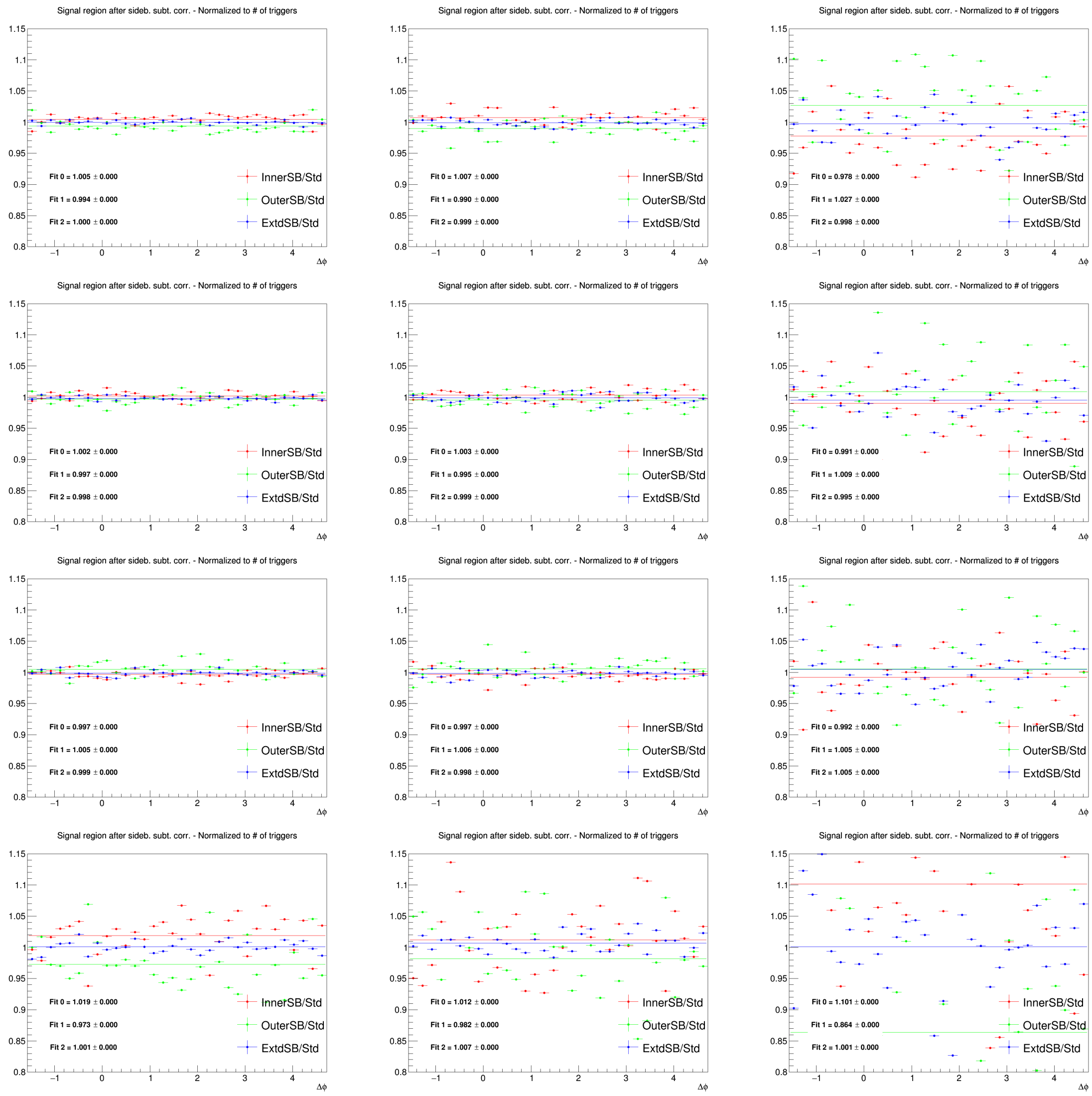

Figure 23: Ratios of D^0-h correlation plots obtained by changing the sideband ranges over those obtained with standard sideband ranges. Rows: $p_T(D^0)$ 3-5, 5-8, 8-16, 16-24 GeV/c. In each row, the panels show the associated track p_T ranges 0.3-1, 1-2, >3 GeV/c, respectively.

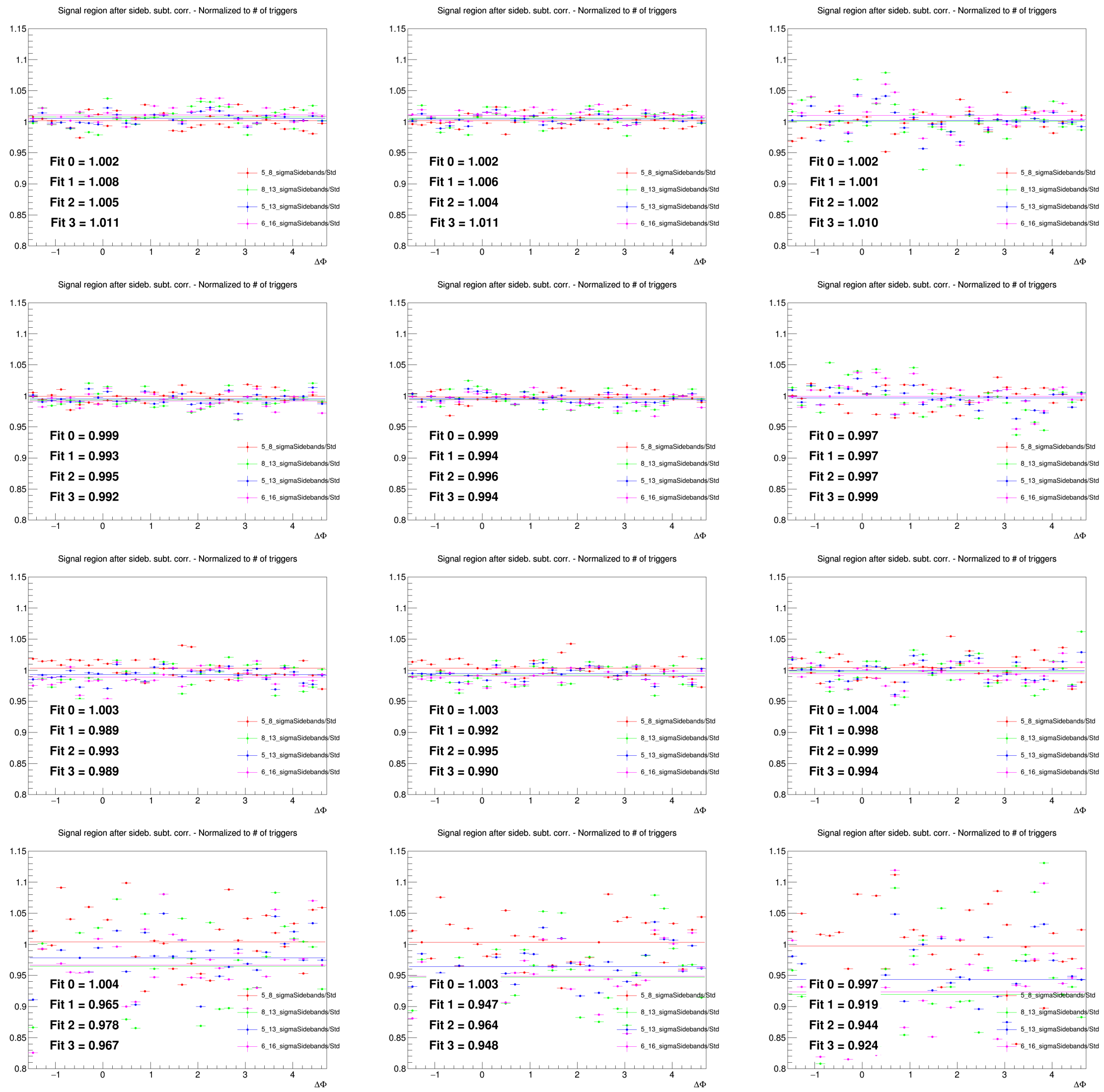

Figure 24: Ratios of D^{*+}-h correlation plots obtained by changing the sideband ranges over those obtained with standard sideband ranges. Rows: $p_T(D^{*+})$ 3-5, 5-8, 8-16, 16-24 GeV/c. In each row, the panels show the associated track p_T ranges 0.3-1, >0.3 GeV/c and >1 GeV/c, respectively.

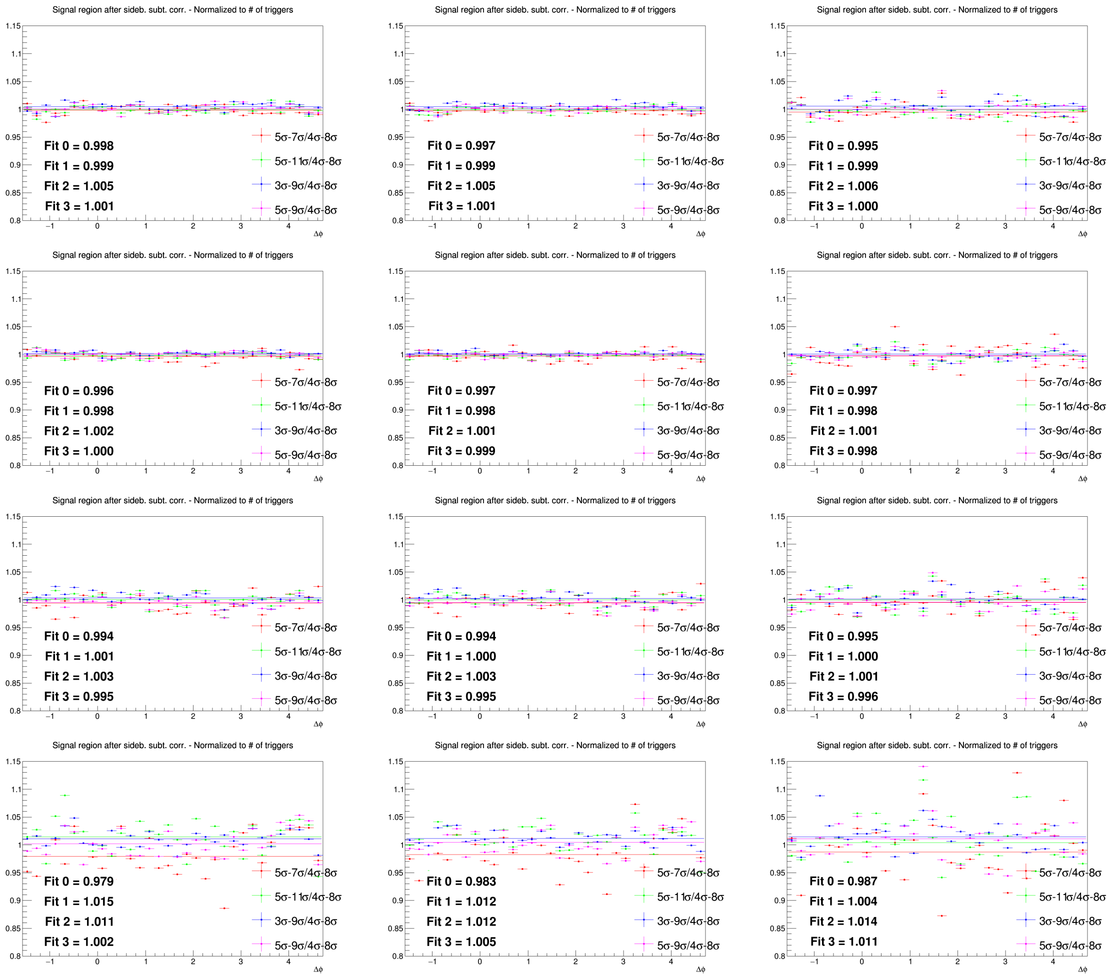

Figure 25: Ratios of D$^+$-h correlation plots obtained by changing the sideband ranges over those obtained with standard sideband ranges. Rows: p_T(D$^+$) 3-5, 5-8, 8-16, 16-24 GeV$/c$. In each row, the panels show the associated track p_T ranges 0.3-1, >0.3 GeV$/c$ and >1 GeV$/c$, respectively.

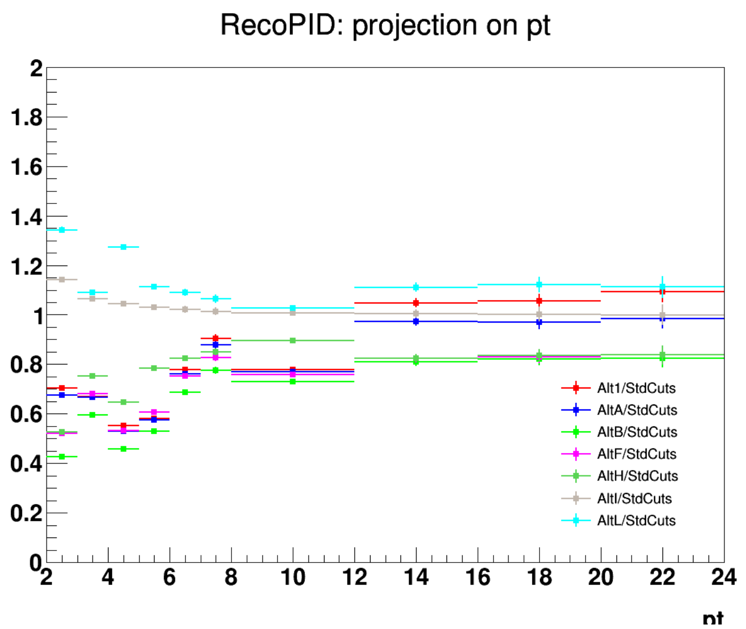

Figure 26: Ratio of D^0 efficiencies with alternate cut variations w.r.t. the standard cut used for the analysis.

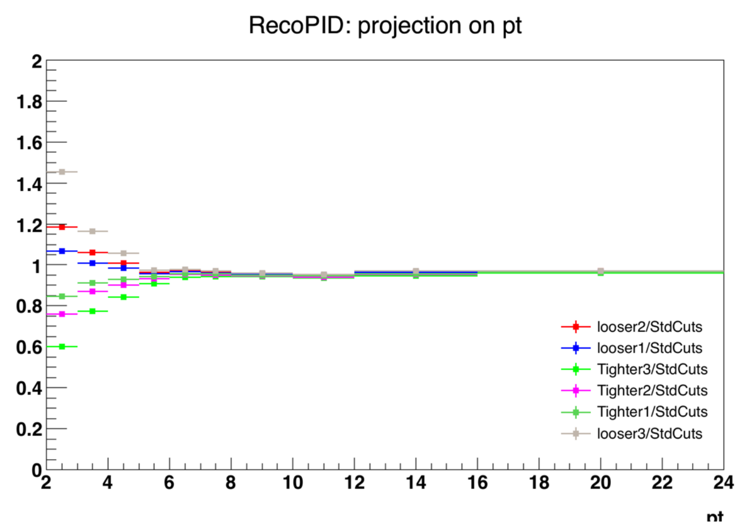

Figure 27: Ratio of D^{*+} efficiencies with alternate cut variations w.r.t. the standard cut used for the analysis.

4.5 Uncertainty on secondary particle contamination

Secondary particles, i.e. particles coming from strange hadrons decays or particles produced in interactions with the material, are expected to be tagged and removed by means of a distance of closest approach (DCA) from primary vertex cut. The uncertainty arising from the residual contamination of secondary tracks can be estimated from a Monte Carlo study, at reconstructed level. The number of primary/secondary tracks which are accepted/rejected from the DCA cut was determined for different values of the DCA selection, and the correlation distributions for the various cases were evaluated. The variations were done in the *xy* direction, where the DCA resolution is better, and the following cases were tried (in addition to the default 1 cm cut): 0.1 cm, 0.25 cm, 0.5 cm, filtering DCA cut (i.e. 2.4 cm).

Figure **??** shows the amount of secondary tracks which are accepted by the DCA cut, over the total number of tracks (primary and secondary) accepted by the selection, for the various DCA selections that were tried. This is shown for the exemplary case of $5 < p_T < 8$ GeV/c (there's no p_T(D) dependence) and as a function of the associated track p_T ranges. Hence, this quantity represents the residual contamination

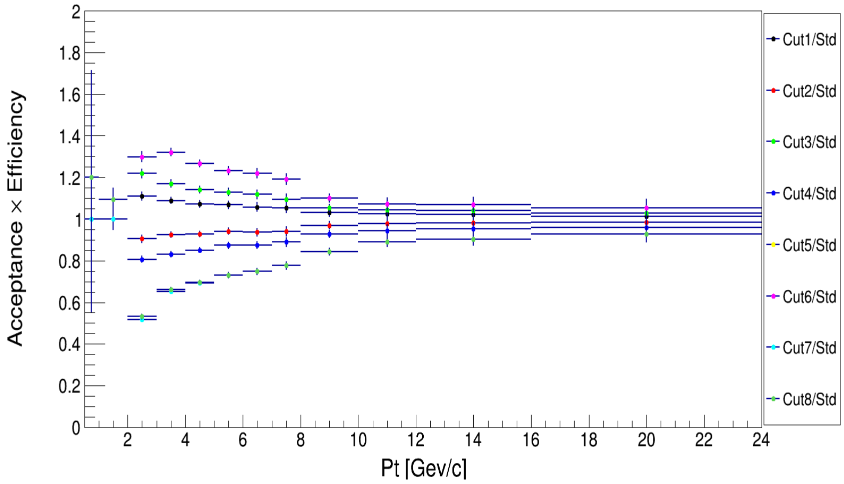

Figure 28: Ratio of D^+ efficiencies with alternate cut variations w.r.t. the standard cut used for the analysis.

of secondary tracks in our reconstructed track sample. From these values, the corresponding primary track purities (1-contamination) were extracted, in each of the momentum ranges. It was also verified that, for all the cut selections, the $\Delta\varphi$ distributions of the residual contaminations were flat within 1%.

As a second step of the procedure to verify the DCA cut stability, the D^0-h data analysis was performed with all the different DCA selection (each time with the proper tracking efficiency map). After having extracted the correlation distributions, these were rescaled for the corresponding purities and compared with the purity-corrected correlation distributions obtained with the standard DCA selection. The ratios of the alternate selections over the standard selection, after the purity correction of both, are shown in Figures **??** and **??**.

The ratios show a flat trend along the $\Delta\varphi$ axis and, in general, a discrepancy from the value of 1 of no more than 3% (the worst case being the 0.3-1 GeV/c range for the associated track). Hence, a flat and symmetric 3% systematical uncertainty on the evaluation of the secondary contamination was assigned on the base of this check in 0.3-1 GeV/c, reduced to 2.5% in > 0.3 GeV/c and to 1.5% for the other ranges. This amount also covers possible biases in the estimation of the purity (the $\Delta\varphi$ distribution of the residual contamination is always contained inside 1%, as previously said).

4.6 Uncertainty on feed-down subtraction

As described in the **??** section, the feed-down subtraction from the data distributions is performed by means of simulation templates of B$\rightarrow$D-h correlation distributions from PYTHIA6 generator, with Perugia2011 tune, and considering the central value of f_{prompt} to extract the feed-down D-meson contribution. In order to evaluate a systematic uncertainty on this procedure, the feed-down subtraction procedure was repeated considering, together with PYTHIA6+Perugia2011 templates, also PYTHIA6+Perugia2010 and PYTHIA8 simulations. In each case, not only the central value of the measured f_{prompt} was considered to rescale the distributions, but also the maximum and minimum values of its total uncertainty.

Then, the envelope of nine the different cases obtained by varying the templates and the f_{prompt} assumption was considered, and a value of the systematics defined as the envelope spread divided by $\sqrt{3}$ was taken as systematic uncertainty. This uncertainty was assumed uncorrelated among the different $\Delta\varphi$ points.

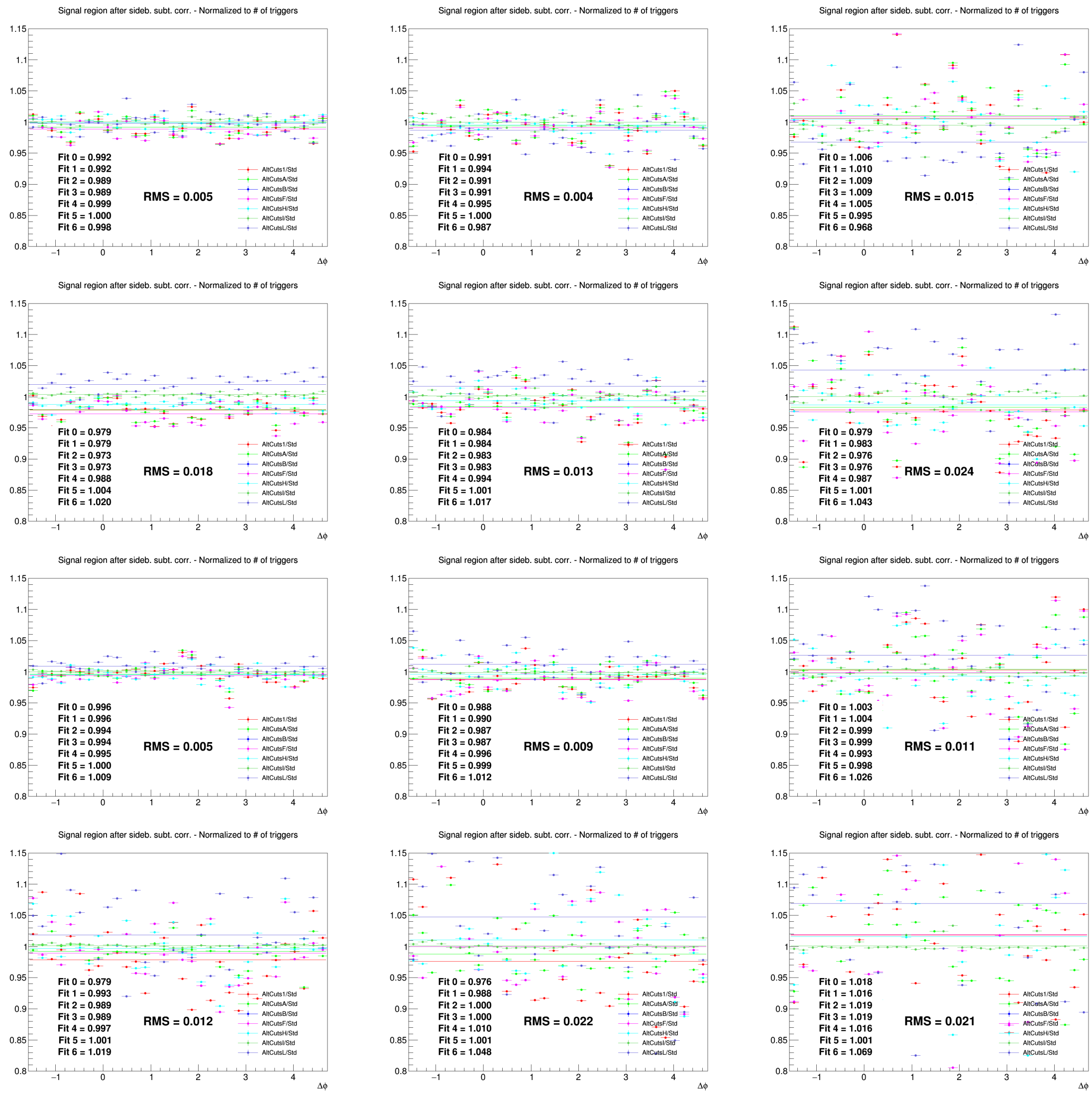

Figure 29: Ratios of D^0-h correlation plots obtained with alternate D-meson cut sets over those obtained with standard selection. Rows: $p_T(D^0)$ 3-5, 5-8, 8-16, 16-24 GeV/c. In each row, the panels show the associated track p_T ranges 0.3-1, 1-2, 2-3 GeV/c, respectively.

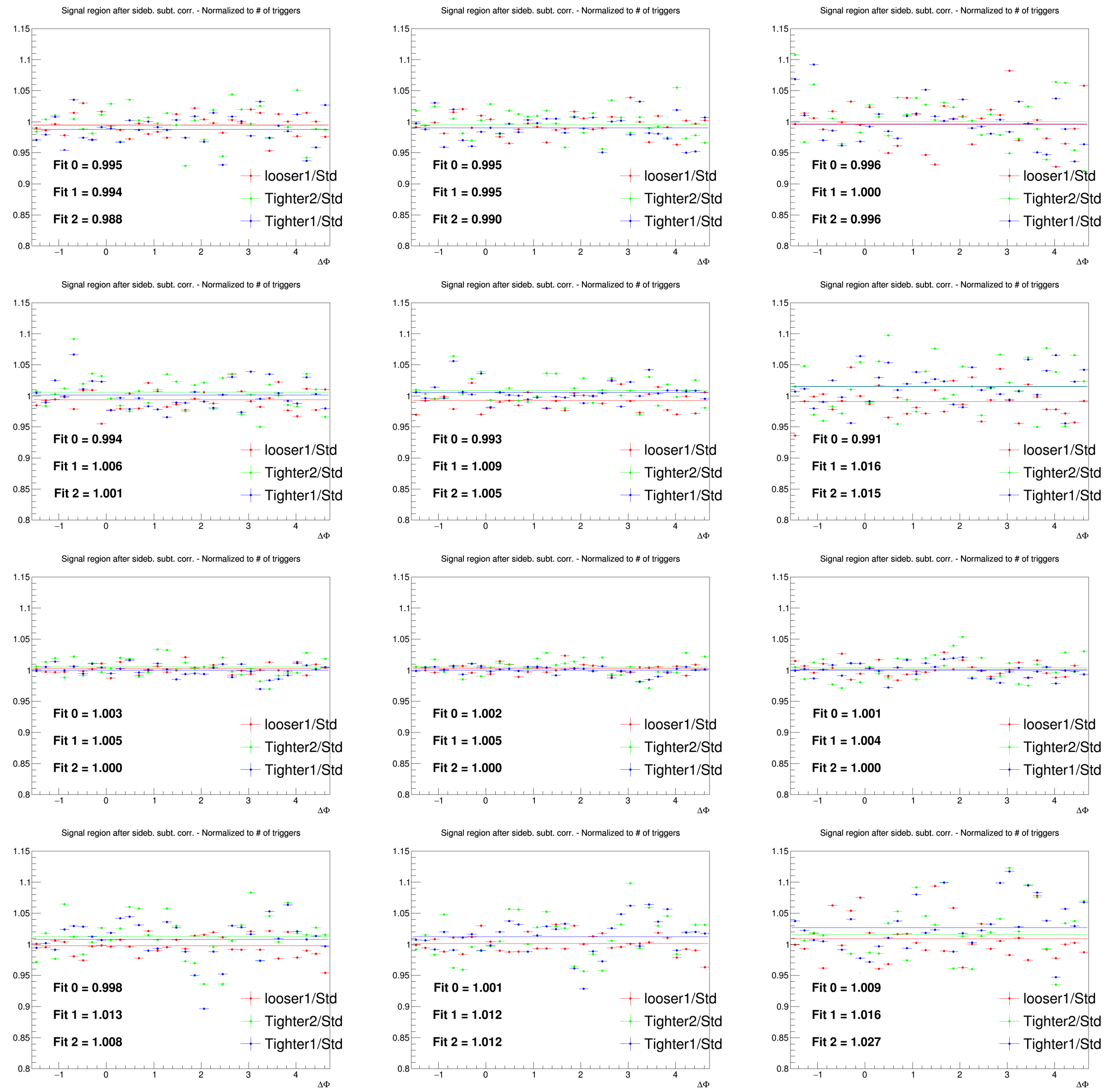

Figure 30: Ratios of D^{*+}-h correlation plots obtained with alternate D-meson cut sets over those obtained with standard selection. Rows: $p_{\mathrm{T}}(D^{*+})$ 3-5, 5-8, 8-16, 16-24 GeV/c. In each row, the panels show the associated track p_{T} ranges 0.3-1, >0.3 GeV/c, >1 GeV/c, respectively.

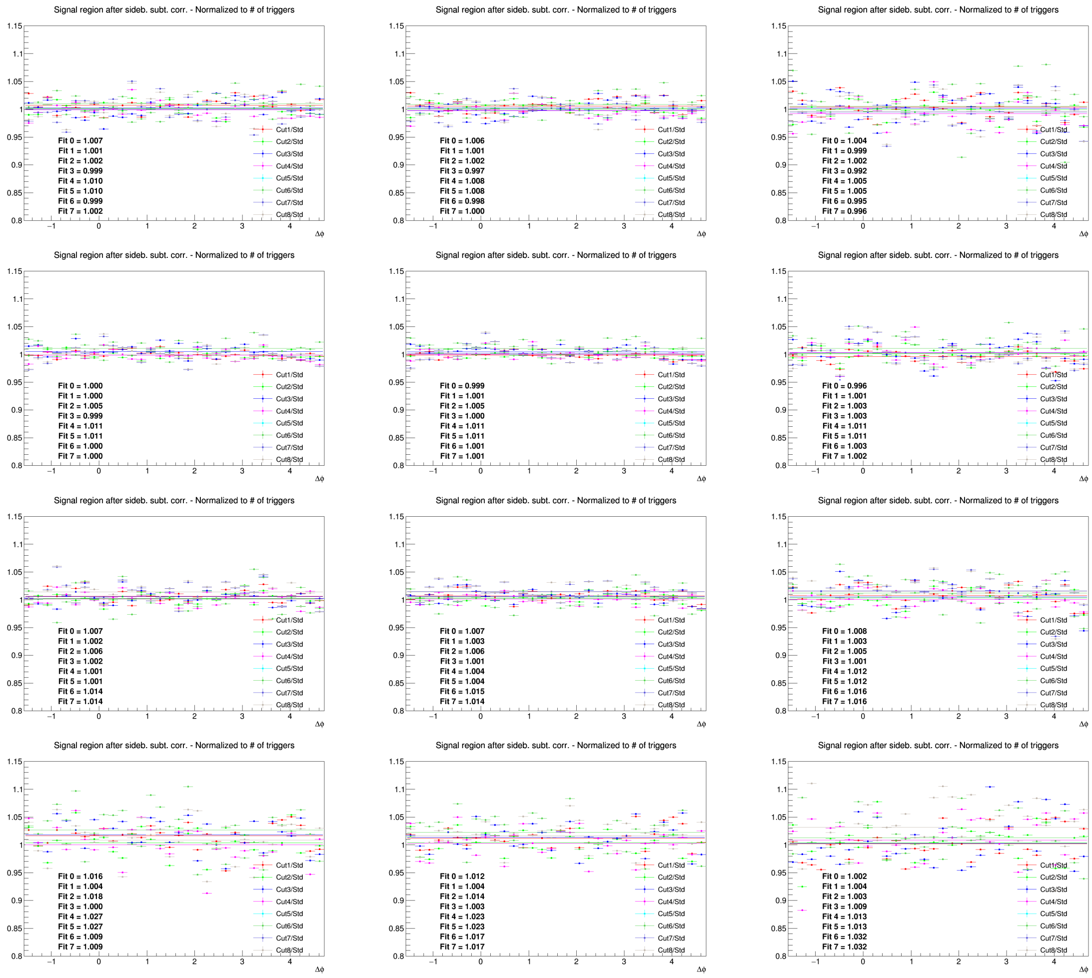

Figure 31: Ratios of D^+-h correlation plots obtained with alternate D-meson cut sets over those obtained with standard selection. Rows: $p_T(D^+)$ 3-5, 5-8, 8-16, 16-24 GeV/c. In each row, the panels show the associated track p_T ranges 0.3-1, >0.3 GeV/c, >1 GeV/c, respectively.

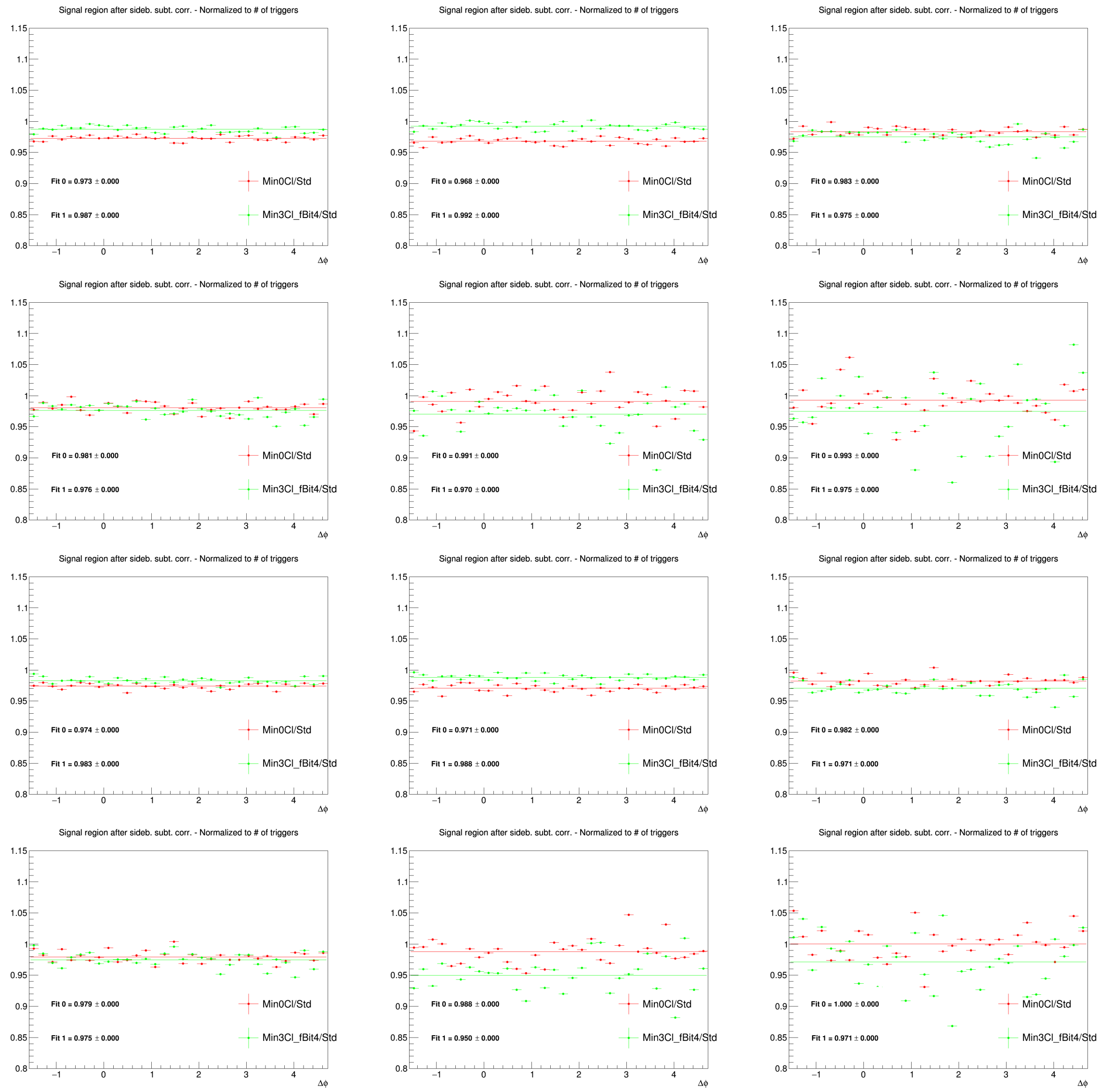

Figure 32: Ratios of D^0-h correlation plots obtained with different associated tracks filtering selections. First 6 plots: p_{T}(D) 3-5 GeV/c, next 6 plots: p_{T}(D) 5-8 GeV/c. Each bunch of 6 plots has p_{T}(assoc) of $>$0.3, 0.3-1, $>$1, 1-2, 2-3, $<$3 GeV/c, respectively.

4.7 Uncertainty on correction for the bias on B to D decay topologies

The evaluation of this systematic uncertainty was already explained in Section 3.3.3. For each of the five data points close to the center of the near-side peak, which are affected by the bias, a bilateral and symmetric uncertainty of amplitude $|C(\Delta\varphi)_{\mathrm{corr}} - C(\Delta\varphi)_{\mathrm{raw}}|/\sqrt{12}$ was assigned.

This because the uncorrected data points are expected to be the extreme (with the current D-meson selection, the bias is always upwards at the centre of the peak, and always upwards on its sides). We then assume that, if the correction is properly evaluated, the corrected data points are at the centre of the possible spread of the true unbiased results. In this case, the span of the possible true results (in case of underestimation/overestimation of the bias) goes from the uncorrected data points to its symmetric value, with respect to the corrected data point, on the other direction. If this distribution is uniform, and constrained by these two values, the 1σ confidence region for the position of the is in a bilateral $|C(\Delta\varphi)_{\mathrm{corr}} - C(\Delta\varphi)_{\mathrm{raw}}|/\sqrt{12}$ window, centered on the $C(\Delta\varphi)_{\mathrm{corr}}$ points.

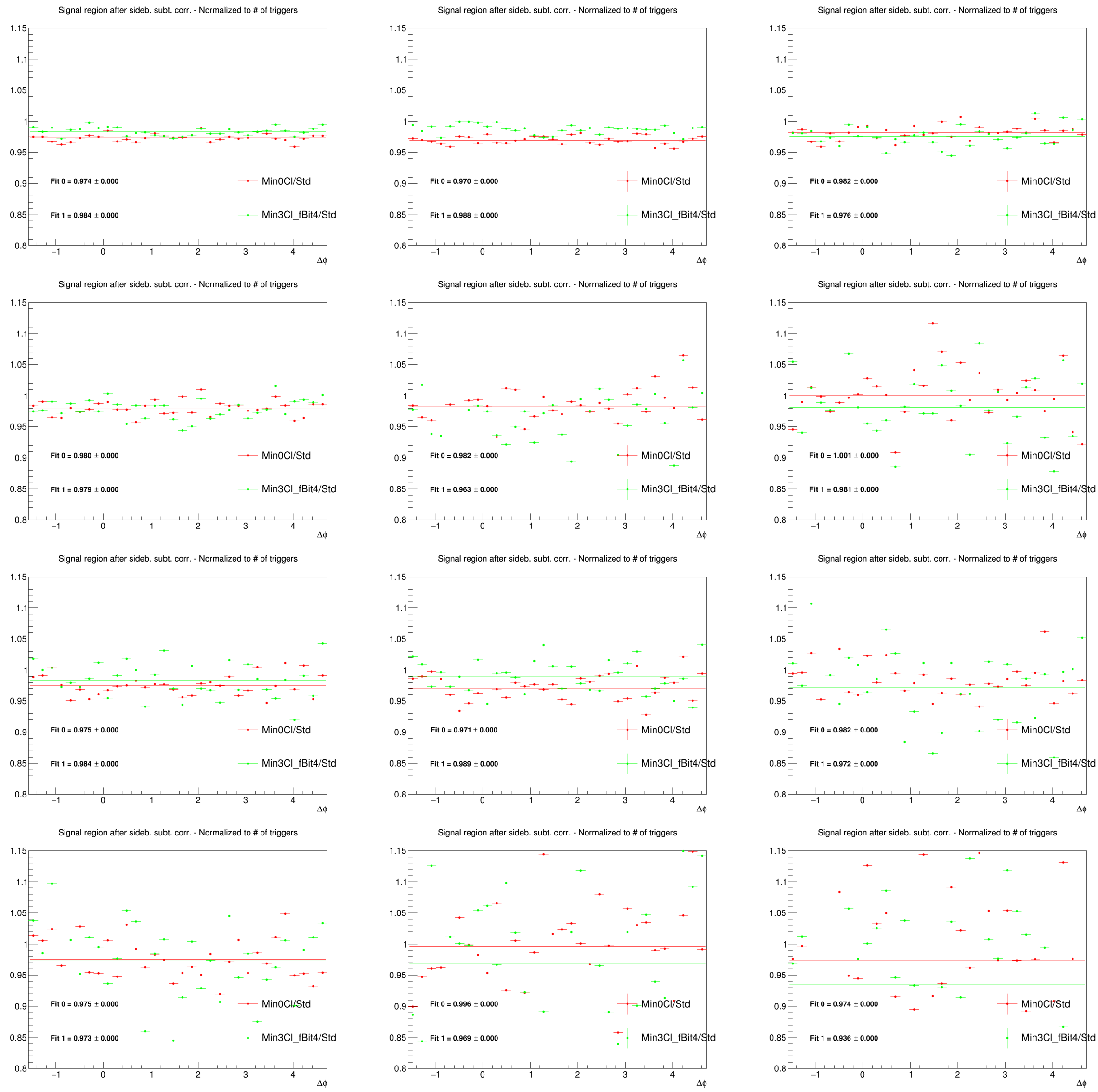

Figure 33: Ratios of D^0-h correlation plots obtained with different associated tracks filtering selections. First 6 plots: p_T(D) 8-16 GeV$/c$, next 6 plots: p_T(D) 16-24 GeV$/c$. Each bunch of 6 plots has p_T(assoc) of $>$0.3, 0.3-1, $>$1, 1-2, 2-3, $<$3 GeV$/c$, respectively.

This source of uncertainty was assumed uncorrelated among the $\Delta\varphi$ points.

4.8 Summary table

A summary of the $\Delta\varphi$-correlated uncertainties affecting the correlation distributions is show in Figure **??**. They are the S and B extraction uncertainty, the background shape uncertainty, the cut variation uncertainty, the tracking efficiency uncertainty and the secondary particle contamination uncertainty.

The overall amount of $\Delta\varphi$-correlated uncertainties is about 5-6% (depending on the p_T bin) for the single D-meson cases; when evaluating the averages of the distributions (see next section), this uncertainty shrinks to 4-5%. This uncertainty is a global scale factor of the distributions, and is quoted as a label in the plots.

The systematics uncertainties from feed-down subtraction and B→D decay topology bias, instead are $\Delta\varphi$ dependent, and are hence reported as uncorrelated boxes in the plots. They do not amount to more than 4%, in every bin of all the kinematic ranges studied.

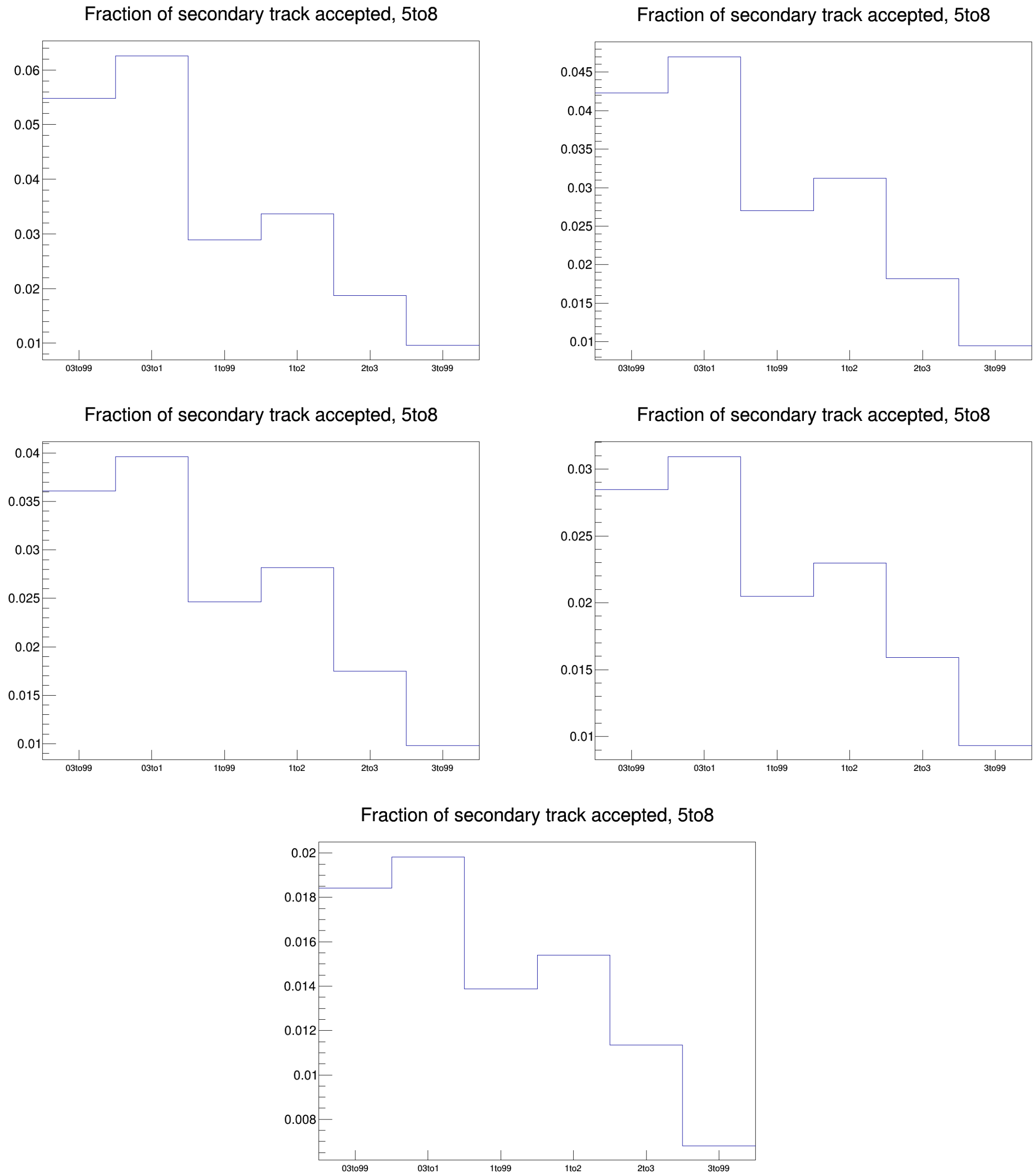

Figure 34: Secondary track contamination as a funciton of the associated track p_{T}, for the various DCA selections tried. The plots are ordered from the loosest to the tightest selection, i.e.: DCA(xy) <2.4 cm, <1 cm, <0.5 cm, <0.25 cm, <0.1 cm.

5 Results

5.1 Comparing the three D meson correlation distributions

To check the compatibility of three D meson analyses, Figures 20, 21, 22, 23 show the corrected azimuthal correlation distributions (except for the feed-down subtraction and the secondary contamination removal) for D^0-h, D^{*+}-h and D^+-h, in each column, on the data sample used in the analysis. Results are shown for $3 < D\ p_{\mathrm{T}} < 5$ GeV/c, $5 < D\ p_{\mathrm{T}} < 8$ GeV/c, $8 < D\ p_{\mathrm{T}} < 16$ GeV/c and $16 < D\ p_{\mathrm{T}} < 24$ GeV/c with associated tracks $p_{\mathrm{T}} > 0.3$, $p_{\mathrm{T}} > 1$, $0.3 < p_{\mathrm{T}} < 1$ GeV/c, $1 < p_{\mathrm{T}} < 2$ GeV/c, $2 < p_{\mathrm{T}} < 3$ GeV/c and $p_{\mathrm{T}} > 3$ GeV/c.

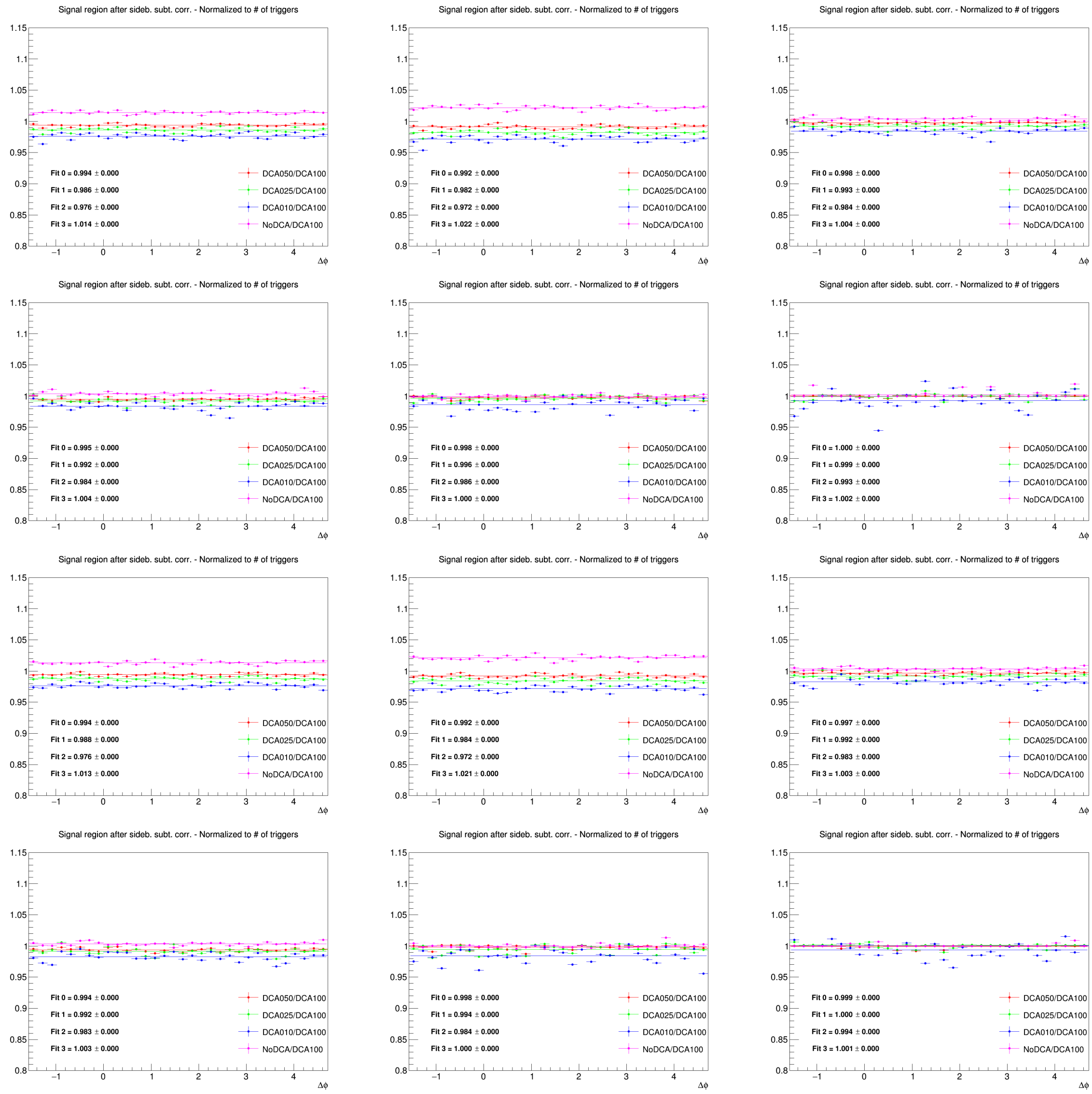

Figure 35: Ratios of correlation plots (with D^0 as trigger meson) obtained with different associated DCA selections, after purity correction. First 6 plots: p_T(D) 3-5 GeV/c, next 6 plots: p_T(D) 5-8 GeV/c. Each bunch of 6 plots has p_T(assoc) of >0.3, 0.3-1, >1, 1-2, 2-3, <3 GeV/c, respectively.

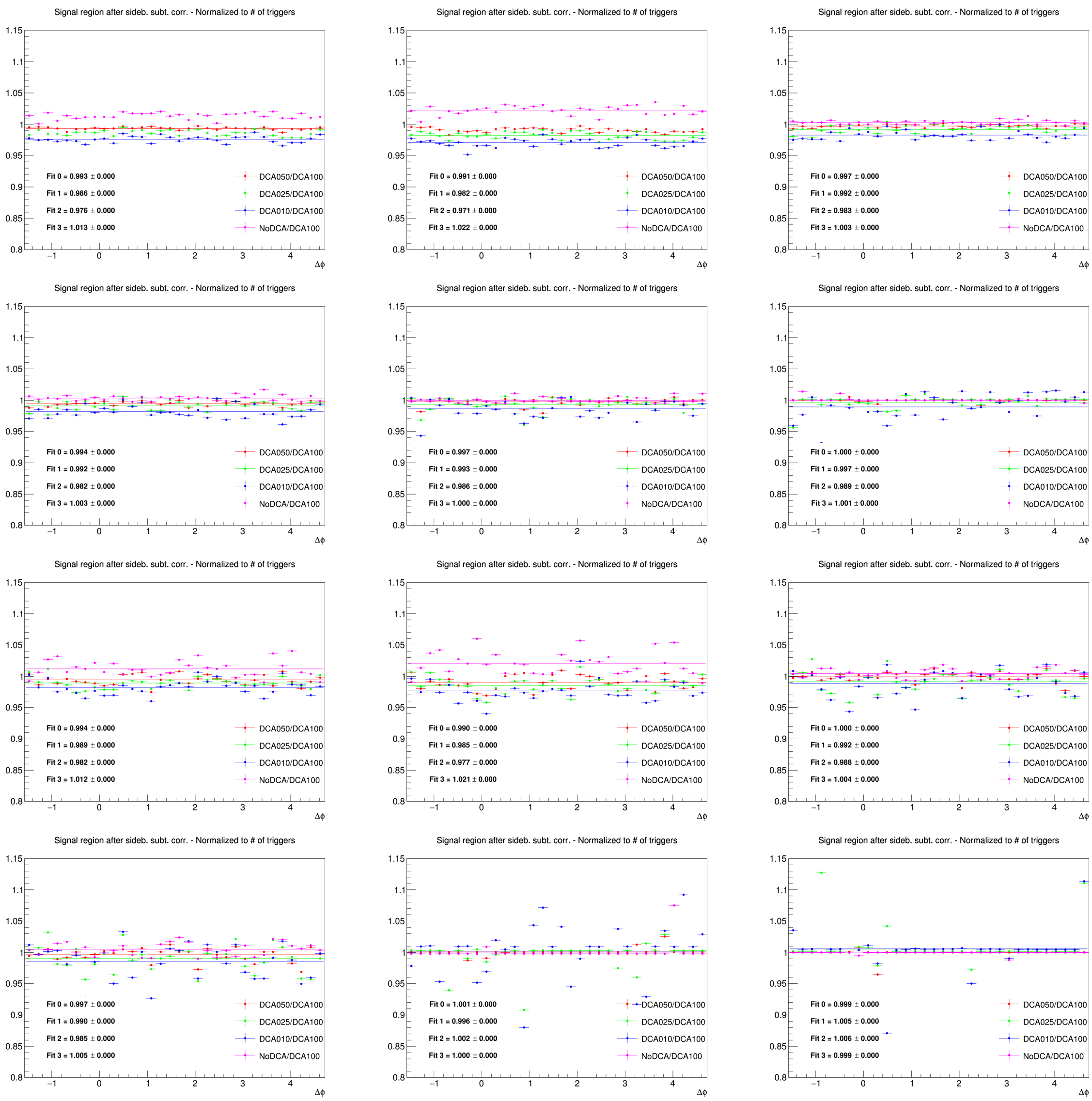

Figure 36: Ratios of correlation plots (with D^0 as trigger meson) obtained with different associated DCA selections, after purity correction. First 6 plots: p_T(D) 8-16 GeV/c, next 6 plots: p_T(D) 16-24 GeV/c. Each bunch of 6 plots has p_T(assoc) of >0.3, 0.3-1, >1, 1-2, 2-3, <3 GeV/c, respectively.

pPb Sample	D^0				D^*				D^+			
D p_T Range (GeV/c)	3-5	5-8	8-16	16-24	3-5	5-8	8-16	16-24	3-5	5-8	8-16	16-24
S and B Extraction	1%	1%	1%	2%	1%	1%	1%	2%	1%	1%	1%	2%
Background Correlation Shape	1%	1%	1%	2.5%	1%	1%	1%	4%	1%	1%	1%	2%
D meson Cut Variation	2%	2%	2%	2%	1.5%	1.5%	1%	1%	1%	1%	1%	2%

pPb Sample	D^0, D^* and D^+ (common for all the p_T(D) ranges)						
Assoc (p_T) Ranges (GeV/c)	> 0.3	> 1.0	> 2.0	> 3.0	0.3-1.0	1.0-2.0	2.0-3.0
Track Efficiency	3.5%	3.5%	3.5%	3.5%	3.5%	3.5%	3.5%
Purity	2.5%	1.5%	1.5%	1.5%	3%	1.5%	1.5%

Figure 37: Summary of the $\Delta\varphi$-correlated uncertainties associated to the correlation distributions, for three D-mesons, in the different kinematic ranges of D meson and hadrons.

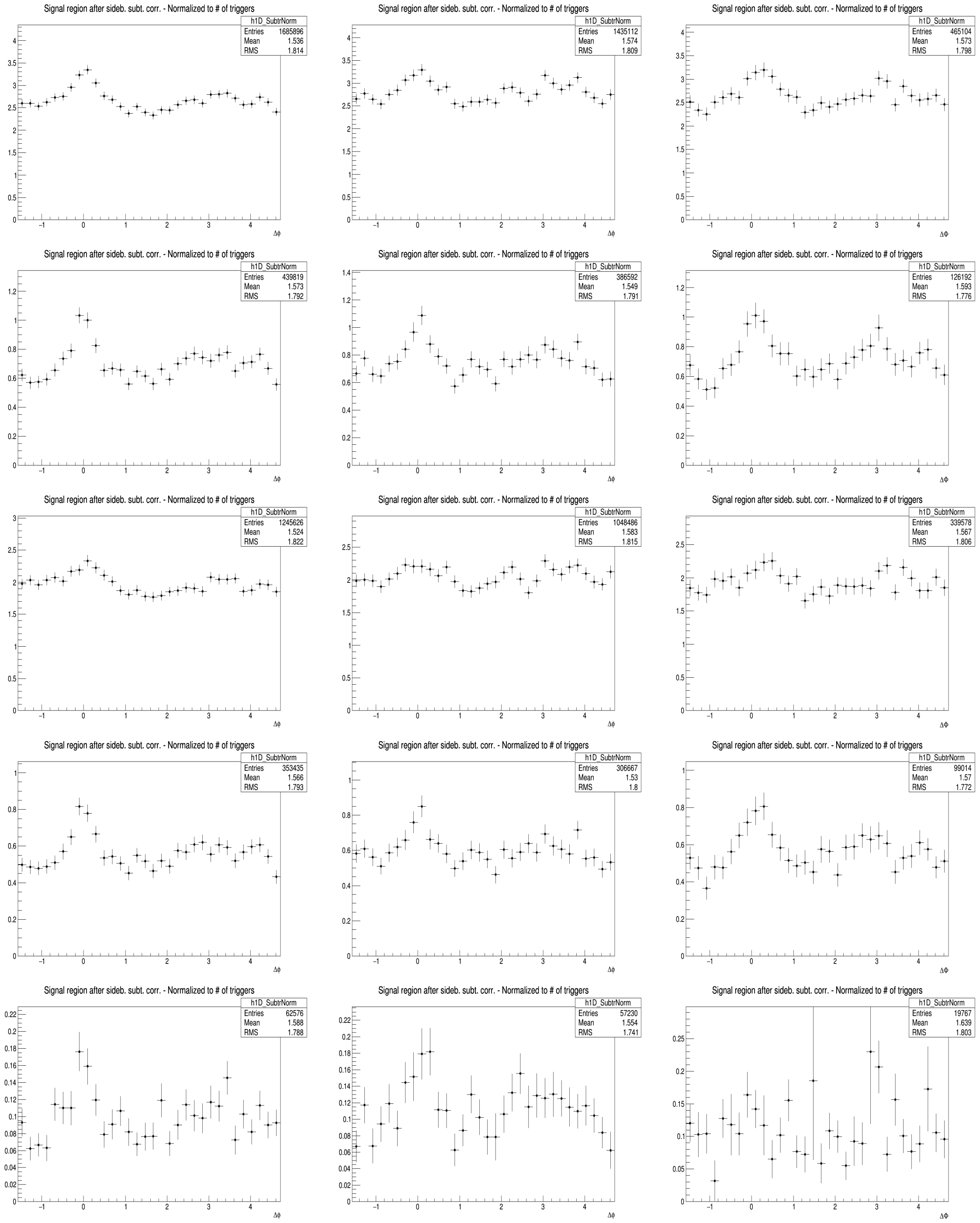

Figure 38: Corrected distribution of D-hadrons azimuthal correlations for the three species (apart from feed-down and purity), from analysis on the data sample, for the analyzed D-meson (**Column-Left:** D^0**, Column-Middle:** D^+ **and Column-Right:** D^{*+}) and different associated tracks p_T ranges (**Row 1-5:** $3 < Dp_\mathrm{T} < 5\ \mathrm{GeV}/c,\ p_\mathrm{T}\ (Assoc) >$ 0.3, $>$1.0, 0.3-1.0, 1.0-2.0 and 2.0-3.0 GeV$/c$ respectively)

.

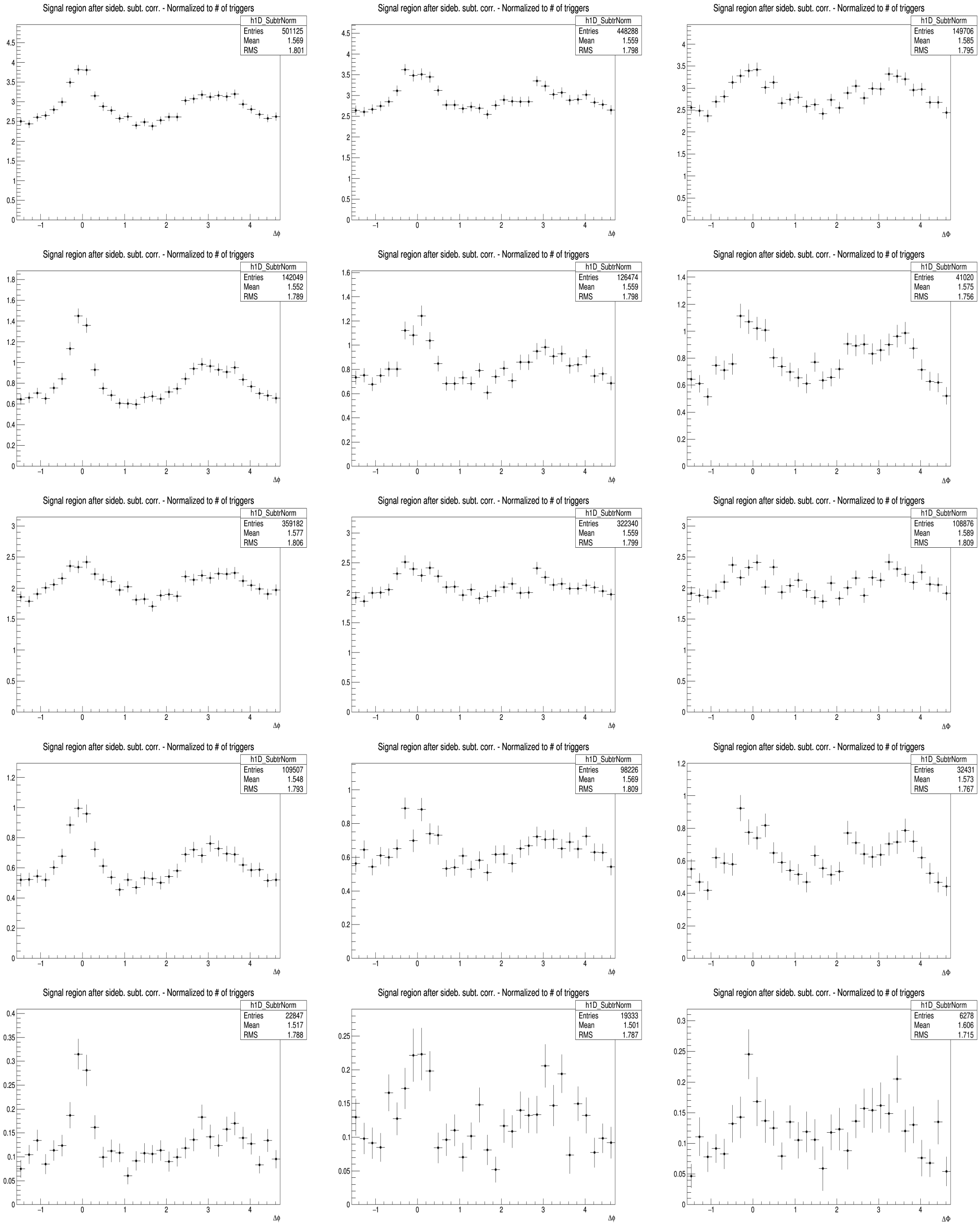

Figure 39: Corrected distribution of D-hadrons azimuthal correlations for the three species (apart from feed-down and purity), from analysis on the data sample, for the analyzed D-meson **(Column-Left:** D^0**, Column-Middle:** D^+ **and Column-Right:** D^{*+}) and different associated tracks p_T ranges (**Row 1-5:** $5 < Dp_T < 8$ GeV/c, $p_T\,(Assoc) >$ 0.3, >1.0, 0.3-1.0, 1.0-2.0 and 2.0-3.0 GeV/c respectively)

.

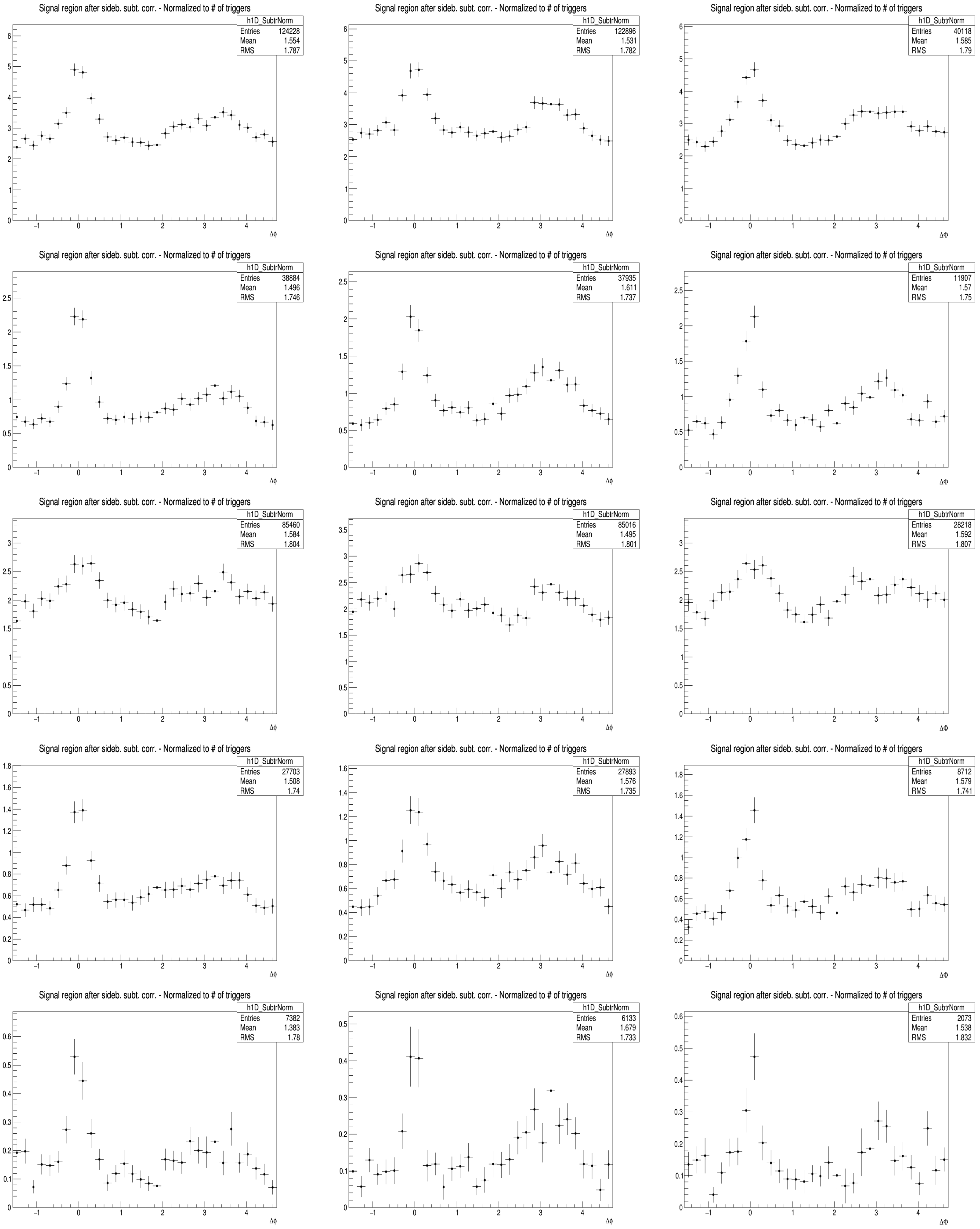

Figure 40: Corrected distribution of D-hadrons azimuthal correlations for the three species (apart from feed-down and purity), from analysis on the data sample, for the analyzed D-meson **(Column-Left: D^0, Column-Middle: D^+ and Column-Right:** D^{*+}) and different associated tracks p_T ranges (**Row 1-5:** $8 < Dp_T < 16$ GeV/c, p_T $(Assoc) > 0.3$, >1.0, 0.3-1.0, 1.0-2.0 and 2.0-3.0 GeV/c respectively)

.

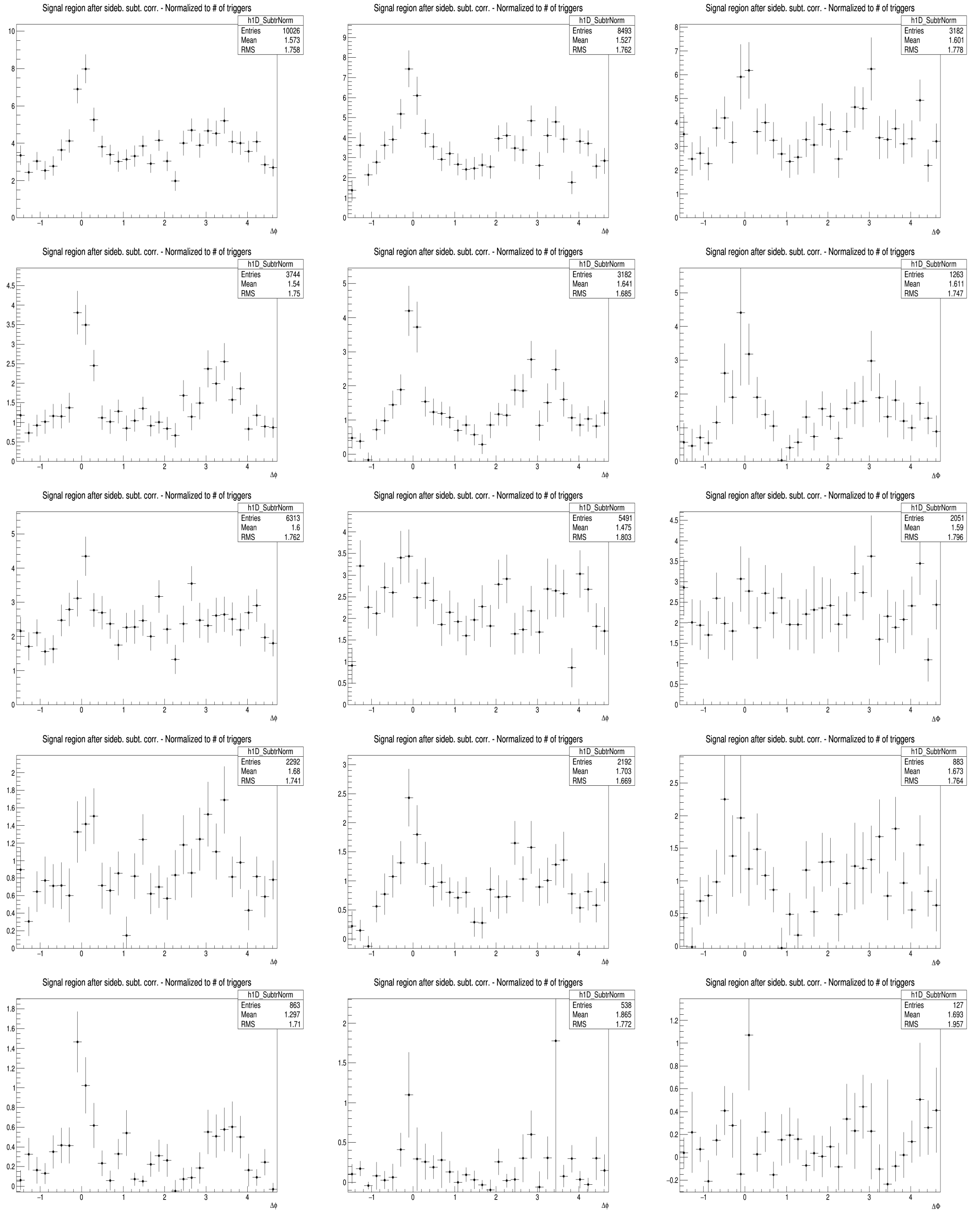

Figure 41: Corrected distribution of D-hadrons azimuthal correlations for the three species (apart from feed-down and purity), from analysis on the data sample, for the analyzed D-meson **(Column-Left:** D^0**, Column-Middle:** D^+ **and Column-Right:** D^{*+}) and different associated tracks p_T ranges (**Row 1-5:** $16 < Dp_T < 24$ GeV$/c$, p_T $(Assoc) > 0.3$, >1.0, 0.3-1.0, 1.0-2.0 and 2.0-3.0 GeV$/c$ respectively)

.

An agreement of the distributions from the three mesons within the uncertainties is found in all the kinematic ranges.

Despite being evaluated in the full 2π range, the range of final results was then reduced to $[0,\pi]$ radians, reflecting the points outside that range over the value of 0. This allowed to reduce the impact of statistical fluctuations on the data points (supposing equal statistics for a pair of symmetric bins, after the reflection the relative statistical uncertainty for the resulting bin is reduced by a factor $1/\sqrt{2}$).

5.2 Average of D^0, D^+ and D^{*+} results

Given the compatibility within the uncertainties among the D^0, D^+ and D^{*+} azimuthal correlations, and since no large differences are visible in the correlation distributions observed in Monte Carlo simulations based on Pythia with Perugia0, 2010 and 2011 tunes[1], it was possible to perform a weighted average (eq. 5) of the azimuthal correlation distributions of D^0, D^+ and D^{*+}, in order to reduce the overall uncertainties. Although some correlation between the mesons could be present (about the 30% of the D^0, and also part of the D^+, come from D^{*+} decays), the three selected D-meson samples can be treated as uncorrelated. The sum of the statistical uncertainties; the systematics uncertainty on S and B extraction and on background shape, are added in quadrature and the inverse of this sum was used as weight, w_i.

$$\left\langle \frac{1}{N_{\mathrm{D}}} \frac{dN^{\mathrm{assoc}}}{dp_{\mathrm{T}}} \right\rangle_{Dmesons} = \frac{\sum_{\mathrm{i=meson}} w_i \frac{1}{N_{\mathrm{D}}} \frac{dN_i^{\mathrm{assoc}}}{d\Delta\varphi}}{\sum_{\mathrm{i=meson}} w_i} \quad , w_i = \frac{1}{\sigma_{i,\mathrm{stat}}^2 + \sigma_{i,\mathrm{uncorr.syst.}}^2} \tag{5}$$

The statistical uncertainty and the uncertainties on S and B extraction and on background shape (those used for the weights) on the average were then recalculated using the following formula:

$$\sigma^2 = \frac{1}{n_{\mathrm{D}}} \frac{\sum_{\mathrm{i=meson}} w_i \sigma_i^2}{\sum_{\mathrm{i=meson}} w_i} \tag{6}$$

where n_{D} is the number of mesons considered in the average. It can be observed that for $\sigma_i^2 = 1/w_i$ the formula coincides with the standard one giving the uncertainty on a weighted average. The contribution to the average systematic uncertainty for those uncertainty sources not included in the weight definition, was evaluated via error propagation on the formula of the weighted average (5), resulting in equation (7) and (8) for sources considered uncorrelated and correlated among the mesons. In particular, the uncertainties on the associated track reconstruction efficiency, on the contamination from secondary, on the feed-down subtraction, and that resulting from the Monte Carlo closure test were considered fully correlated among the mesons, while those deriving from the yield extraction (included in the weight definition) and on the D meson reconstruction and selection efficiency were treated as uncorrelated.

$$\sigma^2 = \frac{\sum_{\mathrm{i=meson}} w_i^2 \sigma_i^2}{\left(\sum_{\mathrm{i=meson}} w_i\right)^2} \tag{7}$$

$$\sigma = \frac{\sum_{\mathrm{i=meson}} w_i \sigma_i}{\sum_{\mathrm{i=meson}} w_i} \tag{8}$$

Figures 24, 25, 26, 27 show the averages of the azimuthal correlation distributions of D^0, D^+ and D^{*+} and charged particles with $p_{\mathrm{T}} > 0.3$ GeV/c, 0.3< $p_{\mathrm{T}} < 1$ GeV/c, $p_{\mathrm{T}} > 1$ GeV/c, 1< $p_{\mathrm{T}} < 2$ GeV/c, 2< $p_{\mathrm{T}} < 3$ GeV/c in the D meson p_{T} ranges $3 < p_{\mathrm{T}} < 5$ GeV/c, $5 < p_{\mathrm{T}} < 8$ GeV/c, $8 < p_{\mathrm{T}} < 16$ GeV/c and $16 < p_{\mathrm{T}} < 24$ GeV/c. As expected, a rising trend of the height of the near-side peak with increasing D-meson p_{T} is observed, together with a decrease of the baseline level with increasing p_{T} of the associated

[1]A slight near side hierarchy is present among the three meson results, with D^{*+} meson having a lower peak amplitude than D^0 and D^+. It was verified that this is induced by the presence of D^0 and D^+ mesons coming from D^{*+}, the latter having on average a larger p_T and coming, hence, on average, from a larger p_T quark parton, which fragments in slightly more tracks in the near-side.

tracks. To further increase the statistical precision on the averaged correlation distributions, given the symmetry around 0 on the azimuthal axis, the distributions were reflected and shown in the range $[0,\pi]$. This reduces the statistical uncertainty on the poins by, approximately, a factor of $1/\sqrt{2}$.

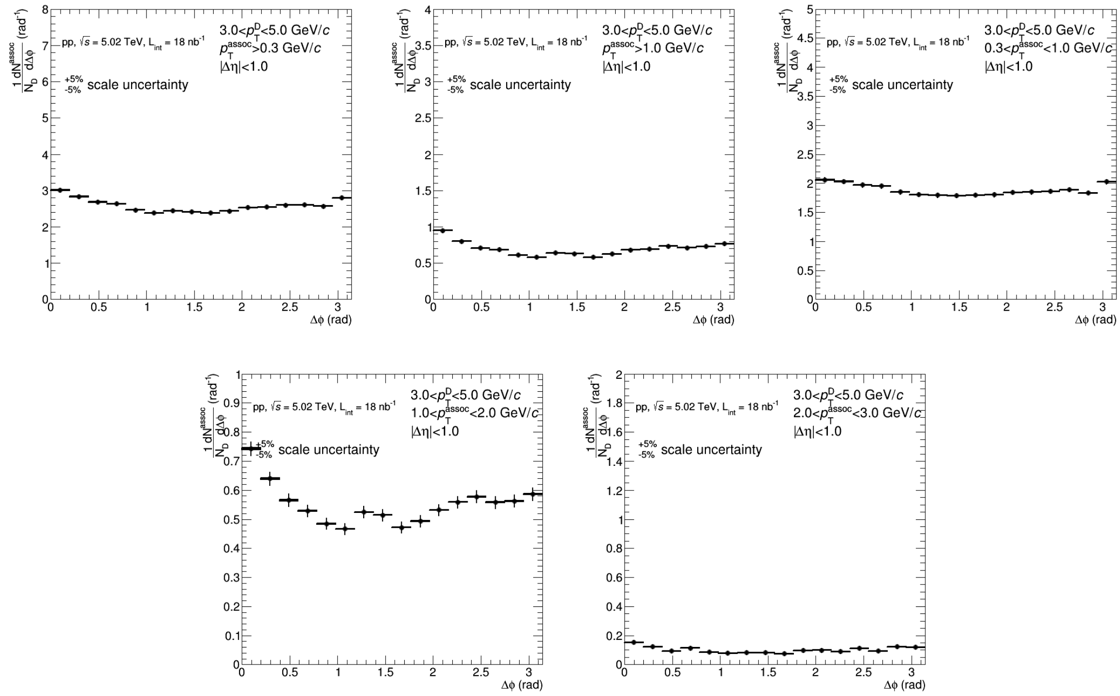

Figure 42: Average of D^0, D^+ and D^{*+} azimuthal correlation distributions, in the D meson p_T range $3 < p_T < 5$ GeV/c with associated tracks with $p_T > 0.3$ GeV/c, $p_T > 1$ GeV/c, $0.3 < p_T < 1$ GeV/c, $1 < p_T < 2$ GeV/c and $2 < p_T < 3$ GeV/c

The usage of weighted average requires, as an underlying assumption, identical results expected for different species (or, at least, compatible within the uncertainties). Anyway, it was also verified that the usage of the arithmetic average instead of the weighted average increases the uncertainties on the points, but produces a negligible shift of their central values.

5.3 Fit observable p_T trends and uncertainties

In order to extract quantitative and physical information from the data correlation patterns, the averaged D-h correlation distributions are fitted with two Gaussian functions (with means fixed at $\Delta\varphi$=0 and $\Delta\varphi$=π values), plus a constant term (baseline). A periodicity condition is also applied to the fit function to obtain the same value at the bounds of 2π range. The expression of the fit function is reported below (equation 9):

$$f(\Delta\varphi) = c + \frac{Y_{NS}}{\sqrt{2\pi}\sigma_{NS}} e^{-\frac{(\Delta\varphi-\mu_{NS})^2}{2\sigma_{NS}^2}} + \frac{Y_{AS}}{\sqrt{2\pi}\sigma_{AS}} e^{-\frac{(\Delta\varphi-\mu_{AS})^2}{2\sigma_{AS}^2}} \tag{9}$$

where baseline is calculated as the weighted average of the points lying in the so-called "transverse region", i.e. the interval $\frac{\pi}{4} < |\Delta\varphi| < \frac{\pi}{2}$.

Results from the fit for the studied kinematical regions are shown in Figure 28

From the fit outcome, it is possible to retrieve the near-side and away-side yield and widths (integral and sigma of the Gaussian functions, respectively), as well as the baseline height of the correlation distribution. The near-side observables give information on the multiplicity and angular spread of the tracks from the fragmentation of the charm jet which gave birth to the D-meson trigger. At first order, instead, the away-side observables are related to the hadronization of the charm parton produced in the opposite direction (though the presence of NLO processes for charm production breaks the full validity

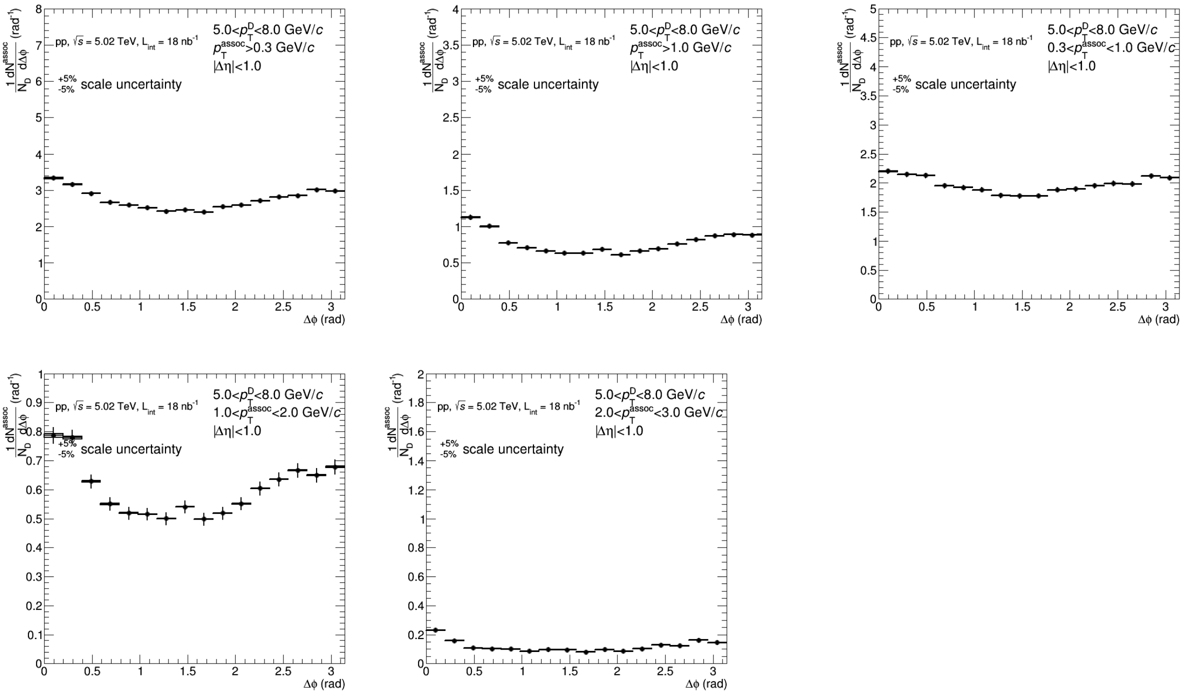

Figure 43: Average of D^0, D^+ and D^{*+} azimuthal correlation distributions, in the D meson p_{T} range $5 < p_{\mathrm{T}} < 8$ GeV$/c$ with associated tracks with $p_{\mathrm{T}} > 0.3$ GeV$/c$, $p_{\mathrm{T}} > 1$ GeV$/c$, $0.3 < p_{\mathrm{T}} < 1$ GeV$/c$, $1 < p_{\mathrm{T}} < 2$ GeV$/c$ and $2 < p_{\mathrm{T}} < 3$ GeV$/c$

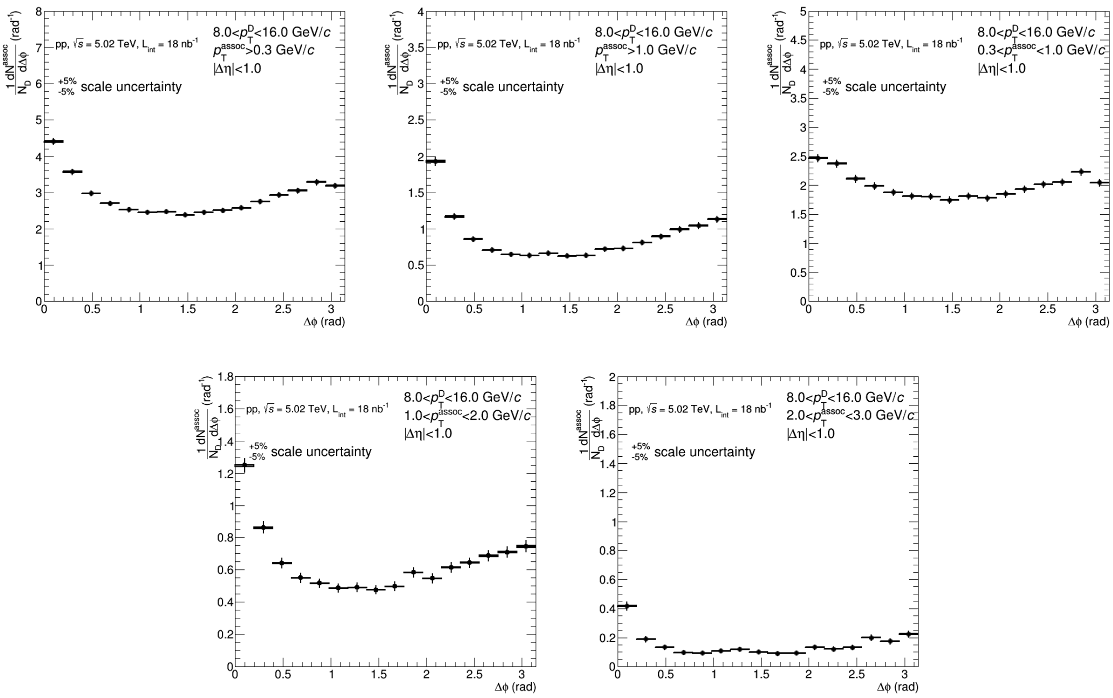

Figure 44: Average of D^0, D^+ and D^{*+} azimuthal correlation distributions, in the D meson p_{T} range $8 < p_{\mathrm{T}} < 16$ GeV$/c$ with associated tracks with $p_{\mathrm{T}} > 0.3$ GeV$/c$, $p_{\mathrm{T}} > 1$ GeV$/c$, $0.3 < p_{\mathrm{T}} < 1$ GeV$/c$, $1 < p_{\mathrm{T}} < 2$ GeV$/c$ and $2 < p_{\mathrm{T}} < 3$ GeV$/c$

of this assumption). The baseline value is a rough indicator of the underlying event multiplicity, though below the baseline level also charm and beauty-related pairs are contained (especially in cases of NLO production for the heavy quarks).

The evaluation of the systematic uncertainties on the observables obtained from the fits is performed as follows (**THIS PARAGRAPH WILL BE UPDATED**):

- The fits are repeated by changing the range of the transverse region in which the baseline is evaluated. Alternate definitions of $\frac{\pi}{4} < |\Delta\varphi| < \frac{3\pi}{8}$, $\frac{3\pi}{8} < |\Delta\varphi| < \frac{\pi}{2}$ and $\frac{\pi}{4} < |\Delta\varphi| < \frac{5\pi}{8}$ are considered.
- In addition, $\Delta\varphi$ correlation points are shifted to the upper and lower bounds of their uncorrelated systematic boxes, and refitted.
- The fits are also repeated by moving the baseline value from its default value (i.e. with the default transverse region) on top and on bottom of its statistic uncertainty. This helps to account, though in a systematic uncertainty, for the statistical uncertainty on the baseline position (since in the fit the baseline is constrained, and its error is not propagated to the other observables).
- The envelope between (i) the RMS of the relative variations of the parameters between the fit outcomes defined in the first two points, and (ii) the relative variations of the parameters from the fit outcomes defined in the third point, is considered as systematic uncertainty for the near-side and away-side widths.
- For the estimation of the baseline and of the near-side and away-side yields, instead, the previous value is added in quadrature with the $\Delta\varphi$-correlated systematics in the correlation distributions, since these values are affected by a change in the global normalization of the distributions.
- In addition, for all the fit observables, an additional fit variation is performed assuming, instead of a flat baseline, a $v_{2\Delta}$-like modulation, with the following v_2 values for the associated tracks (assuming $v_{2\Delta} = v_2(\mathrm{h}) \cdot v_2(\mathrm{D})$: 0.04 (0.3-1 GeV/c), 0.06 (>0.3 GeV/c), 0.08 (1-2 GeV/c), 0.09 (>1 GeV/c, 2-3 GeV/c), 0.1 (>3 GeV/c), on the basis of ATLAS preliminary results for heavy-flavour muons at 8 TeV; for the D-meson triggers the following v_2 values were instead assumed: 0.05 (3-5 GeV/c), 0.03 (5-8 GeV/c), 0.02 (8-24 GeV/c), on the basis of previous ALICE measurements in p-Pb collisions at 5 TeV [3]. The difference of the fit observables with respect to the standard fits is taken as uncertainty. Due to its peculiarity, this systematic uncertainty is summed in quadrature with the others to obtain the total uncertainty, but is also shown separately in the figures.

$$\sigma^{syst} = \sqrt{(Max\,(\Delta par^{ped.mode}, \Delta par^{\Delta\varphi point}))^2 + (\sigma^{corr}_{Syst})^2} \tag{10}$$

NOTE: THE SYSTEMATIC BOXES IN ALL THE FIT OBSERVABLES FOR THE pp AT 5 TeV SAMPLE WILL BE UPDATED AFTER THE SYSTEMATICS EVALUATION, HENCE THEY ARE NOT FINAL.

5.3.1 Results for near-side yield and width, away-side yield and width, and baseline

(**TO BE UPDATED. ANYWAY, THE RESULTS OF THE FIT ARE PRESENTED IN THE COMPARISON FIGURES, SO ALL THE INFORMATION IS ALREADY PRESENT.**) Figures **??**, **??**, **??**, **??** and **??** show the near-side associated yield, width (the sigma of the Gaussian part of the fit functions), away-side associated yield, width and the height of the baseline, for the average correlation distributions, in the kinematic ranges studied in the analysis, together with their statistical and systematic uncertainties. For each kinematic range, the correspondent plot showing the systematic uncertainty of the considered observable from the variation of the fit procedure is reported as well (which is the full systematic uncertainty for the widths).

5.3.2 Comparisons of pp and p–Pb at 5 TeV

Figure 29 (two pages) shows the average of D^0, D^+ and D^{*+} azimuthal correlations for 2017 pp and 2016 p–Pb for all the kinematic ranges of trigger and associated particles p_T. Overall, compatibility within uncertainties between the two collision systems is found for all the common kinematic ranges analyzed, and a similar evolution of the correlation pattern with transverse momentum holds for the two systems. Focusing on the peak regions, while one can appreciate a full near-side compatibility, for some kinematic regions the away-side region seems to be enhanced in p–Pb with respect to pp. As it could be already noticed from the comparison of the distributions, near-side observables are fully consistent. For the away-side region, instead, the peak widths are roughly compatible (wichin rather large uncertainties), while a hint of larger yields in p–Pb can be observed, especially from 5 to 16 GeV/c for the D-meson p_T, generally in all the associated track p_T regions. In Figs. 30,**??** the comparison of the observables extracted from the fits (near-side yield and width) is also presented.

5.3.3 Comparisons of pp at 5, 7 and 13 TeV

Figure 32 shows the average of D^0, D^+ and D^{*+} azimuthal correlations for pp at 5 TeV compared with pp at 7 TeV and 13 TeV for all the common kinematic ranges of trigger and associated particles p_T analysed. The data distribution of pp at 5 TeV have much better uncertainties than 7 TeV and also quite better than 13 TeV. Compatibility within uncertainties between the three energy systems is found for all the common kinematic ranges analyzed. In Figs. 33 and 34, the comparison of the observables extracted from the fits (near-side yield and width for first page, away-side yield and width for second page) is also presented. The near-side observables do not show difference above the uncertainties, which are not small (especially for past results), not allowing to quantitatively appreciate any energy dependence of the yields, expected to be of the order of 8-10% for 5 vs 7 TeV and of 15-20% for 5 vs 13 TeV results from Pythia6 and Pythia8 simulations. Qualitatively, anyway, it can be observed that yield values at 13 TeV are generally larger than yields at 5 TeV, following the expectations of some mild energy scaling of this observable. Nothing can be said, instead, for the away-side observables, where the precision is not enough to draw any conclusion, even qualitatively - also because model expectations for away-side observables at different energies predict much similar results at the three energies, much smaller than the current uncertainties. Indeed, away-side results at 7 and 13 TeV were not approved at all, in the past).

5.3.4 Comparisons of pp at 5 TeV and model predictions

Figure 35 (two pages) shows the average of D^0, D^+ and D^{*+} azimuthal correlations for pp for several ranges of trigger and associated p_T, compared to different Pythia6 tunes (Perugia 0, 2010, 2011), Pythia 8 (tune 4C) and POWHEG+PYTHIA at the same collision energy. A substantial agreement in the overall momentum evolution of the correlation pattern is observed within uncertainties for what concerns the near-side region, apart from very high p_T of the D-meson, where the peak seems to be slightly underestimated, at least by PYTHIA predictions. For the away-side region, the models themselves differentiate in predicting the height of the peak, and generally the strenght of the peak overestimate the data measurements, especially for the older Perugia tunes (PYTHIA6-Perugia0 and PYTHIA6-Perugia2010). In Figs. 36 and 37 (two pages for each) the comparison of the extracted physical observables (near-side and away-side yield, width and baseline height) is presented. For the near-side yields, POWHEG tends to predict larger values than PYTHIA6,8, in all associated track p_T regions. Data results seem to behave in-between of the two predictions, apart from $16 < p_T(\mathrm{D}) < 24\mathrm{GeV}/c$ range, where excluding the lowest associated p_T range, data are better described by POWHEG. For the near-side width, POWHEG also tends to predict wider peaks, in this case generally overpredicting the observed values, which are better matched by PYTHIA predictions (though no model can be ruled out with current uncertainties). Focusing on the away-side region, POWHEG expectation foresee smaller and narrower peaks, with respect to all PYTHIA6,8 predictions, which is confirmed by data, especially for the yields, and in the intermediate D-meson p_T region.. All the models, except possibly PYTHIA6-Perugia0, predict similar baseline values, which generally describe well the data measurements.

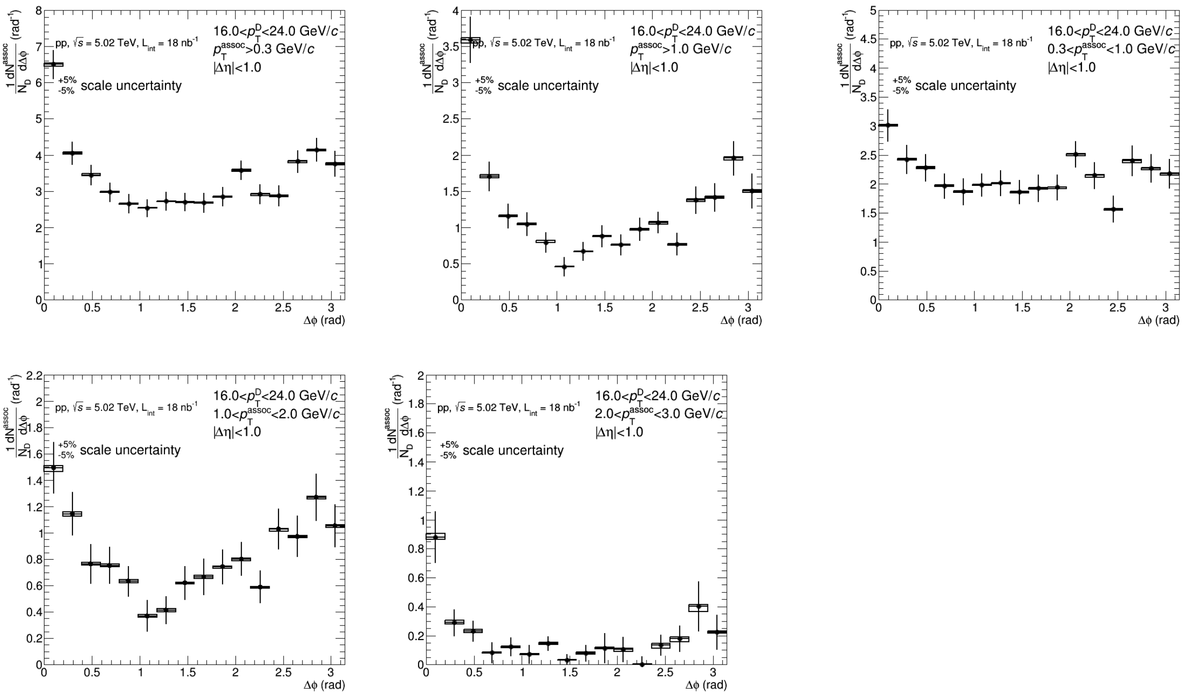

Figure 45: Average of D^0, D^+ and D^{*+} azimuthal correlation distributions, in the D meson p_{T} range $16 < p_{\mathrm{T}} < 24$ GeV$/c$, with associated tracks with $p_{\mathrm{T}} > 0.3$ GeV$/c$, $p_{\mathrm{T}} > 1$ GeV$/c$, $0.3 < p_{\mathrm{T}} < 1$ GeV$/c$, $1 < p_{\mathrm{T}} < 2$ GeV$/c$ and $2 < p_{\mathrm{T}} < 3$ GeV$/c$

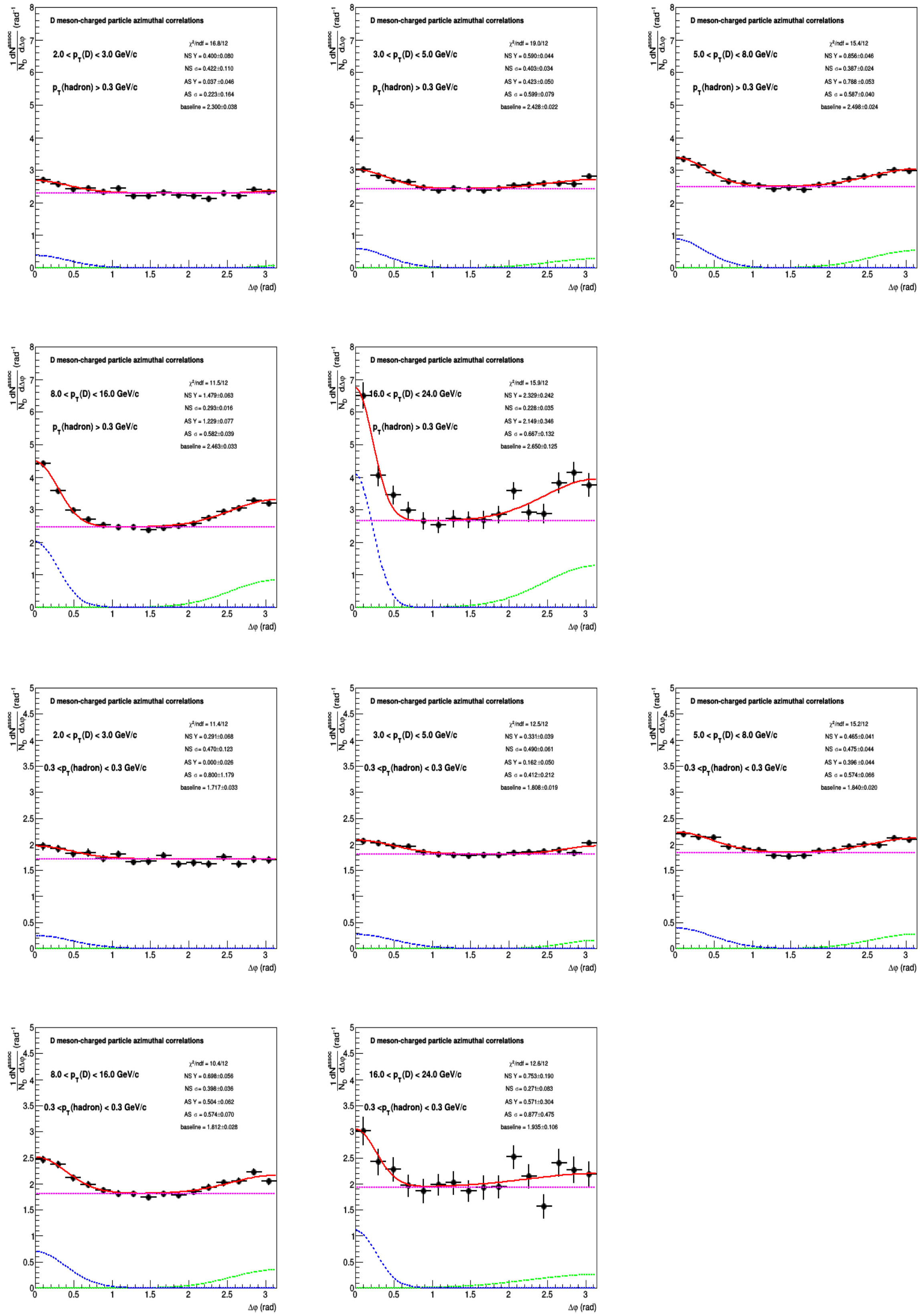
D meson-charged particle azimuthal correlations
2.0 < p_T(D) < 3.0 GeV/c
p_T(hadron) > 0.3 GeV/c
χ²/ndf = 16.8/12
NS Y = 0.400±0.080
NS σ = 0.422±0.110
AS Y = 0.037±0.046
AS σ = 0.223±0.164
baseline = 2.300±0.038
D meson-charged particle azimuthal correlations
3.0 < p_T(D) < 5.0 GeV/c
p_T(hadron) > 0.3 GeV/c
χ²/ndf = 19.0/12
NS Y = 0.590±0.044
NS σ = 0.403±0.034
AS Y = 0.423±0.050
AS σ = 0.599±0.079
baseline = 2.428±0.022
D meson-charged particle azimuthal correlations
5.0 < p_T(D) < 8.0 GeV/c
p_T(hadron) > 0.3 GeV/c
χ²/ndf = 15.4/12
NS Y = 0.856±0.046
NS σ = 0.387±0.024
AS Y = 0.788±0.053
AS σ = 0.587±0.040
baseline = 2.498±0.024
D meson-charged particle azimuthal correlations
8.0 < p_T(D) < 16.0 GeV/c
p_T(hadron) > 0.3 GeV/c
χ²/ndf = 11.5/12
NS Y = 1.479±0.063
NS σ = 0.293±0.016
AS Y = 1.229±0.077
AS σ = 0.582±0.039
baseline = 2.463±0.033
D meson-charged particle azimuthal correlations
16.0 < p_T(D) < 24.0 GeV/c
p_T(hadron) > 0.3 GeV/c
χ²/ndf = 15.9/12
NS Y = 2.329±0.242
NS σ = 0.228±0.035
AS Y = 2.149±0.346
AS σ = 0.667±0.132
baseline = 2.650±0.125
D meson-charged particle azimuthal correlations
2.0 < p_T(D) < 3.0 GeV/c
0.3 < p_T(hadron) < 0.3 GeV/c
χ²/ndf = 11.4/12
NS Y = 0.291±0.068
NS σ = 0.470±0.123
AS Y = 0.000±0.026
AS σ = 0.800±1.179
baseline = 1.717±0.033
D meson-charged particle azimuthal correlations
3.0 < p_T(D) < 5.0 GeV/c
0.3 < p_T(hadron) < 0.3 GeV/c
χ²/ndf = 12.5/12
NS Y = 0.331±0.039
NS σ = 0.490±0.061
AS Y = 0.162±0.050
AS σ = 0.412±0.212
baseline = 1.808±0.019
D meson-charged particle azimuthal correlations
5.0 < p_T(D) < 8.0 GeV/c
0.3 < p_T(hadron) < 0.3 GeV/c
χ²/ndf = 15.2/12
NS Y = 0.465±0.041
NS σ = 0.475±0.044
AS Y = 0.396±0.044
AS σ = 0.574±0.066
baseline = 1.840±0.020
D meson-charged particle azimuthal correlations
8.0 < p_T(D) < 16.0 GeV/c
0.3 < p_T(hadron) < 0.3 GeV/c
χ²/ndf = 10.4/12
NS Y = 0.698±0.056
NS σ = 0.398±0.036
AS Y = 0.504±0.062
AS σ = 0.574±0.070
baseline = 1.812±0.028
D meson-charged particle azimuthal correlations
16.0 < p_T(D) < 24.0 GeV/c
0.3 < p_T(hadron) < 0.3 GeV/c
χ²/ndf = 12.6/12
NS Y = 0.753±0.190
NS σ = 0.271±0.083
AS Y = 0.571±0.304
AS σ = 0.877±0.475
baseline = 1.935±0.106
Δφ (rad)

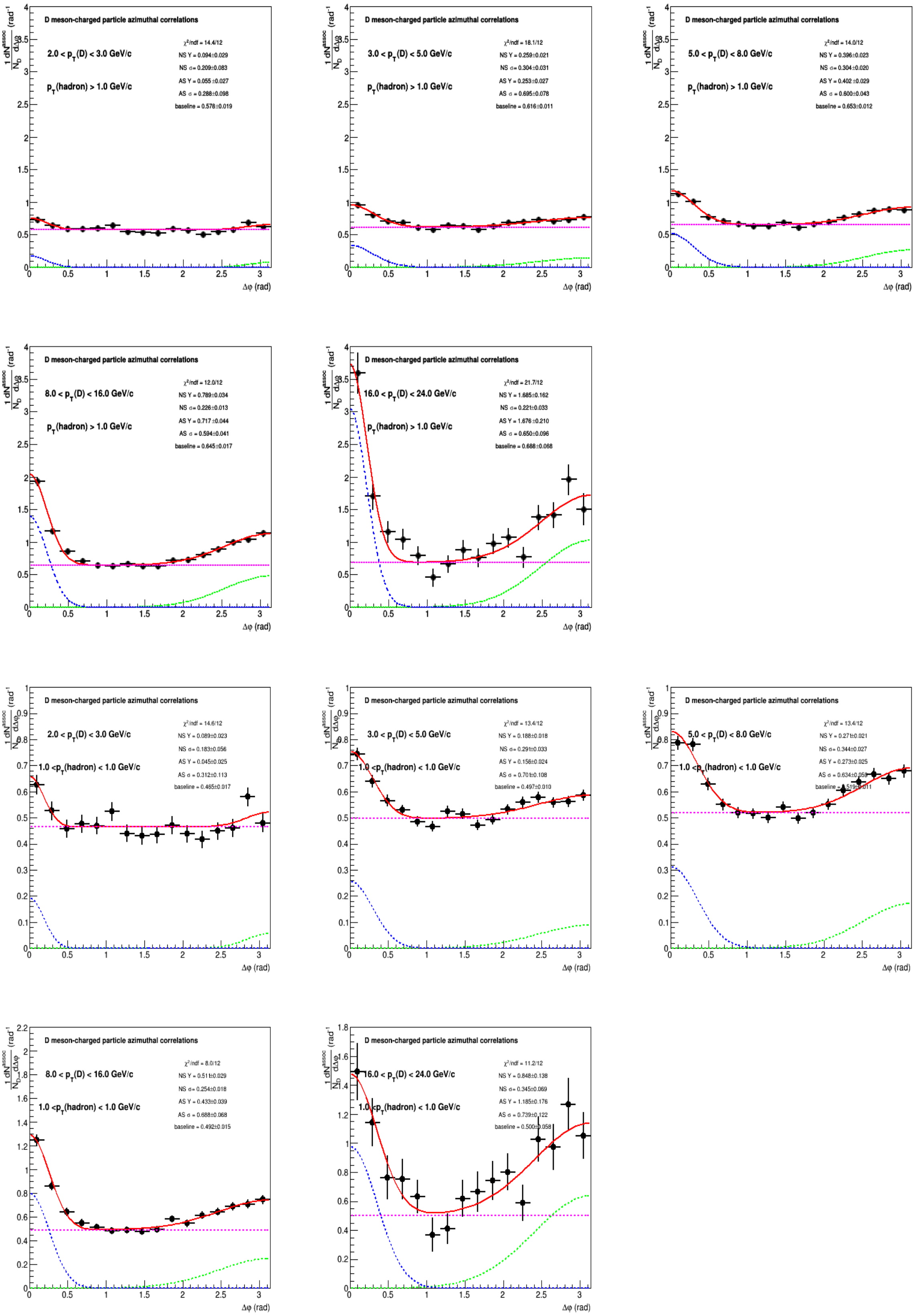
D meson-charged particle azimuthal correlations
2.0 < p_T(D) < 3.0 GeV/c
p_T(hadron) > 1.0 GeV/c
χ²/ndf = 14.4/12
NS Y = 0.094±0.029
NS σ= 0.209±0.083
AS Y = 0.055±0.027
AS σ = 0.288±0.098
baseline = 0.578±0.019
D meson-charged particle azimuthal correlations
3.0 < p_T(D) < 5.0 GeV/c
p_T(hadron) > 1.0 GeV/c
χ²/ndf = 18.1/12
NS Y = 0.259±0.021
NS σ= 0.304±0.031
AS Y = 0.253±0.027
AS σ = 0.695±0.078
baseline = 0.616±0.011
D meson-charged particle azimuthal correlations
5.0 < p_T(D) < 8.0 GeV/c
p_T(hadron) > 1.0 GeV/c
χ²/ndf = 14.0/12
NS Y = 0.396±0.023
NS σ= 0.304±0.020
AS Y = 0.402±0.029
AS σ = 0.600±0.043
baseline = 0.653±0.012
D meson-charged particle azimuthal correlations
8.0 < p_T(D) < 16.0 GeV/c
p_T(hadron) > 1.0 GeV/c
χ²/ndf = 12.0/12
NS Y = 0.789±0.034
NS σ= 0.226±0.013
AS Y = 0.717±0.044
AS σ = 0.594±0.041
baseline = 0.645±0.017
D meson-charged particle azimuthal correlations
16.0 < p_T(D) < 24.0 GeV/c
p_T(hadron) > 1.0 GeV/c
χ²/ndf = 21.7/12
NS Y = 1.685±0.162
NS σ= 0.221±0.033
AS Y = 1.676±0.210
AS σ = 0.650±0.096
baseline = 0.688±0.068
D meson-charged particle azimuthal correlations
2.0 < p_T(D) < 3.0 GeV/c
1.0 <p_T(hadron) < 1.0 GeV/c
χ²/ndf = 14.6/12
NS Y = 0.089±0.023
NS σ= 0.183±0.056
AS Y = 0.045±0.025
AS σ = 0.312±0.113
baseline = 0.465±0.017
D meson-charged particle azimuthal correlations
3.0 < p_T(D) < 5.0 GeV/c
1.0 <p_T(hadron) < 1.0 GeV/c
χ²/ndf = 13.4/12
NS Y = 0.188±0.018
NS σ= 0.291±0.033
AS Y = 0.156±0.024
AS σ = 0.701±0.108
baseline = 0.497±0.010
D meson-charged particle azimuthal correlations
5.0 < p_T(D) < 8.0 GeV/c
1.0 <p_T(hadron) < 1.0 GeV/c
χ²/ndf = 13.4/12
NS Y = 0.271±0.021
NS σ= 0.344±0.027
AS Y = 0.273±0.025
D meson-charged particle azimuthal correlations
8.0 < p_T(D) < 16.0 GeV/c
1.0 <p_T(hadron) < 1.0 GeV/c
χ²/ndf = 8.0/12
NS Y = 0.511±0.029
NS σ= 0.254±0.018
AS Y = 0.433±0.039
AS σ = 0.688±0.068
baseline = 0.492±0.015
D meson-charged particle azimuthal correlations
16.0 < p_T(D) < 24.0 GeV/c
1.0 <p_T(hadron) < 1.0 GeV/c
χ²/ndf = 11.2/12
NS Y = 0.848±0.138
NS σ= 0.345±0.069
AS Y = 1.185±0.176
AS σ = 0.739±0.122
Δφ (rad)

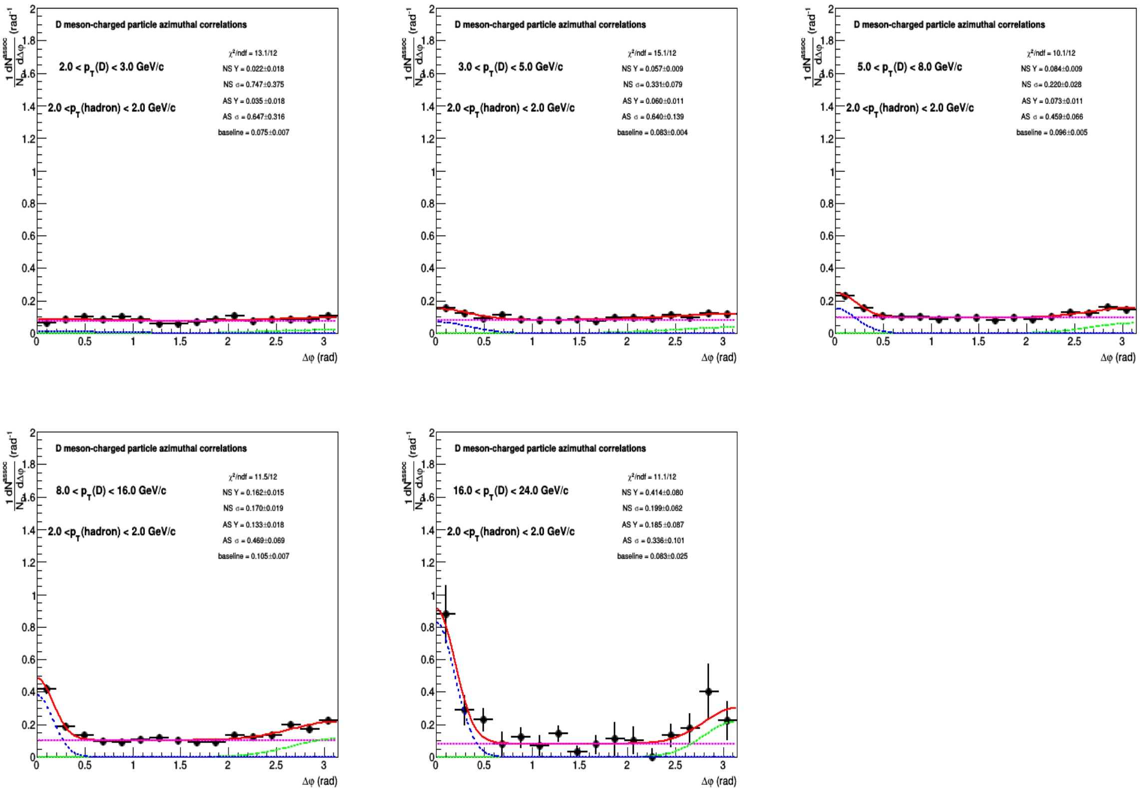

Figure 46: Fits to azimuthal correlation distributions and baseline estimation. Each set of five panels is for, from top to bottom: $p_T > 0.3$ GeV/c, $0.3 < p_T < 1$ GeV/c, $p_T > 1$ GeV/c, $1 < p_T < 2$ GeV/c and $2 < p_T < 3$ GeV/c. The corresponding p_T ranges of D-mesons are reported in each panel.

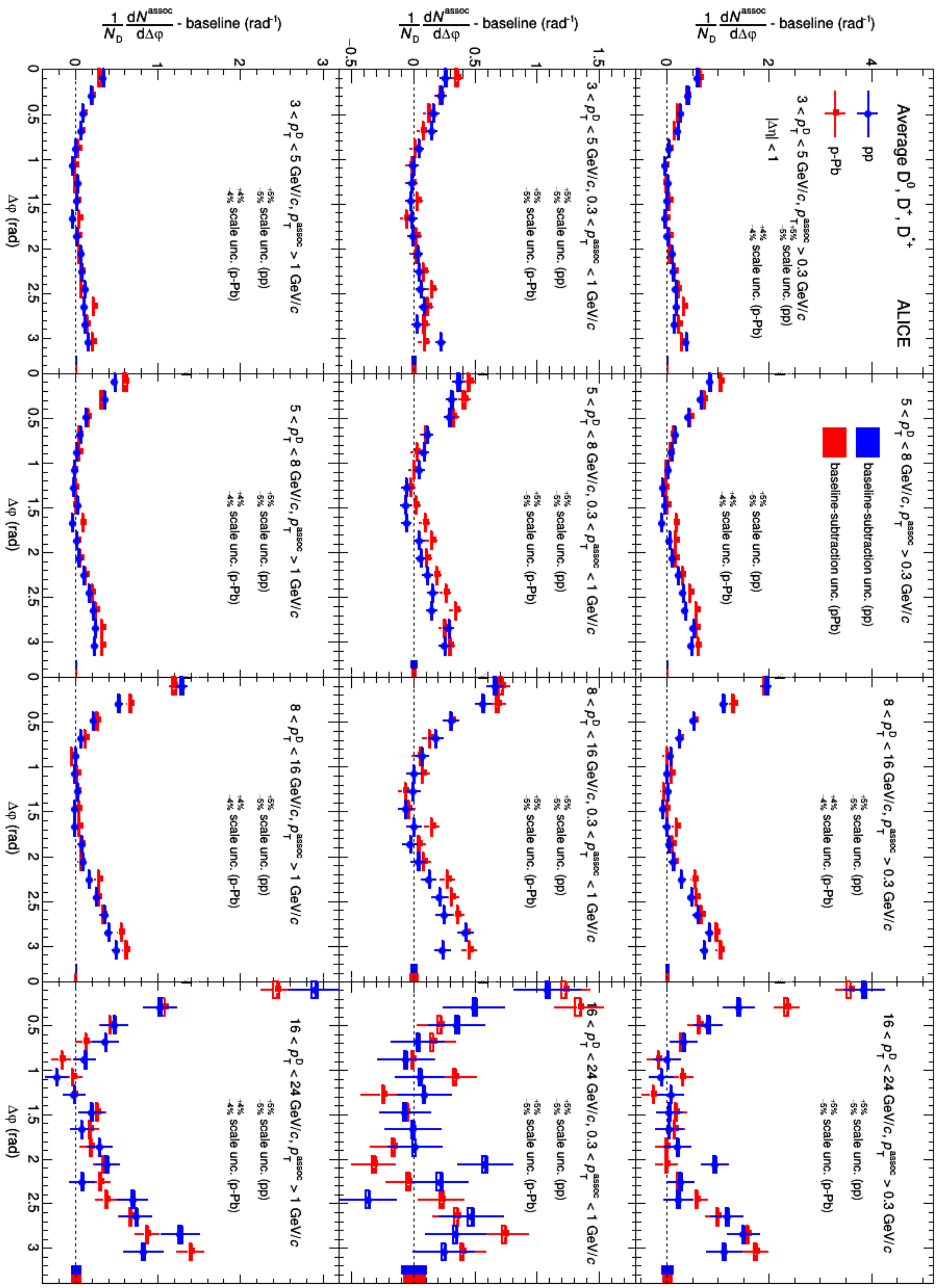
Average D0, D+, D*+
ALICE
pp
p-Pb
|Δη| < 1
baseline-subtraction unc. (pp)
baseline-subtraction unc. (pPb)
3 < pTD < 5 GeV/c, pTassoc > 0.3 GeV/c
5 < pTD < 8 GeV/c, pTassoc > 0.3 GeV/c
8 < pTD < 16 GeV/c, pTassoc > 0.3 GeV/c
16 < pTD < 24 GeV/c, pTassoc > 0.3 GeV/c
3 < pTD < 5 GeV/c, 0.3 < pTassoc < 1 GeV/c
5 < pTD < 8 GeV/c, 0.3 < pTassoc < 1 GeV/c
8 < pTD < 16 GeV/c, 0.3 < pTassoc < 1 GeV/c
16 < pTD < 24 GeV/c, 0.3 < pTassoc < 1 GeV/c
3 < pTD < 5 GeV/c, pTassoc > 1 GeV/c
5 < pTD < 8 GeV/c, pTassoc > 1 GeV/c
8 < pTD < 16 GeV/c, pTassoc > 1 GeV/c
16 < pTD < 24 GeV/c, pTassoc > 1 GeV/c
scale unc. (pp)
scale unc. (p-Pb)
1/ND dNassoc/dΔφ - baseline (rad-1)
Δφ (rad)

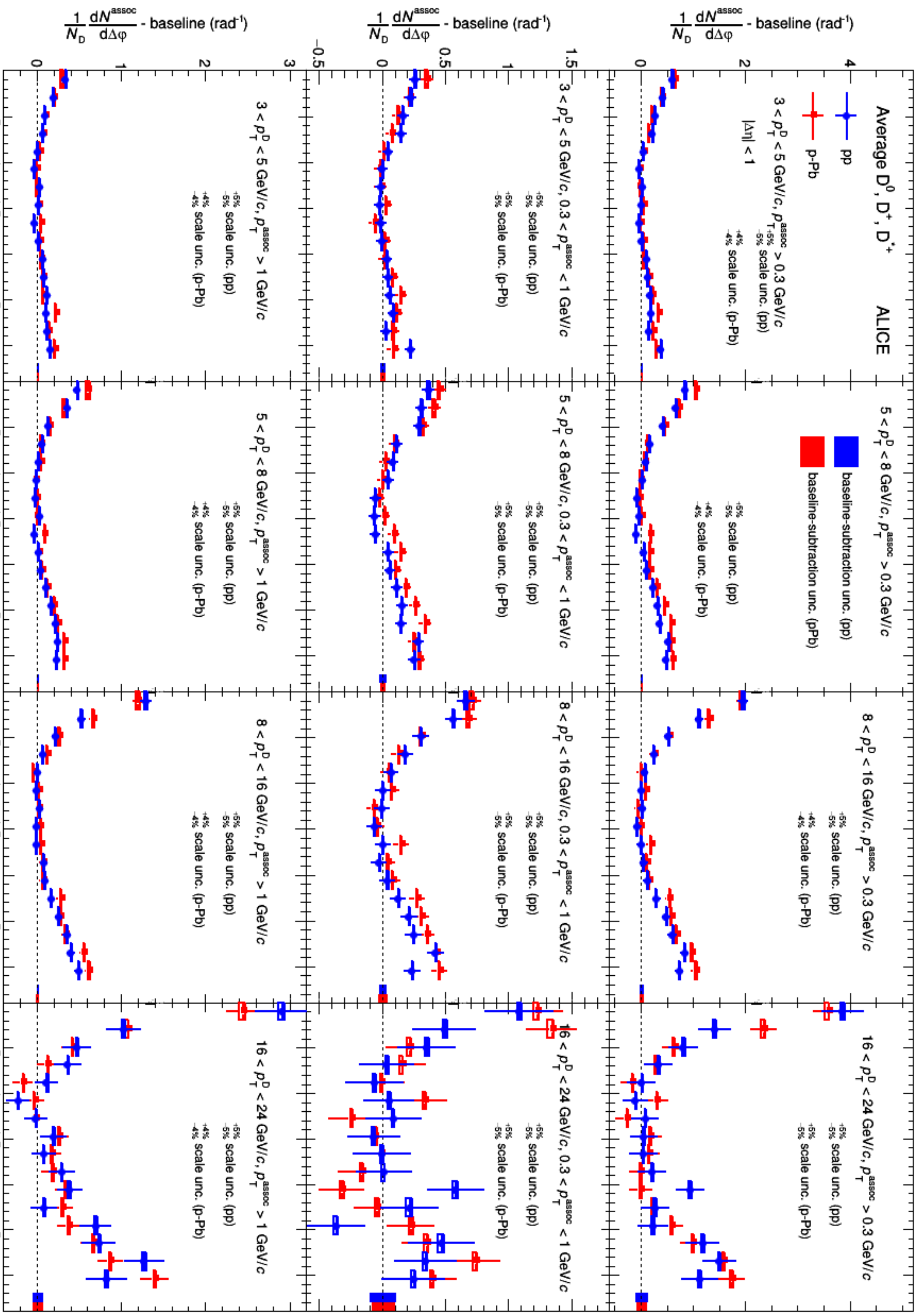

Figure 47: Average of D^0, D^+ and D^{*+} azimuthal correlations in pp (blue) and p-Pb (red) in all the kinematic ranges of trigger and associated particles.

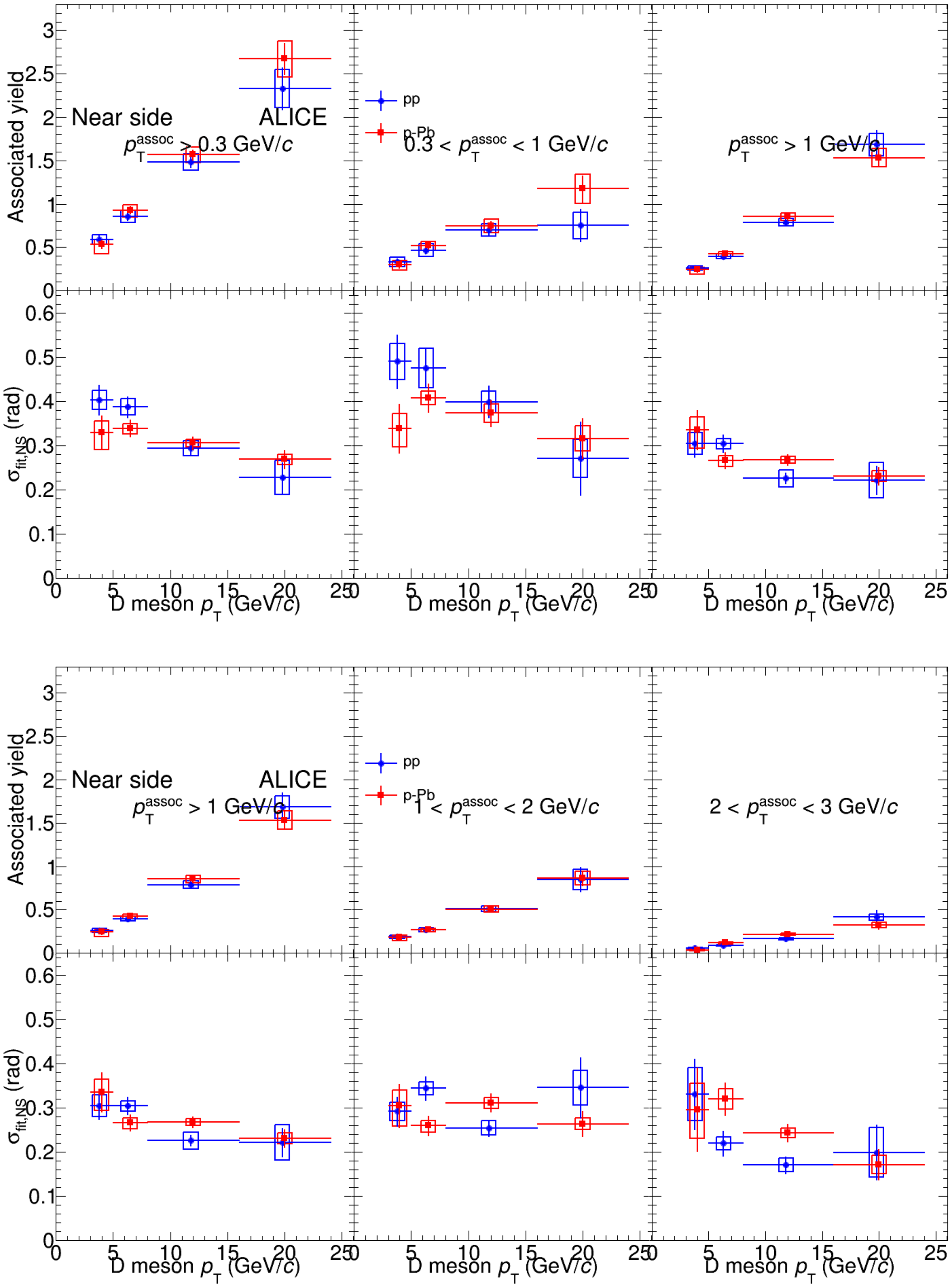

Figure 48: Near-side yield and sigmas for the average of D^0, D^+ and D^{*+} azimuthal correlations in pp (red) and p-Pb (black) in all the kinematic regions of trigger and associated track.

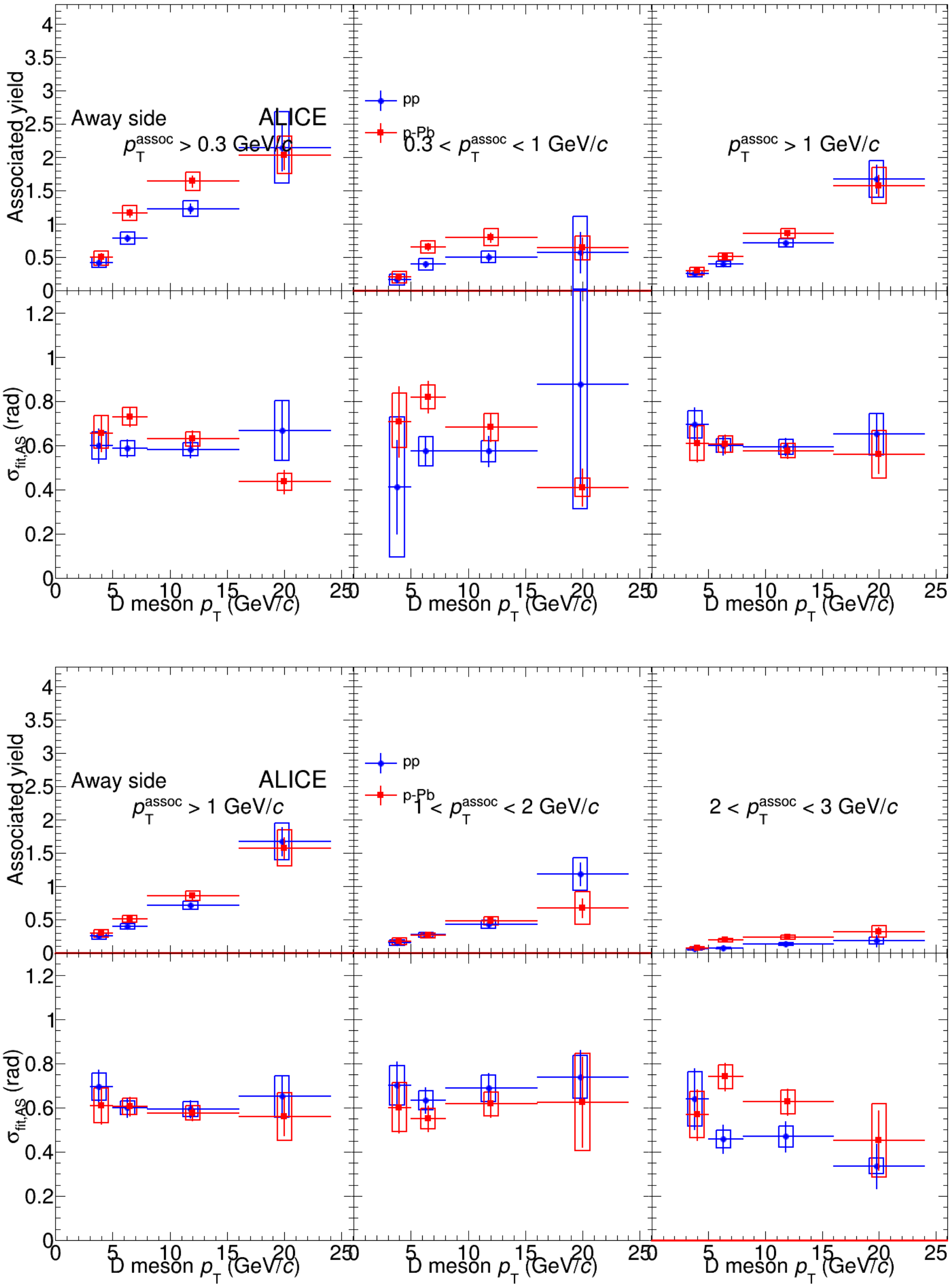

Figure 49: Away-side yield and sigmas for the average of D^0, D^+ and D^{*+} azimuthal correlations in pp (red) and p-Pb (black) in all the kinematic regions of trigger and associated track.

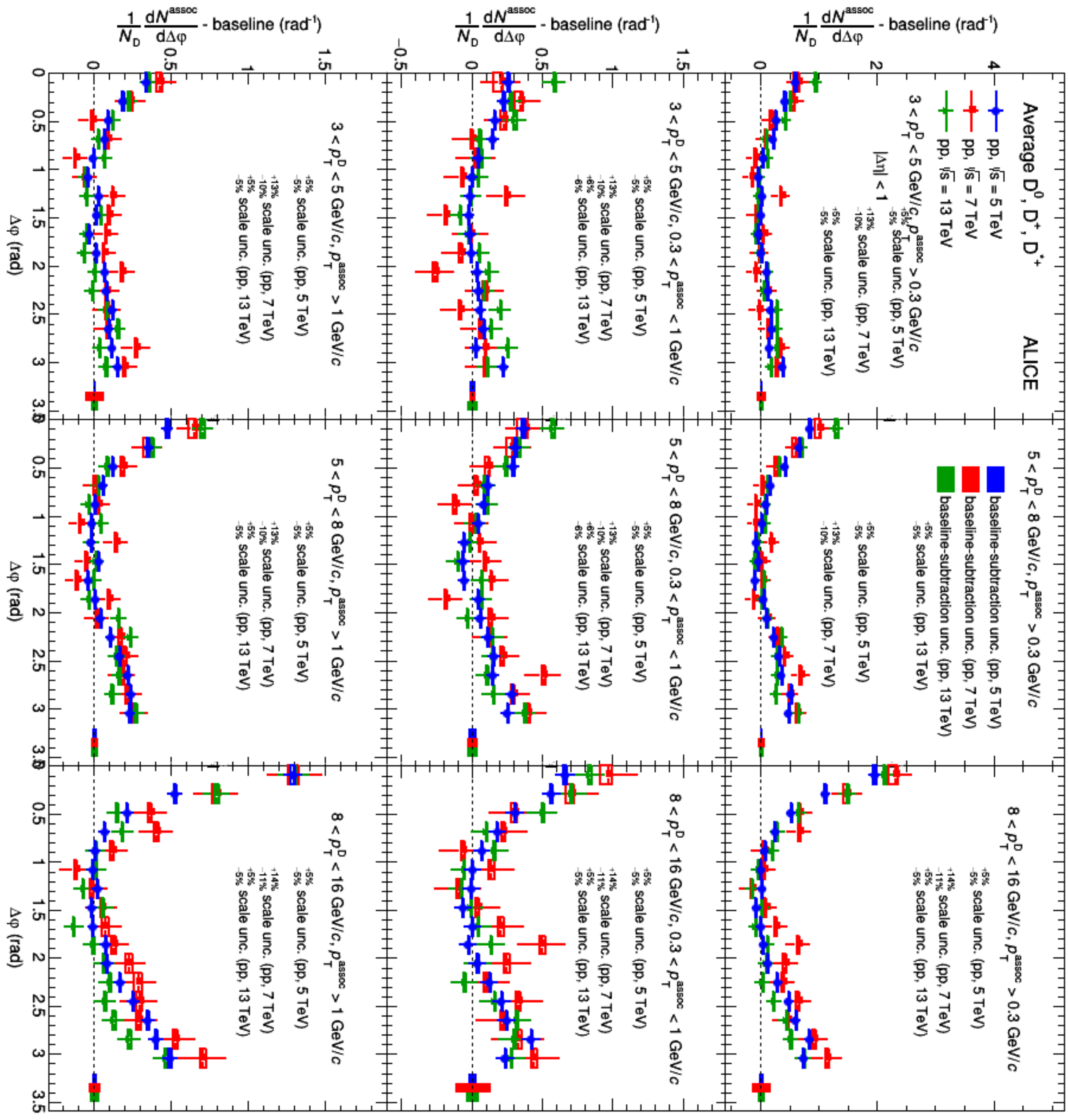

Figure 50: Average of D^0, D^+ and D^{*+} azimuthal correlations in pp at 5 (blue), 7 (red) and 13 (green) TeV in all the common kinematic ranges of trigger and associated particles.

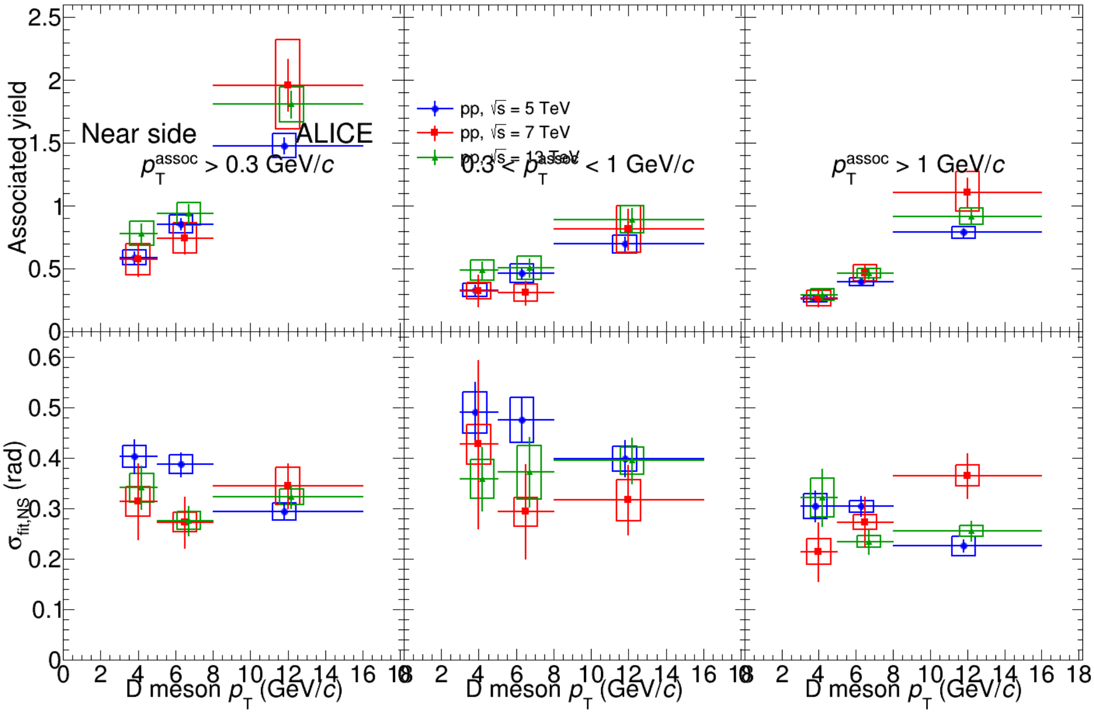

Figure 51: Near-side yield and width for the average of D^0, D^+ and D^{*+} azimuthal correlations in pp at 5 (blue), 7 (red) and 13 (green) TeV in all the common kinematic regions of trigger and associated track.

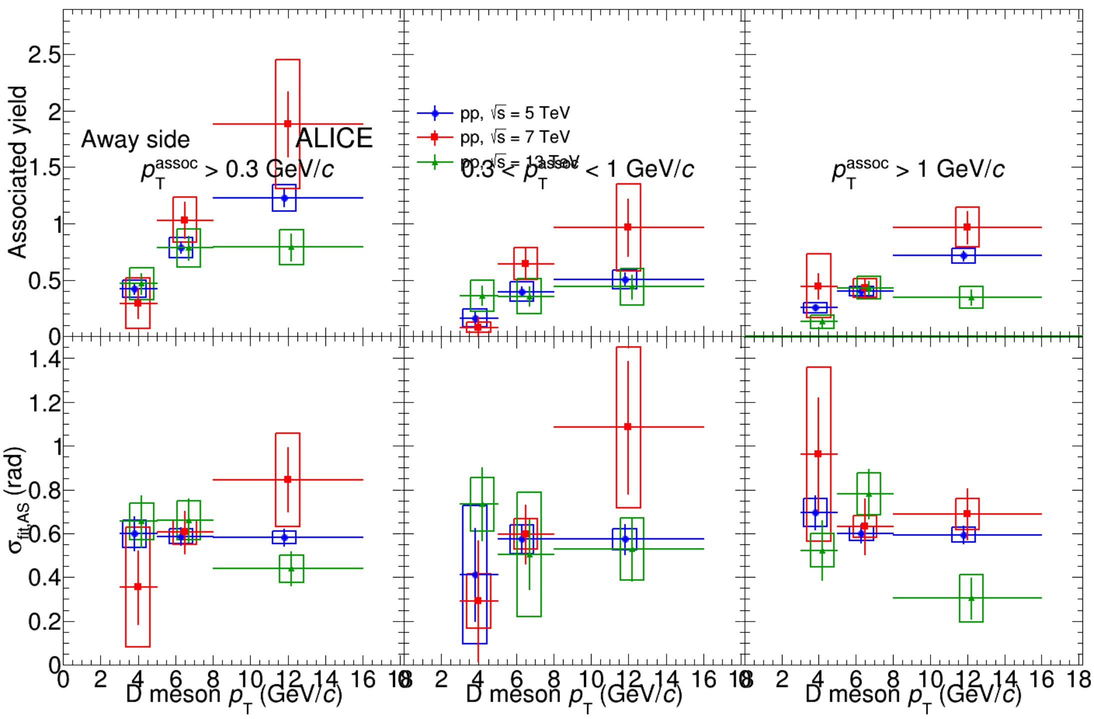

Figure 52: Away-side yield and width for the average of D^0, D^+ and D^{*+} azimuthal correlations in pp at 5 (blue), 7 (red) and 13 (green) TeV in all the common kinematic regions of trigger and associated track.

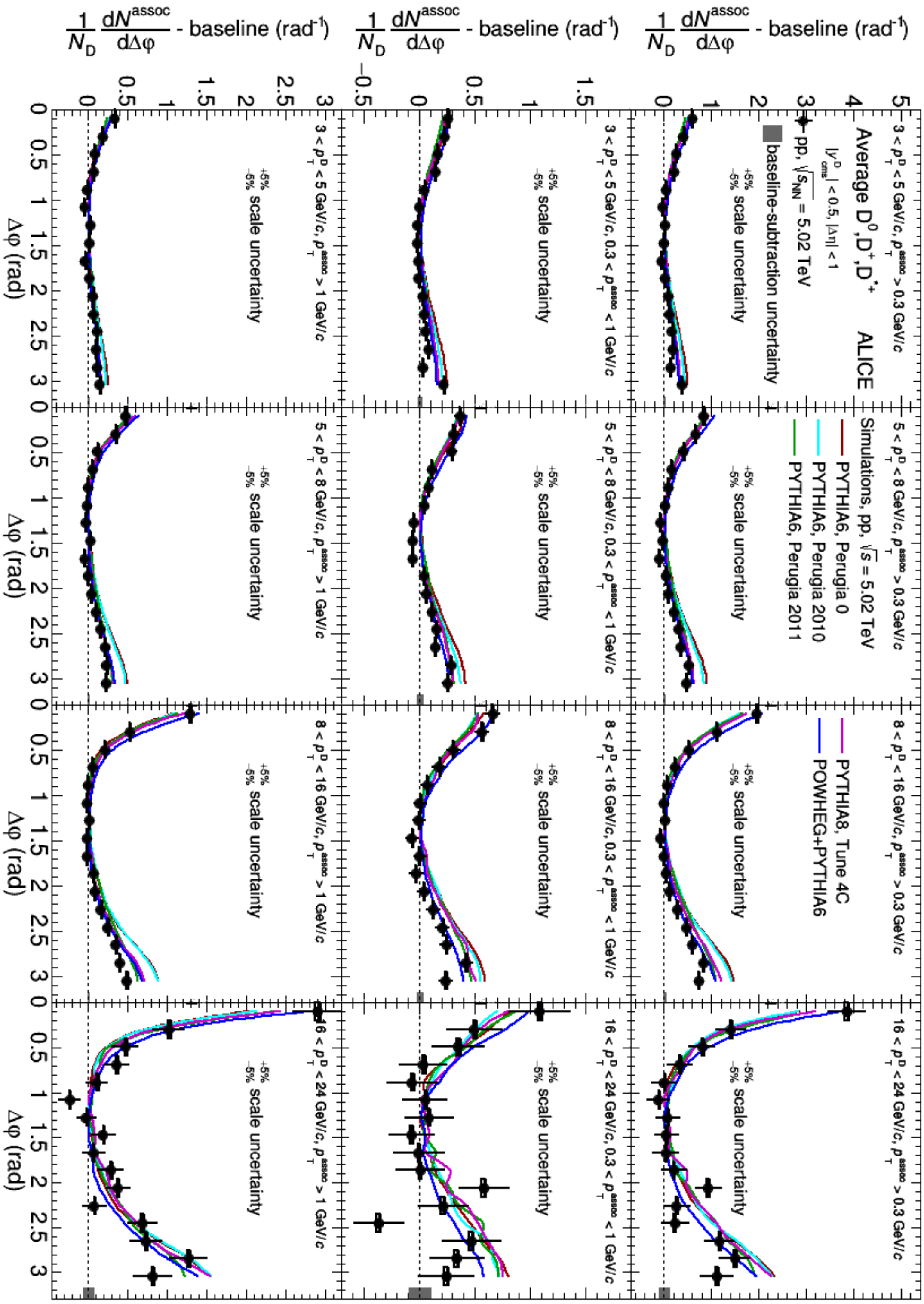
ALICE
Average D⁰,D⁺,D*⁺
pp, √s_NN = 5.02 TeV
baseline-subtraction uncertainty
Simulations, pp, √s = 5.02 TeV
PYTHIA6, Perugia 0
PYTHIA6, Perugia 2010
PYTHIA6, Perugia 2011
PYTHIA8, Tune 4C
POWHEG+PYTHIA6
+5% −5% scale uncertainty
Δφ (rad)
- baseline (rad⁻¹)

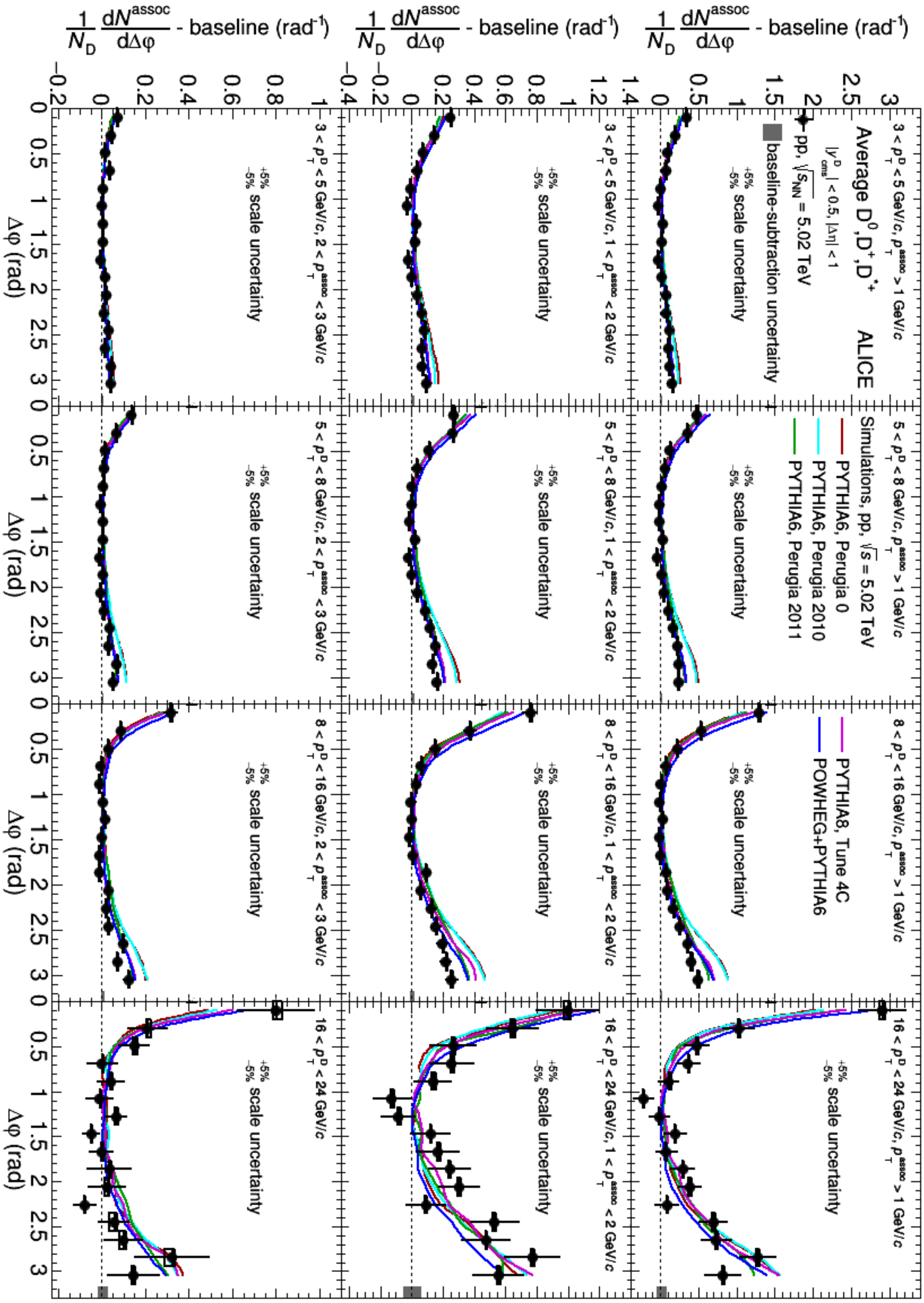

Figure 53: Comparison of $\Delta\varphi$ azimuthal distribution for D-meson averages, obtained from data and simulations different event generators (PHYTIA, with three tunes, and POWHEG+PYTHIA), in the different kinematic ranges analyzed.

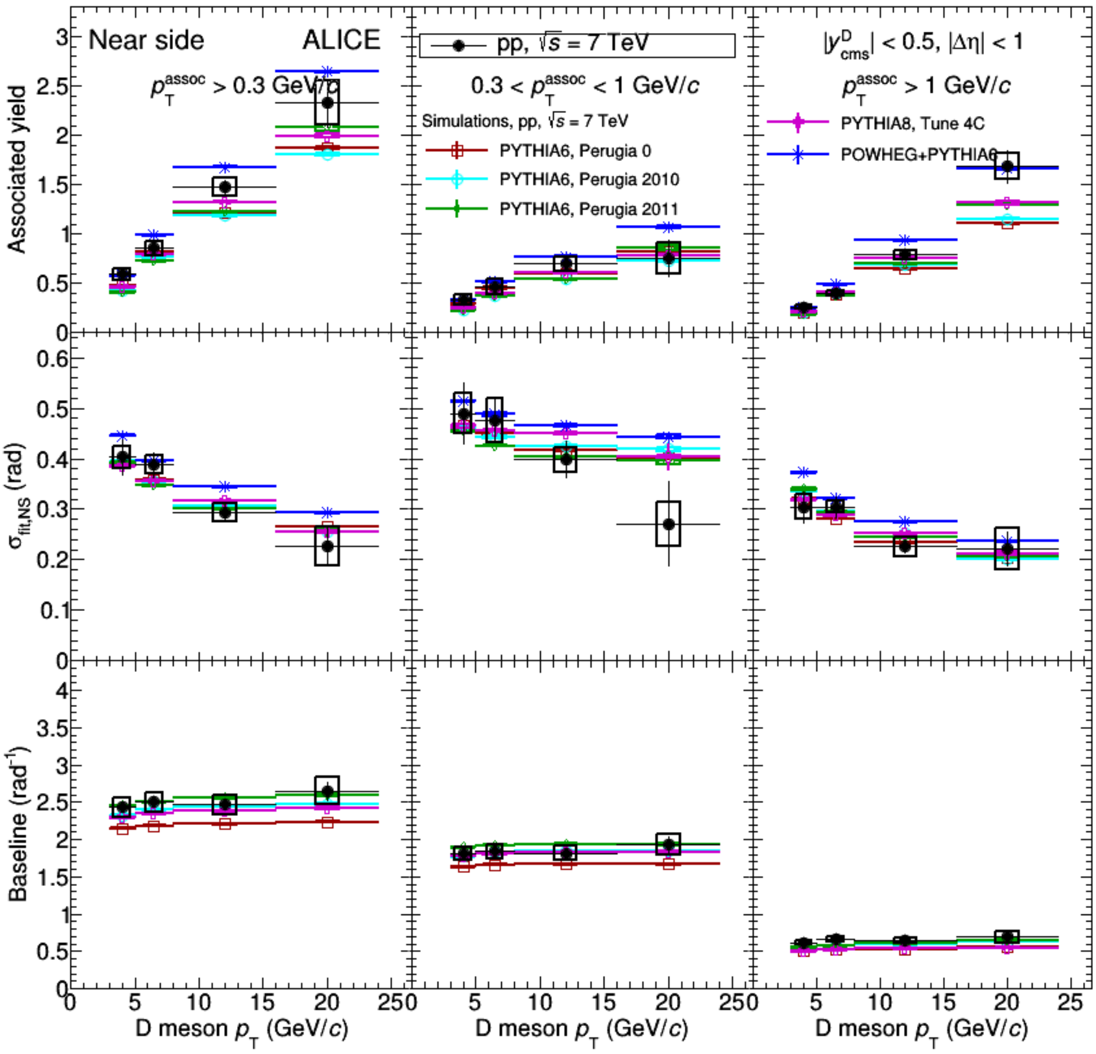

Near side
ALICE
p_T^{assoc} > 0.3 GeV/c
pp, $\sqrt{s}$ = 7 TeV
0.3 < p_T^{assoc} < 1 GeV/c
Simulations, pp, $\sqrt{s}$ = 7 TeV
PYTHIA6, Perugia 0
PYTHIA6, Perugia 2010
PYTHIA6, Perugia 2011
$|y^D_{cms}|$ < 0.5, $|\Delta\eta|$ < 1
p_T^{assoc} > 1 GeV/c
PYTHIA8, Tune 4C
POWHEG+PYTHIA6
Associated yield
$\sigma_{fit,NS}$ (rad)
Baseline (rad^{-1})
D meson p_T (GeV/c)

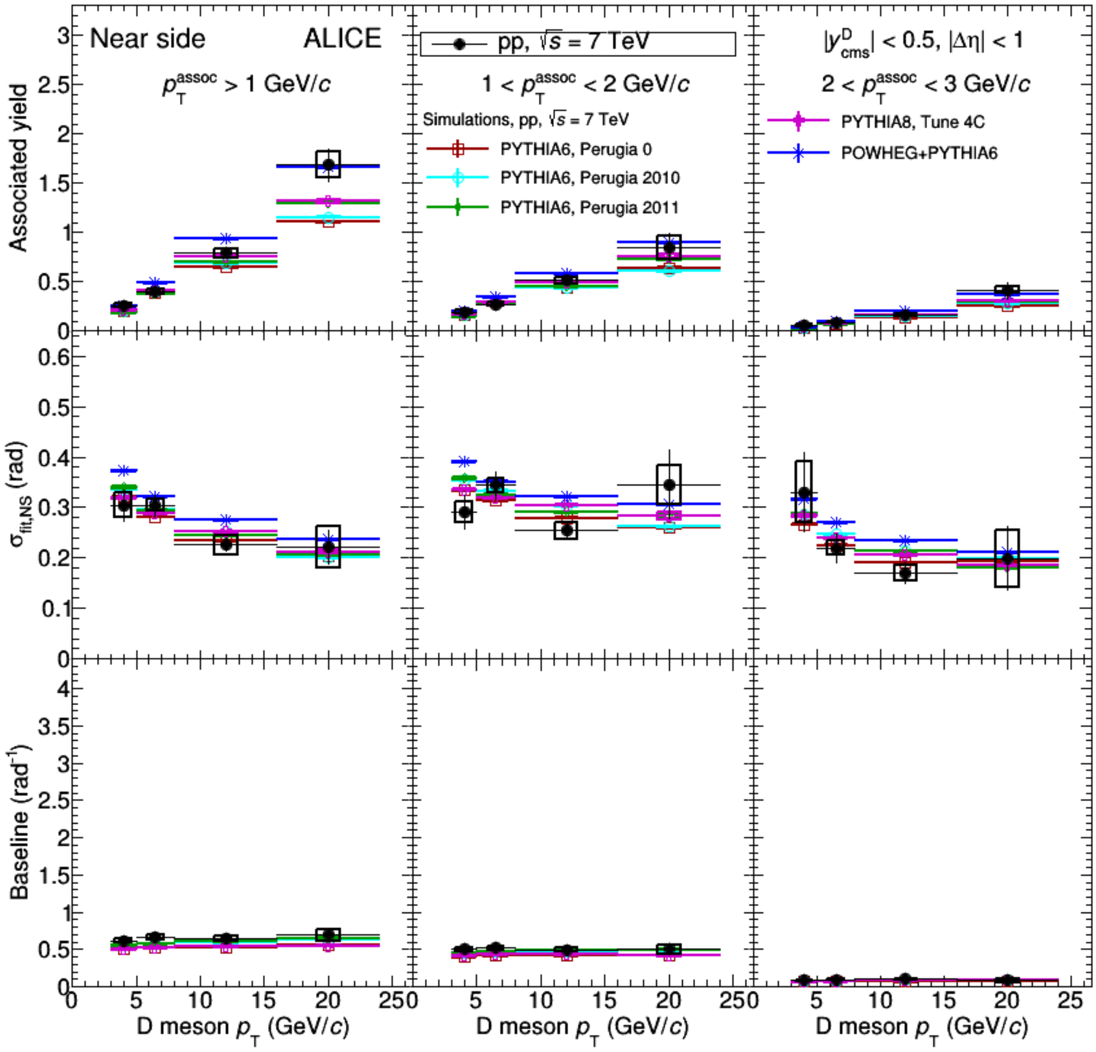

Figure 54: Near-side fit parameters obtained for D-meson averages, extracted from data and simulations different event generators (PYTHIA,6 with three tunes, PYTHIA8 and POWHEG+PYTHIA), in the different kinematic ranges analyzed.

.

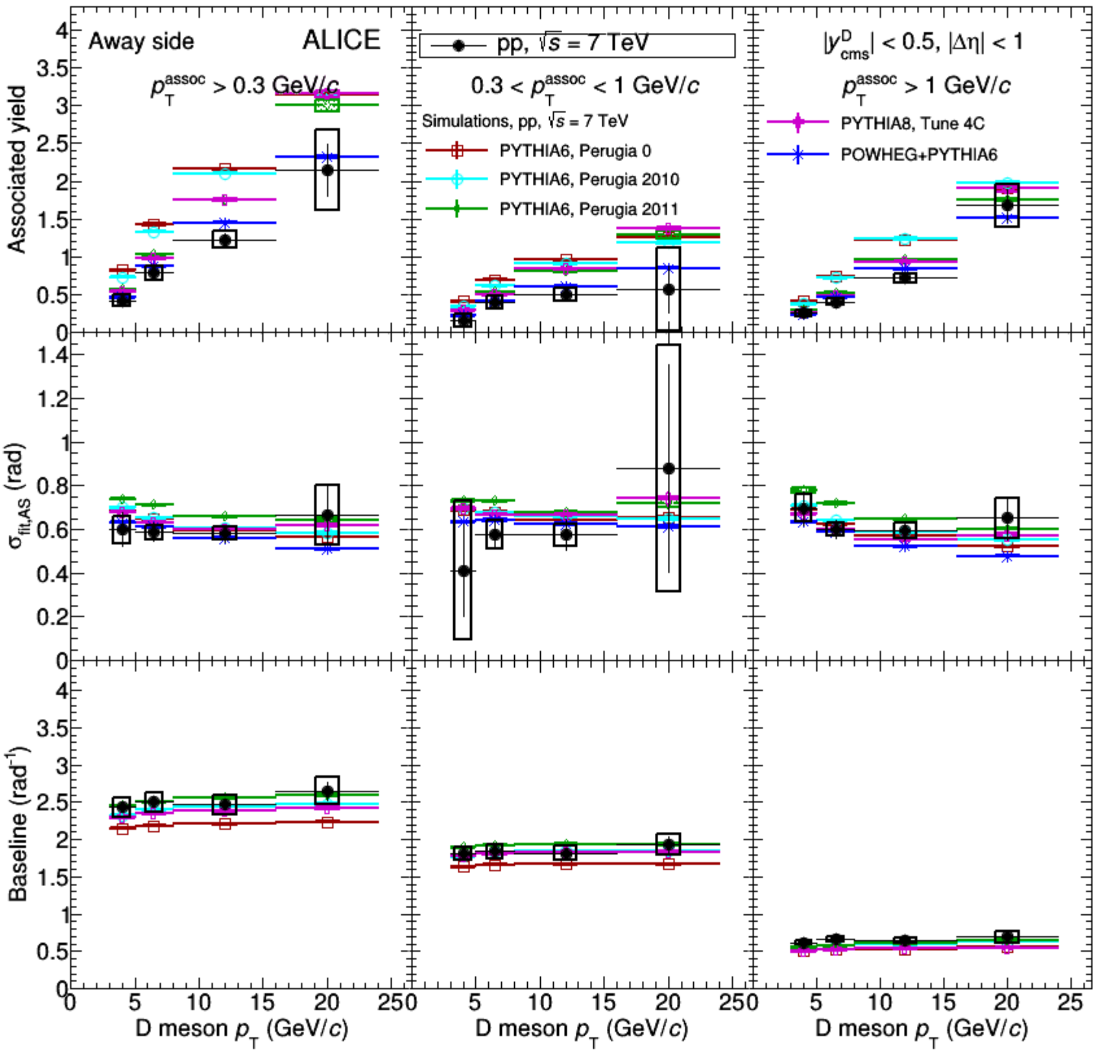

Away side
ALICE
p_T^{assoc} > 0.3 GeV/c
pp, $\sqrt{s}$ = 7 TeV
0.3 < p_T^{assoc} < 1 GeV/c
Simulations, pp, $\sqrt{s}$ = 7 TeV
PYTHIA6, Perugia 0
PYTHIA6, Perugia 2010
PYTHIA6, Perugia 2011
$|y^D_{cms}|$ < 0.5, $|\Delta\eta|$ < 1
p_T^{assoc} > 1 GeV/c
PYTHIA8, Tune 4C
POWHEG+PYTHIA6
Associated yield
$\sigma_{fit,AS}$ (rad)
Baseline (rad^{-1})
D meson p_T (GeV/c)

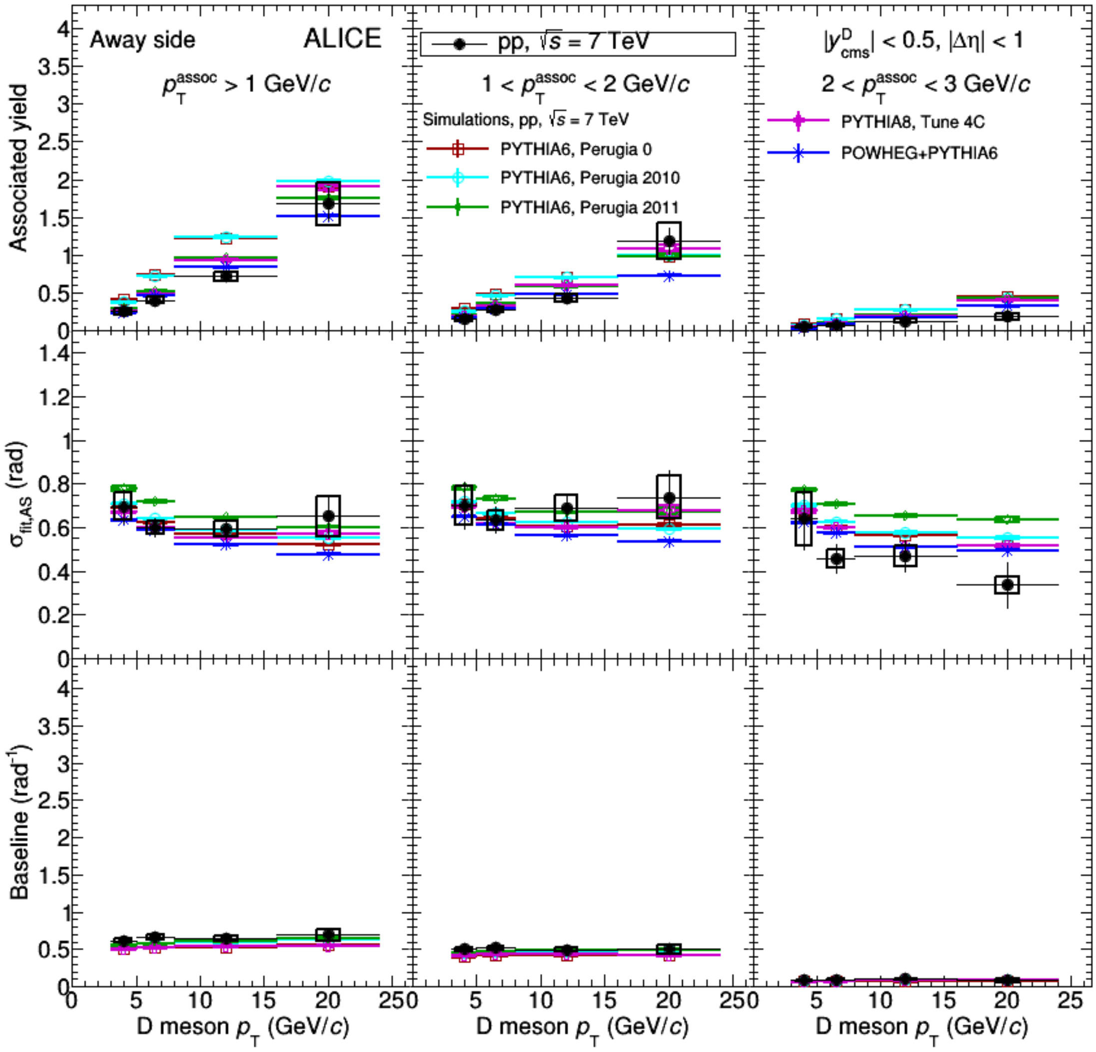

Figure 55: Near-side fit parameters obtained for D-meson averages, extracted from data and simulations different event generators (PYTHIA6, with three tunes, PYTHIA8 and POWHEG+PYTHIA), in the different kinematic ranges analyzed.

.

6 Bibliography

References

[1] B. Abelev et al. [ALICE Collaboration], JHEP **01** (2012) 128
[2] B. Abelev et al. [ALICE Collaboration], Eur. Phys. J. C (2017) 77:245
[3] B. Abelev et al. [ALICE Collaboration], Phys.Lett. B719 (2013) 29-41
[4] B. Abelev et al. [ALICE Collaboration], Phys.Lett. B726 (2013) 164-177
[5] https://aliceinfo.cern.ch/Figure/node/12130 (ALI-PREL-138003)
[6] ALICE Collaboration, arXiv:1609.06643 [nucl-ex]
[7] https://aliceinfo.cern.ch/Notes/node/785
[8] https://aliceinfo.cern.ch/Notes/node/238
[9] https://aliceinfo.cern.ch/Notes/node/201